

# **Integration of Functional DNA-Nanoscaffolds into Supramolecular Polymers**

Inauguraldissertation

der Philosophisch-naturwissenschaftlichen Fakultät

der Universität Bern

vorgelegt von

Mariusz Kownacki

von Polen

Leiter der Arbeit:

Prof. Dr. Robert Häner

Departement für Chemie und Biochemie der Universität Bern

# **Integration of Functional DNA-Nanoscaffolds into Supramolecular Polymers**

Inauguraldissertation

der Philosophisch-naturwissenschaftlichen Fakultät

der Universität Bern

vorgelegt von

Mariusz Kownacki

Von Polen

Leiter der Arbeit:

Prof. Dr. Robert Häner

Departement für Chemie und Biochemie der Universität Bern

Von der Philosophisch-naturwissenschaftlichen Fakultät angenommen.

Der Dekan:

Bern, 28.06.2018

Prof. Dr. Z. Balogh

## **Acknowledgments**

I sincerely thank Prof. Robert Häner for the support during the past 4 years. My thanks indeed go to Simon Langenegger and Shi-Xia Liu for their great input in my scientific development. Many thanks go to the former and the current group members who helped me during my PhD journey. Additionally I want to thank Simon Langenegger, Markus Probst and Simon Rothenbühler for proofreading my thesis.

# Contents

<b>1 Summary.....</b>	<b>1</b>
<b>2 General Introduction.....</b>	<b>2</b>
2.1 Supramolecular Polymers .....	2
2.1.1 DNA-Functionalized Supramolecular Polymers .....	4
2.2 Structural Aspects of DNA.....	5
2.2.1 Solid phase synthesis .....	8
2.3 Light-Harvesting and Energy Transfer.....	10
2.4 FRET in DNA-Photonic Wires.....	13
2.5 Aim of the Thesis.....	15
<b>3 Integration of Functional DNA-Nanoscaffolds into Supramolecular Polymers .....</b>	<b>16</b>
Introduction .....	16
3.1 Integrating DNA - Photonic Wires into Light-Harvesting Supramolecular Polymers.....	18
3.1.1 Abstract.....	18
3.1.2 Introduction .....	19
3.1.3 Results.....	19
3.1.3.1 Oligomers Synthesis and LHCs Composition.....	19
3.1.3.2 Formation of LHCs.....	20
3.1.3.3 AFM and TEM Measurements .....	21
3.1.3.4 Photophysical and FRET Properties of the Fluorophores .....	22
3.1.3.5 Energy Transfer in Phenanthrene Based LHCs.....	24
3.1.3.6 Titration Experiments .....	26
3.1.3.7 Additional Titration Experiments.....	27
3.1.3.8 FRET Efficiency and Antenna Effects.....	28
3.1.3.9 Spectroscopic Measurements.....	30
3.1.4 Conclusions .....	34
3.1.5 Supporting information.....	34
3.1.5.1 Synthesis and purification of oligophosphates .....	34
3.1.5.2 Mass spectra of Oligomers.....	35
3.1.5.3 UV-Vis Spectra.....	37

3.1.5.4 Fluorescence Spectra of Cy7 (Cyanine)-Containing Light-Harvesting Complexes .....	37
3.1.5.5 Structures of the Cyanine Fluorophores used for FRET Cascade Design .....	38
3.1.5.6 Spectra of T <sub>m</sub> Measurements .....	39
3.2 Further Experiments .....	42
3.2.1 Introduction .....	42
3.2.2 Results and Discussion .....	42
3.2.2.1 Composition of Light Harvesting Complexes and DNA Sequences.....	42
3.2.2.2 Spectroscopic Measurements.....	44
3.2.2.3 Energy Transfer in Modified Light-Harvesting Complexes.....	47
3.2.2.4 Influence of the PEG Linker on Phenanthrene Based Light-Harvesting Complexes .....	49
3.2.2.5 Pyrene Influence on the Phenanthrene Based Light-Harvesting Complexes .....	50
3.2.2.6 Distance Dependent Energy Transfer .....	52
3.2.2.7 Conclusions .....	55
3.2.4 Supporting Information .....	55
3.2.4.3 Spectra of T <sub>m</sub> Measurements .....	60
3.3 Integration of DNA-Modified Gold Nanoparticles into Supramolecular Polymers.....	61
3.3.1 Introduction .....	61
3.3.2 Results .....	63
3.3.2.1 DNA Sequences .....	63
3.3.2.2 Arrangements of Gold Nanoparticles .....	63
3.3.3 Conclusions and outlook .....	65
3.3.4 Supporting Information .....	65
3.3.4.1 Synthesis of Gold Nanoparticles .....	65
3.3.4.2 AuNPs-DNA conjugation .....	66
<b>4 Self-Assembly and Aggregation-Induced Emission Properties of a Dialkynyl-Tetraphenylethylene Oligophosphate .....</b>	<b>67</b>
4.1 Introduction .....	67
4.2 Results .....	69
4.2.1 Oligomer Synthesis .....	69
4.2.2 Photophysical Properties .....	69
4.2.3 Temperature Dependent AIE .....	71
4.2.4 AFM Images.....	73
4.3 Conclusions .....	75

4.4 Supporting Information .....	76
4.4.1 Oligomers Synthesis .....	76
4.4.2 Mass Spectra of Oligomer 1 .....	76
5 References .....	78
6 Appendix.....	84
6.1 General Methods .....	84
6.2 Declaration.....	85
6.3 Curriculum Vitae .....	86

## Abbreviations

AIE	Aggregation-induced emission
AFM	Atomic force microscopy
APTES	3-Aminopropyltriethoxy silane
DCM	Dichloromethane
DMT-Cl	4,4'-Dimethoxytriphenylmethyl chloride
EET	Excitation energy transfer
FRET	Förster resonance energy transfer
LCAA-CPG	Long chain alkylamine controlled pore glass
LHC	Light-harvesting complex
PAH	Polycyclic aromatic hydrocarbon
PAM-Cl	2-Cyanoethyl <i>N,N</i> -diisopropylchlorophosphoramidite
r.t.	Room temperature
SPs	Supramolecular Polymers
TEM	Transmission electron microscopy
ESI – MS	Electrospray Ionization Mass Spectrometry
TPE	Tetraphenylethylene

## 1 Summary

The thesis starts with a general introduction that consists of the description of supramolecular polymers (SPs), followed by structural aspects of the DNA and solid phase synthesis based on phosphoramidite chemistry. Furthermore, the light harvesting, energy transfer and application of the Förster resonance energy transfer (FRET) in DNA photonic wires is presented.

The work presented herein consists of two parts:

Part I is composed of three subchapters (3.1-3.3) and describes the integration of functional DNA-nanoscaffolds into supramolecular polymers (SPs). Such systems were designed to mimic the light-harvesting complex (LHC), i.e. key component in photosynthesis. In addition, it is demonstrated that DNA photonic wires as well as gold nanoparticles (AuNPs) can be successfully incorporated into SPs.

In more detail, Subchapter 3.1 (page 21), describes the incorporation of DNA-photonic wires into SPs for the efficient and directional propagation of light-harvesting cascades, while Subchapter 3.2 (page 54) focuses on the influence of modified oligomeric components on the energy transfer in different LHCs. In the same Subchapter (page 65) the effects on energy transfer in LHCs by varying the donor-acceptor pair distance is presented. And finally, Subchapter 3.3 (page 77) describes the functionalization of the, in the previous subchapters introduced, SPs with AuNPs.

Part II of this work (page 83) presents a similar topic – SPs with interesting photophysical properties – but addresses a different aspect: Here, the oligomers self-assemble into vesicles and exhibit aggregation-induced emission (AIE). In this case, phosphodiester-linked dialkynyl-tetraphenylethylene (DATPE) trimers were synthesized and then characterized in aqueous medium.

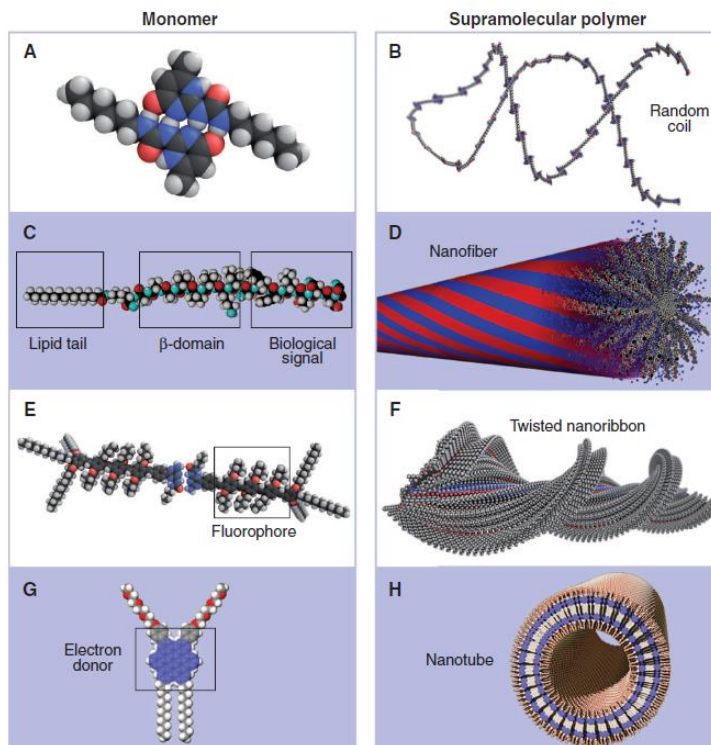
Designing and construction of functional, multicomponent DNA-based supramolecular polymers can be used as platforms in molecular cargo for the delivery of small molecules, proteins, and nanoparticles.

## 2 General Introduction

### 2.1 Supramolecular Polymers

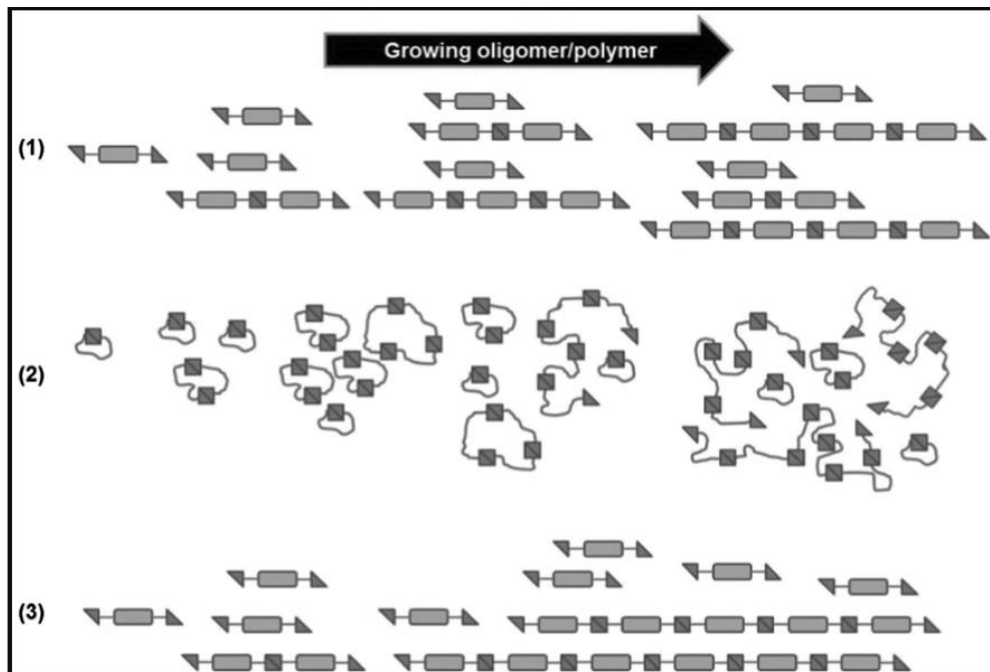
Supramolecular polymers are polymeric arrays of non-covalently linked monomer units usually assembled in well-ordered structures in one or two dimensions.<sup>[1]</sup> In aqueous medium, supramolecular structures are formed due to secondary interactions, among others noncovalent interactions like hydrogen bonding, hydrophobic interactions, π-π interactions and electrostatic interactions.<sup>[2]</sup> Non-covalent bonds ensure high reversibility in supramolecular architectures.

Figure 1 demonstrates molecular building blocks which self-assemble into supramolecular structures with mechanical (Figure 1, A and B), biological (Figure 1, C and D), optical (Figure 1, E and F) or electronic (Figure 1, G and H) properties.<sup>[3]</sup>



**Figure 1.** Representation of four different monomeric building blocks and the corresponding supramolecular assemblies with mechanical (A and B), biological (C and D), optical (E and F) or electronic (G and H) functionalities.<sup>[3]</sup>

SPs growth can follow three different mechanistic pathways: isodesmic, ring-chain, and cooperative growth (Figure 2).<sup>[4-6]</sup> In the isodesmic model, the addition of each monomer to the growing chain of the polymer is ascribed to a single equilibrium constant. This association constant greatly determines the degree of polymerization of the gradually aggregated species.



**Figure 2.** Three main mechanisms for the supramolecular polymer growth: (1) isodesmic, (2) ring-chain, (3) cooperative. <sup>[4]</sup>

The cooperative mechanism is described by two different stages with distinct equilibrium constants. As a result nonlinearly grown supramolecular polymers often occur as nucleated and elongated species. The formation of small polymer nuclei is followed by fast polymer chain growth, which is favourable thermodynamically.

The ring-chain mechanism is characterized by the equilibrium of linear polymers with their cyclic counterparts. Below the critical polymerization concentration (CPC) there are only cyclic species produced, whereas above the CPC, the excess of monomeric species form linear polymers.

Two different types of supramolecular polymers are typically obtained.<sup>[3]</sup> The first type is formed with no internal order (random-coil supramolecular polymer) by the isodesmic

polymerization mechanism. The second type, ordered supramolecular polymers are formed by the cooperative mechanism. So formed ordered supramolecular polymers, in contrast to the disordered one, lack the structural analogy to covalent polymers.

### 2.1.1 DNA-Functionalized Supramolecular Polymers

DNA-Functionalized supramolecular polymers received recently lots of attention.<sup>[7]</sup> DNA hybridization provides control over the structural properties leading to the incorporation of a variety of functionalities into the supramolecular polymer.

In our group, DNA-functionalized systems based on DNA-grafted supramolecular polymers have been demonstrated.<sup>[8]</sup> The pyrene-modified oligonucleotide monomer composed of seven pyrene units modified with additional 10 nucleobases, self-assemble into nanoribbons (Figure 3). Addition of DNA-complementary strand (connector strand) results in a formation of supramolecular network. Formation of networks proceeds via cooperative blunt end stacking interaction.

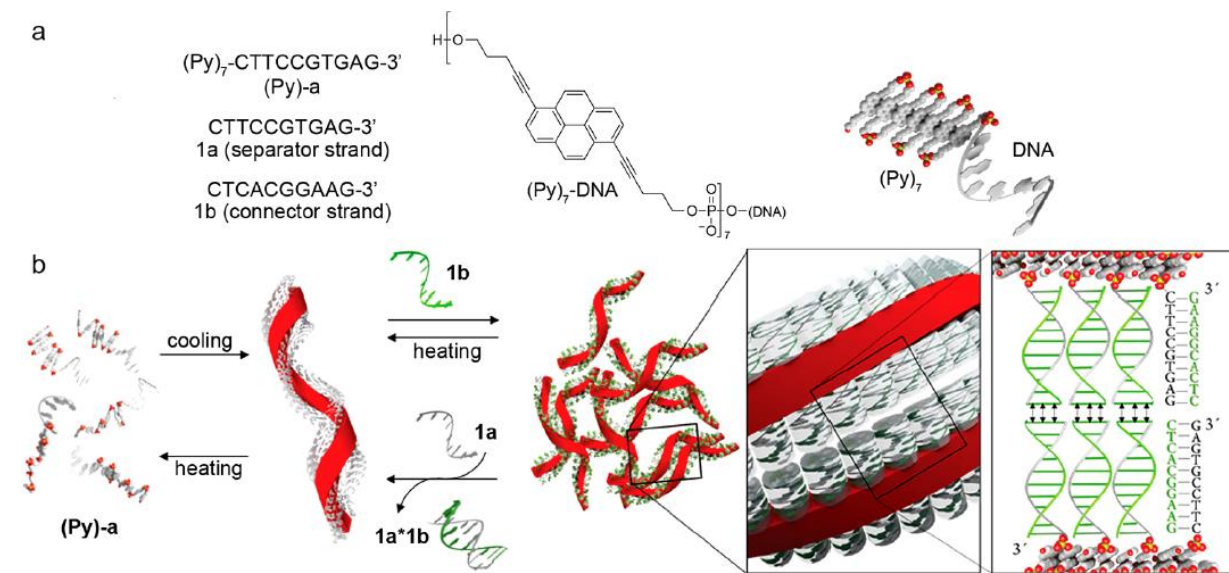


**Figure 3.** Assembly and disassembly of the nanoribbons composed of chimeric oligomers. Hybridization of the complementary oligonucleotide on the pyrene-modified oligonucleotide leads to the formation of networks via cooperative blunt end.<sup>[8]</sup>

Recently, a Brunsfeld group has reported assembly of benzene-1,3,5-tricarboxamide (BTA) into supramolecular polymers. The polymers were used as a platform for recruitment of DNA-conjugated proteins through a selective hybridization (Figure 4).<sup>[9]</sup> The BTA-3OH and BTA modified with 10 nucleobases were mixed together, which resulted in the formation of micrometer-long supramolecular BTA platform. Such robust polymeric platforms can be functionalized with varied DNA content. Mixing  $\beta$ -lactamase and BLIP modified with DNA-sequence containing 21 nucleobases in the presence of an additional inhibitor recruiter hybridized with the oligonucleotides on BTA-DNA and protein-DNA, results in recruitment of protein on the supramolecular polymer.

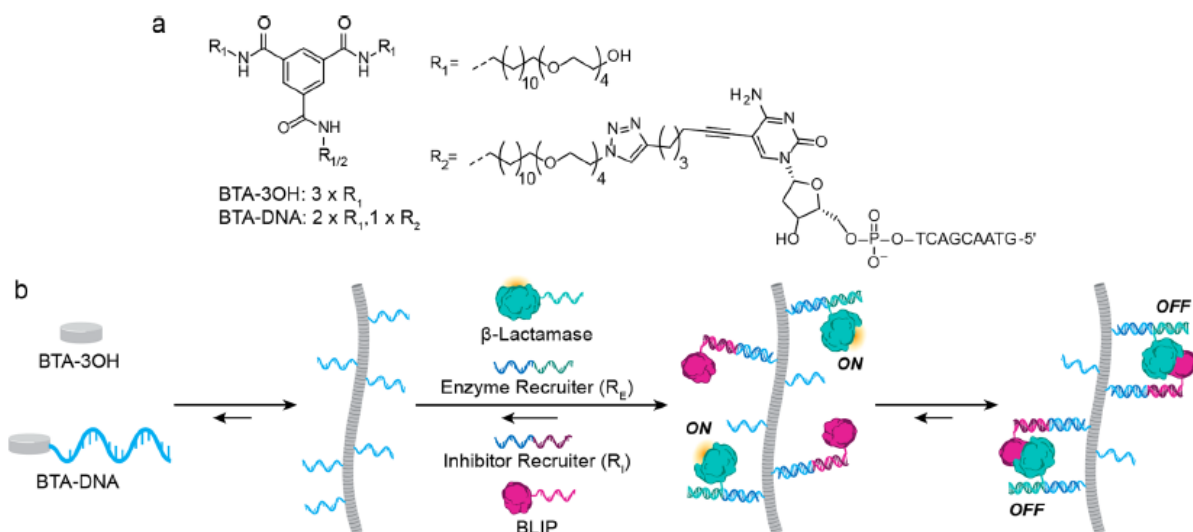


**Figure 4.** Supramolecular BTA platform used for the recruitment of  $\beta$ -lactamase and BLIP. A: Chemical structures of a BTA monomeric building blocks BTA-3OH and BTA-DNA modified with 10 nucleobases. B: Co-assembly of inert BTA and BTA-DNA monomers into DNA-functionalized supramolecular polymers. Selective hybridization of a DNA-modified proteins with the complementary DNA of functionalized polymers is allowed in the presence of a recruiter strand.<sup>[9]</sup>

## 2.2 Structural Aspects of DNA

In 1953 Watson and Crick presented the 3D structure of the DNA double helix. DNA exhibits dynamic secondary structures which can be easily rearranged.<sup>[10]</sup> Such secondary structures result from strong Watson-Crick pairing interactions.<sup>[11]</sup> The two

polynucleotide chains of the DNA double helix are in antiparallel orientation. One complete  $360^\circ$  rotation (helix pitch) in B-DNA structure requires 10.5 base pairs. The other DNA structures (A and Z conformation) are illustrated in the Figure 5.

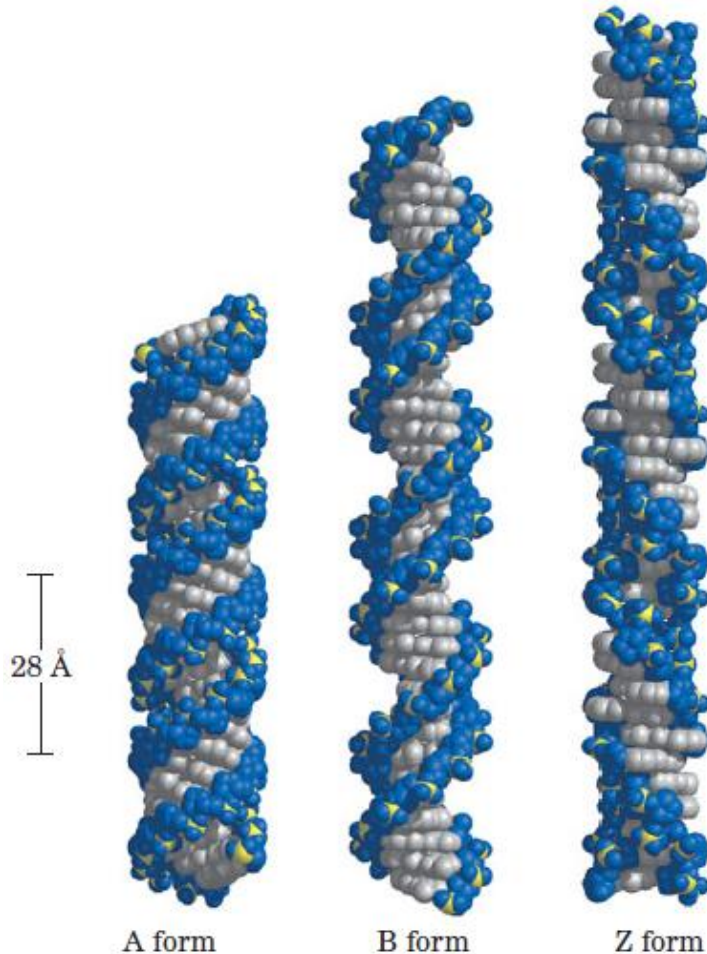


**Figure 5.** Structural variants of DNA (A, B and Z conformation).<sup>[12]</sup>

The DNA double helix is mostly stabilized via noncovalent forces like hydrogen bonding and base stacking.<sup>[13-14]</sup> Hydrogen bonding includes mainly electrostatic interaction,<sup>[14]</sup> while hydrophobic interactions and Van der Waals forces (dipole-dipole and London dispersion interactions) explain stacking interactions between planar bases.<sup>[10]</sup>

The specific hydrogen bonding of DNA base pairs and the molecular recognition system can be used for DNA material purposes.<sup>[15]</sup> In nanotechnology DNA gained lots of attention due to the programmable nature and easiness in controllable formation of two-

and three-dimensional structures.<sup>[16]</sup> DNA is composed of four heterocyclic aromatic bases, the two purines (adenine and guanine) as well as the two pyrimidines (thymine and cytosine), sugar moiety (deoxyribose) and the negatively charged phosphodiester backbone (Figure 6).<sup>[17]</sup>

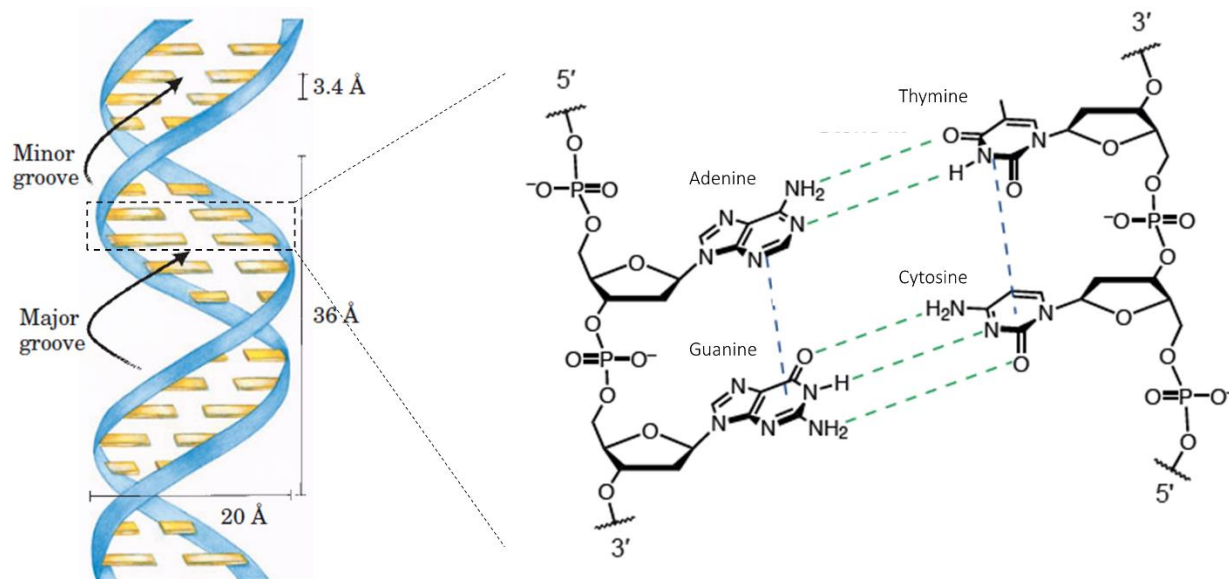


**Figure 6.** Left: schematic illustration of DNA double helix. Right: Watson – Crick base pairs: adenine (A), guanine (G), thymine (T) and cytosine (C).<sup>[12]</sup>

DNA plays a crucial role as versatile scaffold for the selective and precise organization of different auxiliaries, for example quantum dots,<sup>[18-19]</sup> proteins<sup>[20]</sup> or nanoparticles.<sup>[21-22]</sup> Almost for two decades it has become popular to replace natural bases in DNA by flat aromatic molecules, thus it was found that incorporation of polycyclic aromatic hydrocarbons (PAH) enable stabilization of the DNA duplex.<sup>[23]</sup> Over the years multichromophoric systems, e.g. pyrene,<sup>[24-25]</sup> perylene,<sup>[26-27]</sup> or phenanthrene<sup>[28-29]</sup> derivatives, placed along the DNA backbone were studied. A very popular strategy for chromophore-assembly is through a non-nucleosidic approach.<sup>[30-31]</sup> This approach requires artificial and flexible acyclic linkers between the phosphodiester bridges which allows efficient chromophore intercalation into the DNA. Some examples of acyclic linkers involve threoninol<sup>[32]</sup>, carboxamide,<sup>[24]</sup> tetraethylene glycol<sup>[27]</sup> or (S)-aminopropan-2,3-diol<sup>[26]</sup> (Figure 7).

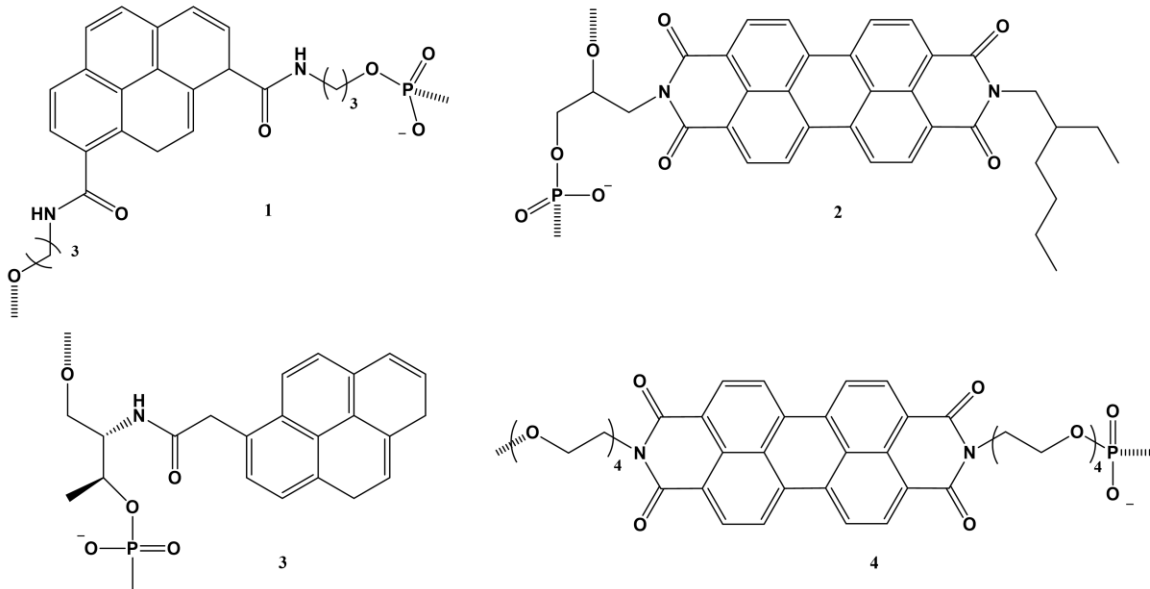


**Figure 7.** Different ways to link non-nucleosidic chromophores, such as pyrene or perylenebisimide, with DNA backbone via acyclic linker, 1: carboxamide-linker,<sup>[24]</sup> 2: (S)-aminopropan-2,3-diol linker,<sup>[26]</sup> 3: threoninol linker,<sup>[32]</sup> 4: tetraethylene glycol-linker.<sup>[27]</sup>

## 2.2.1 Solid phase synthesis

The phosphoramidite approach, pioneered by Marvin Caruthers in the early 1980s,<sup>[33]</sup> significantly enhanced solid phase technology and automation of DNA synthesis.

The growing DNA on the solid support proceeds in the 3' to 5' direction, which is opposite of biosynthesis (Figure 8). Similarly as in Merrifield peptide synthesis, the used solid supports can strongly influence the efficiency of the synthesis. So far many different resins were used, however the most suitable and the most common ones occurred to be controlled pore glass (CPG) and polystyrene solid support.

Rigid and non-swelling CPG has deep pores where the reaction takes place. The pores of 500 Å (50 nm) are suitable for short oligonucleotide synthesis, up to 40 bases in length. This kind of commercially available CPG has usually attached long chain alkylamines and can be loaded with the first 3'-nucleoside or with a modified building block. The long alkylamine linker provides good reagent accessibility.

Alternatively, the polystyrene support has good moisture properties and is suitable for small scale synthesis (e.g. 40 nmol).

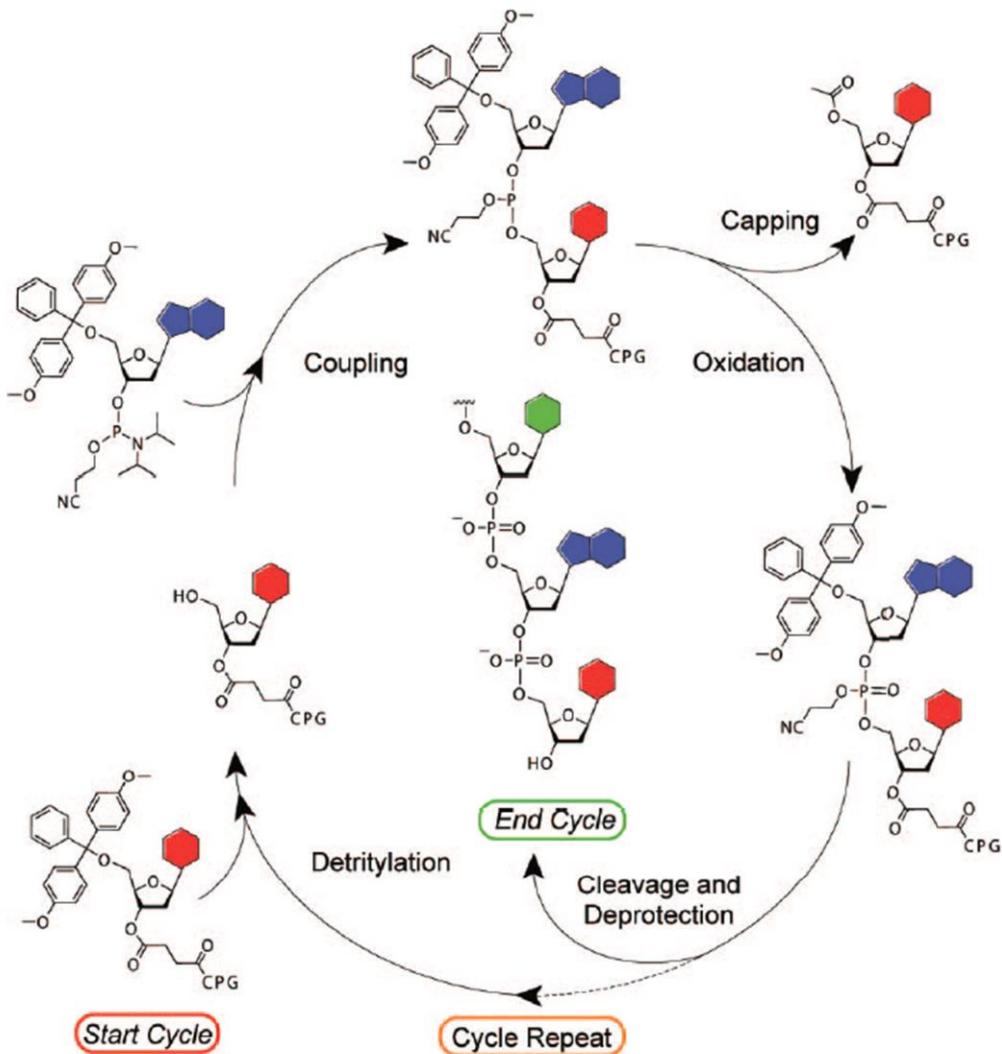


**Figure 8.** Typical cycle for the solid phase synthesis of oligonucleotides.<sup>[34]</sup>

The oligonucleotide synthesis cycle starts with a detriylation reaction, followed by activation and coupling, oxidation, capping and final cleavage from the support (Figure 8).

The support-bound nucleoside contains an acid-labile 4,4'-dimethoxytrityl (DMT) protecting group in 5'-position. To proceed the oligonucleotide synthesis, the DMT group has to be removed. The column is washed with a solution of 3% trichloroacetic acid in

DCM. The reaction is followed spectrophotometrically as the reaction results in colored DMT group.

The next step is activation and coupling reaction. After deprotection step the next base – nucleoside phosphoramidite with protected 5'-OH group is added and mixed with an activator. First protonation of diisopropylamino group of protected phosphoramidite monomer in ACN takes place. Dinucleoside with a new phosphite triester linkage is formed.

The oxidation with iodine in the presence of water and pyridine results in conversion of the unstable triester to a phosphate.

To ensure that there are no side products the remaining unreacted 5'-OH is capped with an acetyl group. Acetylated 5'-OH is a result of a mixture of acetic anhydride, N-methylimidazole in THF and pyridine with unreacted species. The reaction cycles are repeated until the sequence is completed.

In the last step a solution of concentrated ammonium hydroxide ( $\text{NH}_4\text{OH}$ ), overnight at 55 °C is used to provide the free 3'-OH group, deprotected bases and phosphodiester backbone. Finally, the oligonucleotide is purified by reverse-phase HPLC.

## 2.3 Light-Harvesting and Energy Transfer

In photosynthetic organisms, like higher plants, algae and photosynthetic bacteria a big number of light-harvesting pigment molecules absorb the photons and transform them into excitons which afterwards migrate toward the reaction centers (Figure 9) [35-36]. These light-harvesting complexes (LHCs) contain chlorophyll molecules in a well-defined order which allows efficient energy transfer.<sup>[37]</sup>

The photosynthetic mechanism can be explained by the Förster resonance energy transfer (FRET), Dexter electron exchange mechanism, as well as coherent resonance energy transfer.<sup>[38]</sup>

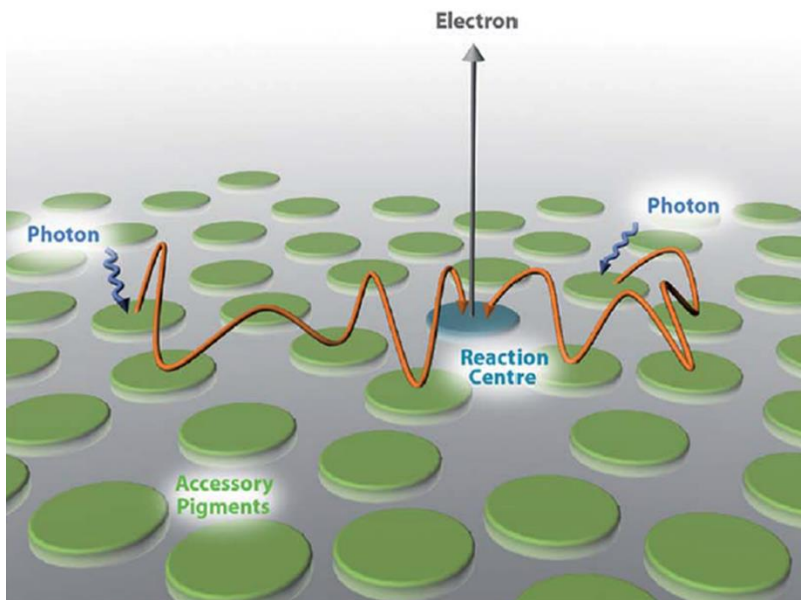


**Figure 9.** Demonstration of the light-harvesting antenna effect. Photons are captured by light-harvesting pigments and transferred to the reaction centre (the acceptor). In the reaction centre the charge separation occurs and the storage of chemical energy takes place.<sup>[37]</sup> Taken from <sup>[39]</sup>.

Energy transfer efficiency between weakly coupled donor (D) and acceptor (A) molecules depends on the distance as well as the relative orientation. In FRET the acceptor distance is between 10 – 100 Å and the energy transfer occurs through electric dipole couplings.<sup>[40]</sup> Unfortunately, conventional Förster's theory does not explain the energy transfer in certain cases.<sup>[37]</sup> In case of small donor – acceptor separations an alternative Dexter theory is considered.

Also, these mechanisms vary depending on the coupling interactions between donor and acceptor. The Dexter electron exchange mechanism considers the overlap of atomic orbitals. In the FRET mechanism, molecular couplings change from strong to very weak. In some case FRET theory is not sufficient and the exciton theory with coherent resonance energy transfer mechanism is taking into account.<sup>[38]</sup>

Recently, the Liu group presented a sequential energy transfer from chiral supramolecular light harvesting nanotubes to acridine orange (AO) (Figure 10). Sequential energy transfer was found to be cooperative with chirality transfer, which provides a better understanding of the natural light-harvesting antenna.<sup>[41]</sup>

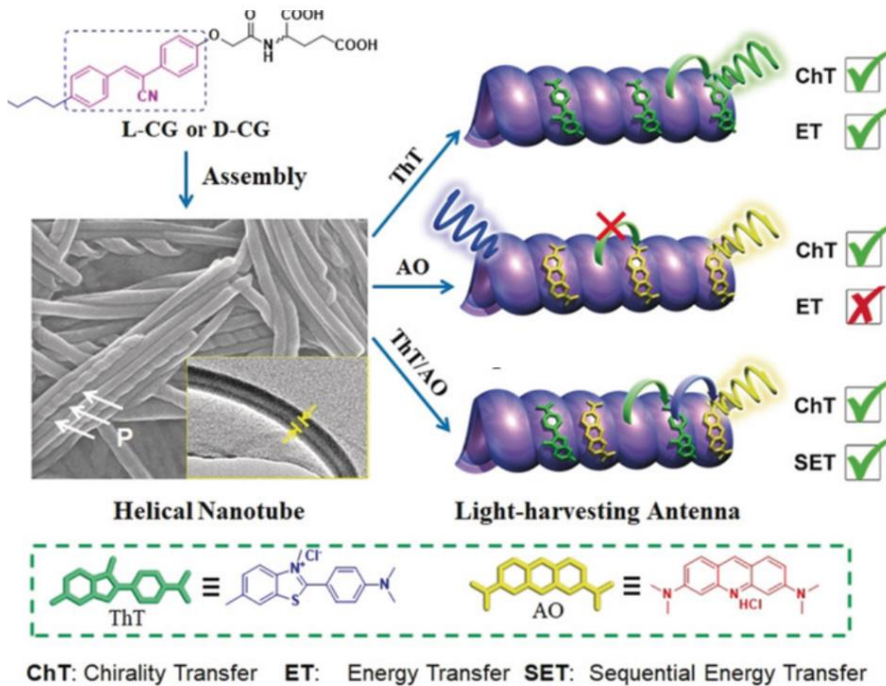


**Figure 10.** Co-assemble of the supramolecular light harvesting nanotube composed of cyanostilbene-appended glutamate compound (CG) with acceptors (ThT, AO) results in three different chirality and energy transfer patterns. Taken from [41].

The mechanism shows that after excitation of donor CG with unpolarized light, a circularly polarized luminescence (CPL) is observed. Co-assemble of two achiral acceptors with the nanotube results in transfer of CPL energy to the acceptor with the emission of the new CPL ascribed to the acceptor (Figure 11).

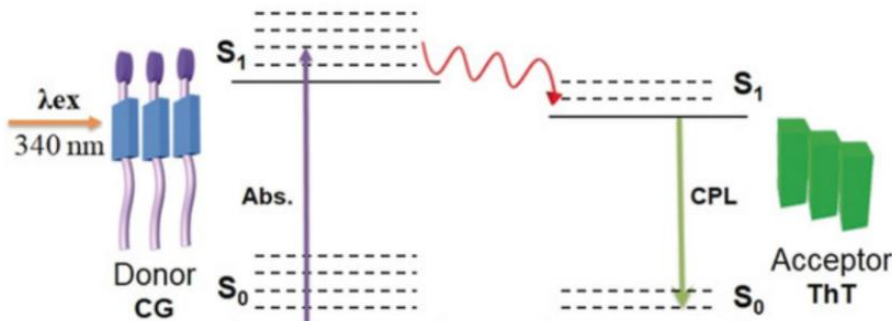


**Figure 11.** Illustration of the energy level diagram for ET-associated CPL mechanism.[41]

## 2.4 FRET in DNA-Photonic Wires

Designing DNA-based molecular photonic wires with FRET properties between multiple dyes has attracted extensive attention.<sup>[42-50]</sup> Increased cascade ET efficiencies in such photonic wires can lead to improvement of artificial light-harvesting arrays. Two kinds of FRET energy transfer mechanisms can be distinguished in DNA-photonic wires (Figure 10). There is the conventional hetero-FRET as well as the promising homo-FRET approach. FRET efficiency can be significantly enhanced by increasing the maximal length of the photonic wires via a homo-FRET mechanism. <sup>[47, 51-52]</sup> This energy transfer has a small Stokes shift and is based on diffusive energy migration between identical chromophores. Instead, hetero-FRET is characterized with energy losses.

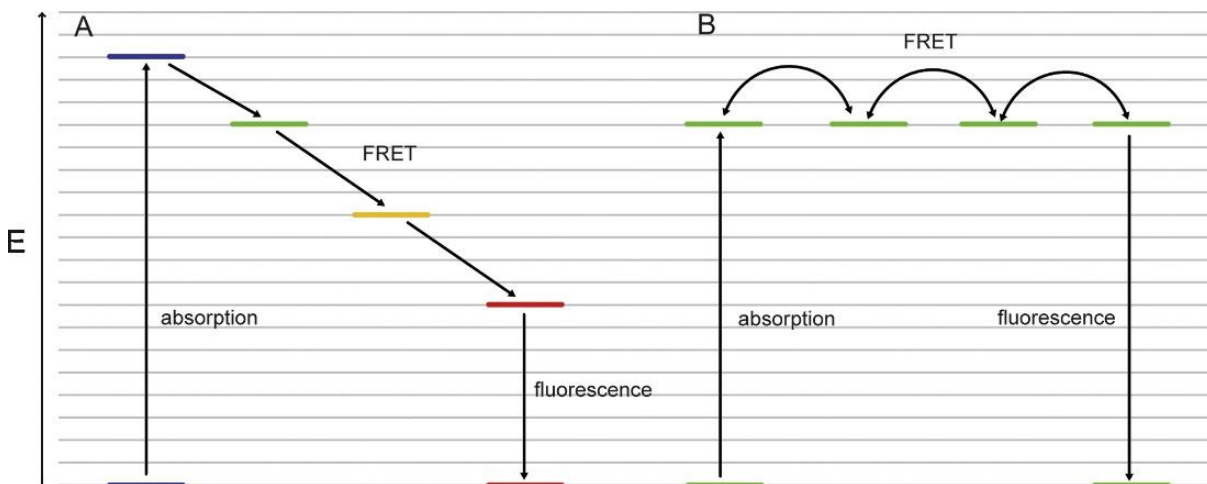


**Figure 10.** Schematic energy level diagram showing examples of multi-step hetero-FRET (A) and homo-FRET (B). Arrows indicate one of many potential energy pathways from the initial absorption at a donor fluorophore to the emission from the final acceptor.<sup>[42]</sup>

Recently Medintz and co-workers presented complex DNA-based FRET networks with dendrimeric structures that were found to exhibit homo-FRET over multiple chromophores with high efficiency. Four or five dye FRET cascades (AF488→Cy3→Cy3.5→Cy5→Cy5.5) consisting of up to six Cy3 repeats are embedded into four-arm, eight-arm or dendrimeric DNA photonic wires (Figure 11, A). A significant six-fold gain in antenna effect was observed in the dendrimer structure containing six Cy3 homo FRET fluorophores.<sup>[53]</sup>

In the same group, a linear DNA photonic wire with up to 7 different dyes was designed (Figure 11, B).<sup>[54]</sup> Chromophores were incorporated along the DNA for long-range energy transfer studies.

Lots of interest gained DNA photonic wires in combination with quantum dots (QDs).<sup>[43]</sup> In such hybrids, the QDs are used as energy harvesting donors that drive cascade energy transfer over 4-consecutive steps (Figure 11, C). Multiple ET over long distances (~180 Å) was found.

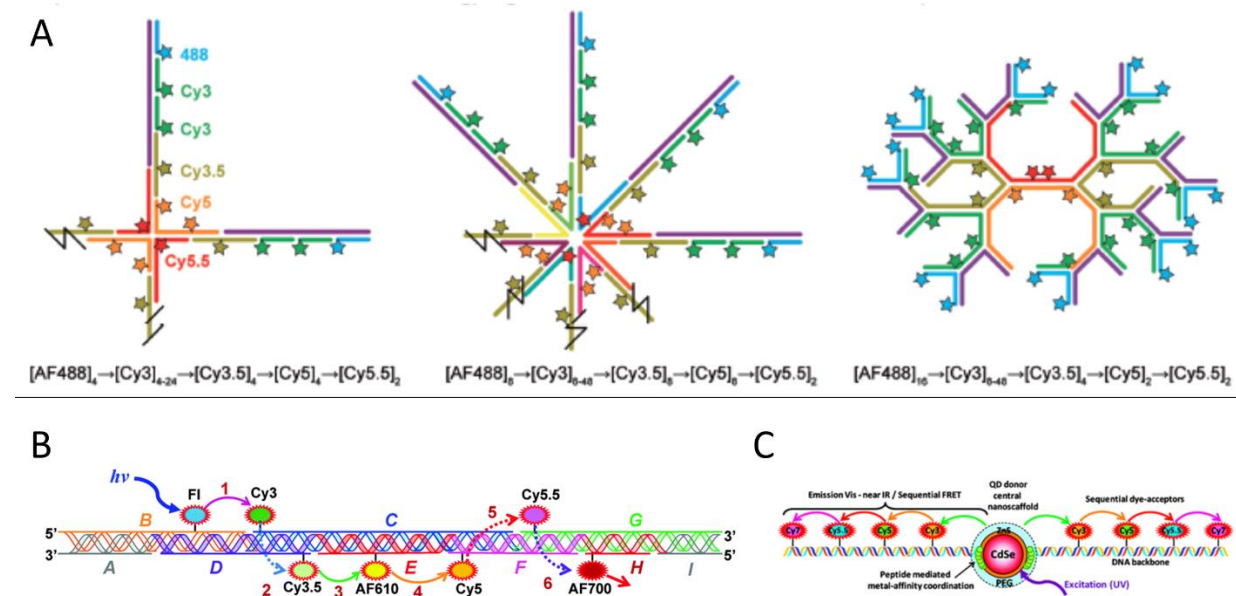


**Figure 11.** Examples of photonic wires designed in Medintz group. A: Four arm, eight-arm, and 2:1 dendrimeric DNA photonic wires with extended homo FRET. B: Linear DNA photonic wires with 7 fluorophores arranged along the DNA scaffold. C: DNA photonic wires that self-assemble around the quantum-dot.

The Liu group designed light-harvesting triads based on DNA nanotechnology.<sup>[45]</sup> Such antenna systems are self-assembled from seven DNA bundles and contain three different types of chromophores (Figure 12, A). This light-harvesting system was used for the estimation of the FRET efficiency and antenna effect. The efficiency of energy transfer and antenna effect was found to be highly dependent on the donor-acceptor ratio.

An interesting example of a self-assembled DNA-based photonic wire showed Albinsson.<sup>[42]</sup> Such photonic wires can transfer excitation energy over a long range of

more than 20 nm (Figure 12, B). The intercalating YO chromophore with its homo transfer properties was used for diffusive energy migration between pacific blue donor and Cy3 acceptor with 85% efficiency.

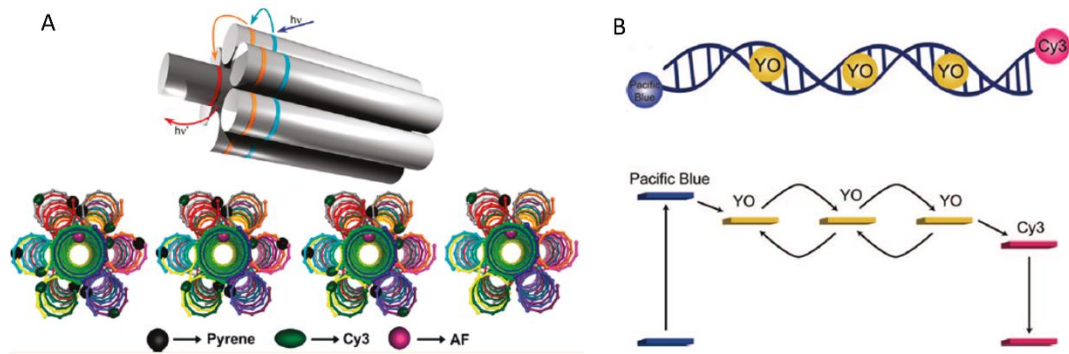


**Figure 12.** A. Liu`s triads for precisely organized donor-acceptor arrays.<sup>[45]</sup> B. Self-assembled DNA based photonic wire and the energy level diagram with a diffusive energy transfer mechanism proposed by Albinsson.<sup>[42]</sup>

## 2.5 Aim of the Thesis

Previous work in the Häner group is based on the precise arrangement of chromophore-arrays in DNA scaffolds. The phosphodiester linked chromophores were used for the assembly of  $\pi$ -stacked artificial oligomeric building blocks in chromophore-DNA conjugates that mimic the naturally occurring process of light harvesting. Additionally, the same non-nucleosidic building blocks were used to synthesize short oligomers that self-assemble into nanostructures such as fibers, tubes, sheets or ribbons.

In this thesis, chromophore-oligomers and chromophore-DNA conjugates build the basis for the self-assembly of versatile SPs. The first aim of this thesis is to functionalize such DNA-appended SPs with DNA-photonic wires or AuNPs.

In more detail, the SPs act as light-harvesting antenna, while the integrated DNA-scaffolds provide a straightforward approach to precisely arrange donor-acceptor pairs with well-defined distances. The so formed LHCs are designed for efficient and directional propagation of light-harvesting cascades.

On the other hand, merging of DNA-scaffolds into SPs allowed them to work as functional platforms. Therefore, the potential of self-assembled cargo systems via hybridization of AuNPs will be discussed as well.

The second aim of this thesis is to design a new class of SPs with interesting luminescent properties. AIE-active SPs exhibit high fluorescence efficiency. Therefore, controlled self-assembly of AIE-active SPs based on the phosphodiester-linked dialkynyl-tetraphenylethylene (DATPE) trimers is demonstrated

### **3 Integration of Functional DNA-Nanoscaffolds into Supramolecular Polymers**

#### **Introduction**

Supramolecular polymers, in which repeating building blocks are held together *via* directional and non-covalent interactions [55-58] represent an appealing alternative to DNA nano-scaffolds for achieving 2D or 3D fluorophore arrangements. [59-71] Encouraged by our finding that energy can be funneled over long distances ( $\geq 100$  nm) in supramolecular phenanthrene polymers, [61, 70] we explored the approach of integrating DNA photonic wires into SPs. Additionally the AuNPs aligned along the SPs are presented.

Previously reported self-assembled oligomeric building blocks developed in our group are illustrated in Figure 13.

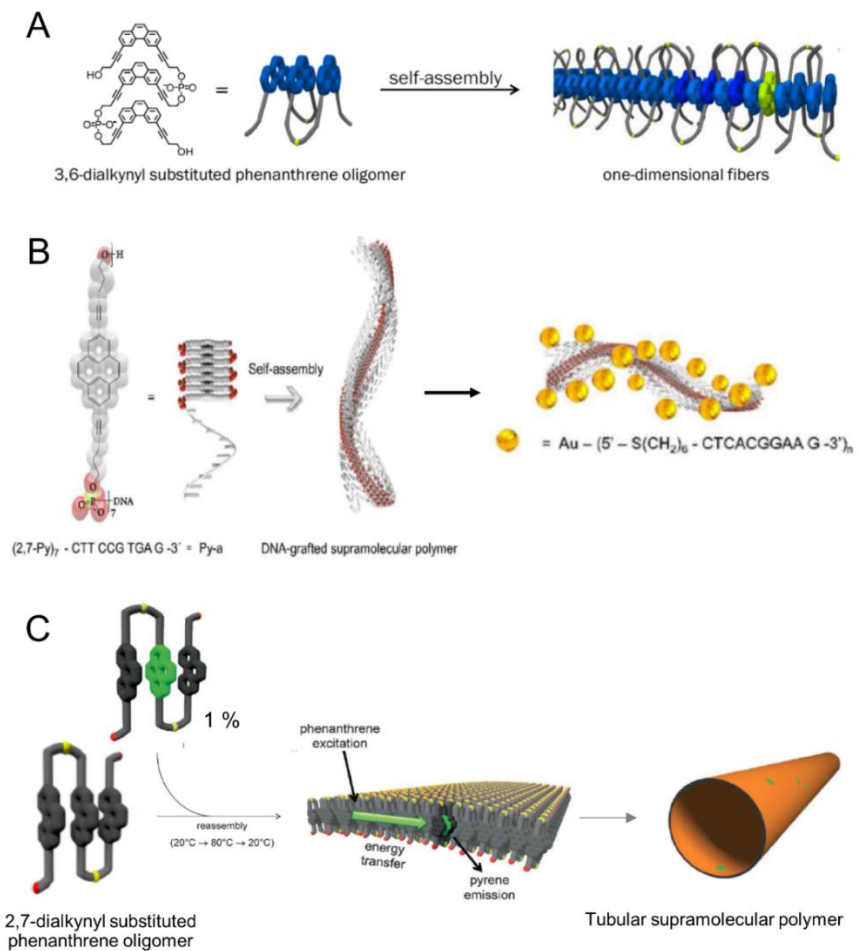


**Figure 13.** Previously investigated oligomers which self-assemble in aqueous medium. A) 3,6-Dialkynyl phenanthrene;<sup>[70]</sup> B) 2,7-Dialkynyl pyrene DNA conjugate and DNA-grafted supramolecular polymers functionalized with AuNPs;<sup>[22]</sup> C) 2,7-dialkynyl phenanthrene;<sup>[61]</sup> the nanotubes and the fibers act as light-harvesting antenna with an incorporated acceptor (pyrene is highlighted in green).

First example illustrates 3,6-dialkynyl phenanthrene doped with tiny amount of pyrene molecules which forms linear SPs in aqueous medium. The supramolecular phenanthrene polymers act as light-harvesting antenna. The absorbed energy is transferred to the pyrene acceptor over long distances (>100 nm). Efficient energy transfer, reported with high quantum yields, indicates quantum coherent energy transfer mechanism. The next case addresses the formation of one-dimensional nanoribbons self-assembled from a DNA-grafted pyrene oligophosphates. Subsequent loading with AuNPs results in arranged particles along the edges of the helical nanoribbons.

The last example demonstrates 2,7-dialkynyl phenanthrenes self-assembled into light-harvesting nanotubes in aqueous media. Nanotubes doped with tiny amount of pyrene exhibit strong fluorescence emission and high fluorescence quantum yields. The nanotubes are several micrometer-long with the diameter of 50-150 nm.

### **3.1 Integrating DNA - Photonic Wires into Light-Harvesting Supramolecular Polymers**

Parts of these results are published in:

*Integrating DNA-Photonic Wires into Light-Harvesting Supramolecular Polymers*

M. Kownacki, S. M. Langenegger, S.-X. Liu, R. Häner, *Angew. Chem. Int. Ed.*, **2019**, 58, 751-755.

#### **3.1.1 Abstract**

The combination of DNA nanoscaffolds with supramolecular polymers for the efficient and directional propagation of light-harvesting cascades has been developed. A series of photonic wires with different arrangements of fluorophores in DNA-organized nanostructures were linked to light-harvesting SPs in a self-assembled fashion. Among them, a LHC composed of SPs and a photonic wire of phenanthrene, Cy3, Cy5 and Cy5.5 chromophores reveals a remarkable energy transfer efficiency of 59%. Stepwise transfer of the excitation energy collected by the light-harvesting SPs via the intermediate Cy3 and Cy5 chromophores to the final Cy5.5 acceptor proceeds by a Förster resonance energy transfer mechanism. In addition, the light-harvesting properties are documented by antenna effects ranging from 1.4 up to 23 for different LHCs.

### 3.1.2 Introduction

The construction of molecular photonic wires for implementations of DNA-based light harvesting systems *via* Förster resonance energy transfer (FRET) between multiple dyes has attracted considerable attention.<sup>[42-50]</sup> The use of DNA as a template provides a straightforward approach to precisely arrange fluorophores with well-defined distances and relative orientations.<sup>[45, 72-81]</sup> and leads to addressable nano-architectures with diverse types of geometries.<sup>[15, 51, 82-93]</sup> Different strategies have been developed to facilitate the processes of light-harvesting and energy transfer. Particularly, FRET efficiency can be significantly improved by increasing the maximal length of the photonic wires *via* a homo-FRET mechanism.<sup>[47, 51-52]</sup> Alternatively, DNA photonic wires have been appended to quantum dots.<sup>[43, 94]</sup> On the other hand, the merging of DNA photonic wires with light-harvesting SPs for an efficient and directional propagation of energy has not yet been explored. The attainment of a LHC was envisaged through the formation of a supramolecular assembly consisting of a phenanthrene trimer (oligomer **A**) and a DNA organized chromophore complex through non-covalent stacking interactions among phenanthrene molecules.

In this studies we described the merging of DNA photonic wires with light-harvesting SPs as efficient artificial LHCs. Energy transfer from the light-absorbing phenanthrene antenna to the acceptor chromophores arranged along the DNA is presented.

### 3.1.3 Results

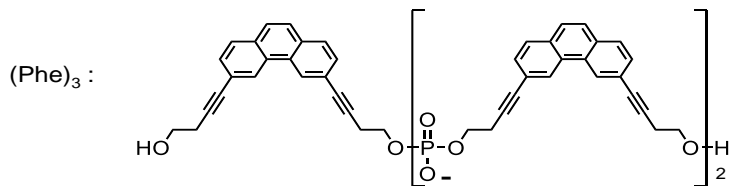
#### 3.1.3.1 Oligomers Synthesis and LHCs Composition

The required 3,6-dibutynylphenanthrene phosphoramidite for the synthesis of oligomers **A**, **B** and **K** was prepared according to the published procedure.<sup>[70]</sup> All three oligomers were assembled by automated oligonucleotide synthesis and purified by reverse phase HPLC and analysed by mass spectrometry (3.1.5.2 Supporting Information). The phenanthrene-containing oligomers and dye-labelled oligonucleotides used in this study as well as composition of light-harvesting complexes are summarized in Table 1.

**Table 1.** Top: Oligomers used in this study; middle: composition of different LHCs; bottom: chemical structure of phosphodiester-linked phenanthrenes.

Oligomer	Sequence
<b>A</b>	(Phe) <sub>3</sub>
<b>B</b>	(Phe) <sub>5</sub> - GAA GGA ACG TAG CCT GGA AC - 5'
<b>C</b>	5' - Cy3 - CTT CCT TGC A - Cy5
<b>D</b>	5' - TCG GAC CTT G - Cy5,5
<b>E</b>	5' - CTT CCT TGC A
<b>F</b>	5' - TCG GAC CTT G
<b>G</b>	Cy3 - CTT CCT TGC A - 3'
<b>H</b>	Cy3 - CTT CCT TGC ATC GGA CCT TG - 3'
<b>I</b>	3' - GAA GGA ACG TAG CCT GGA AC
<b>J</b>	5' - CTT CCT TGC A - Cy5
<b>K</b>	(Phe) <sub>3</sub> - GAA GGA ACG TAG CCT GGA AC - 5'

**LHC1: (A,B,H)    LHC2: (A,B,C,F)    LHC3: (A,B,C,D)    LHC4: (A,B,E,F)**



### 3.1.3.2 Formation of LHCs

Supramolecular assembly of a light-harvesting complex (LHC3) is demonstrated in Figure 14. Self-assembly experiments were typically carried out by mixing oligomer **A** (0.5 μM) and an equimolar ratio of oligomer **B** and the cyanine-labeled oligonucleotides (15 nM) in sodium phosphate buffer (10 mM, pH 7.2) in the presence of NaCl (120 mM). Upon heating to 80 °C and cooling to room temperature over a period of 5 min, the oligomeric building blocks self-organize into DNA functionalized SPs.

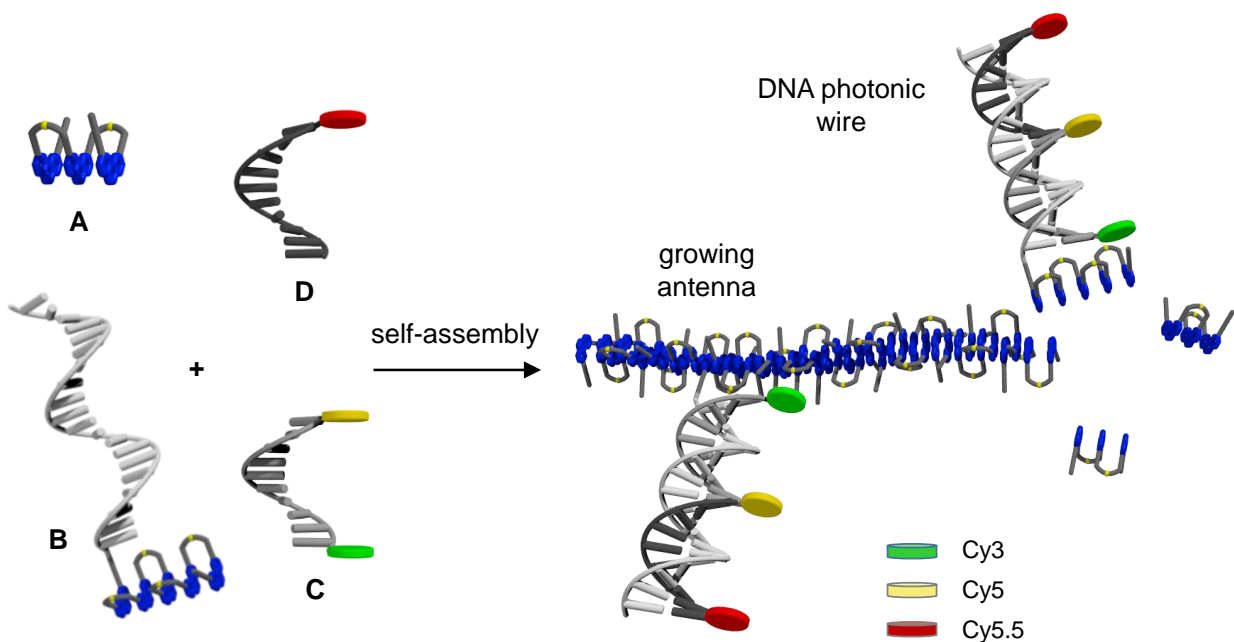
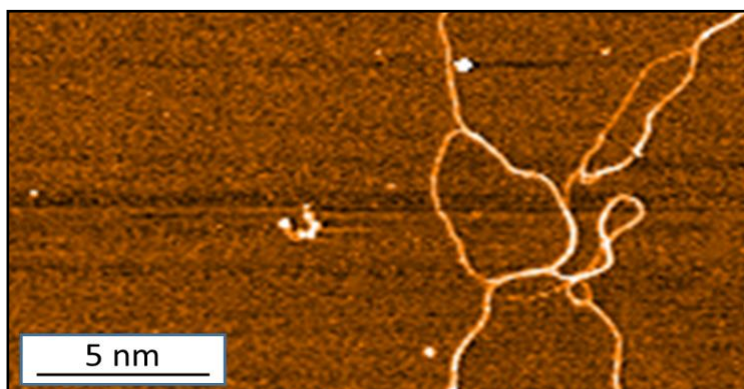


**Figure 14.** Illustration of the supramolecular assembly of a light-harvesting complex (LHC3). Chromophore-modified DNA hybrids containing terminal phenanthrenes (shown in blue) are incorporated into the growing phenanthrene antenna during supramolecular polymerization.

### 3.1.3.3 AFM and TEM Measurements

Self-assembled polymers reach a length of several micrometers, as demonstrated by transmission electron microscopy (TEM) and atomic force microscopy (AFM) (Figure 15). Assembly of the supramolecular nanofibers takes place in the temperature range between 60 and 50 °C (3.1.5.6 Supporting Information).

a)



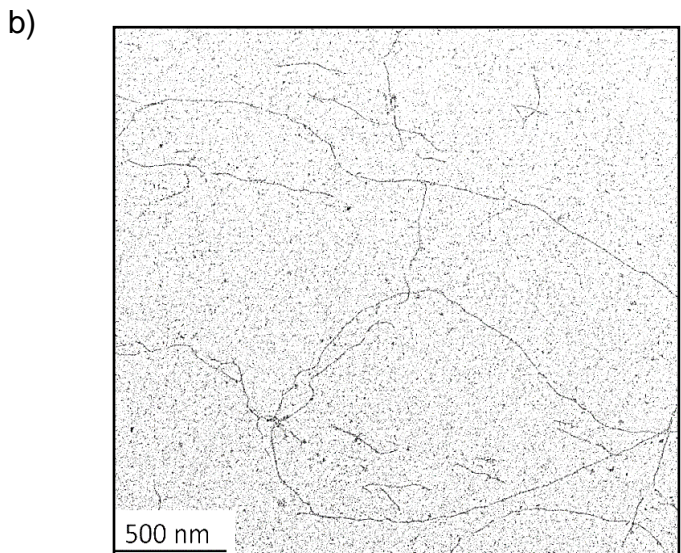


**Figure 15.** a) AFM analysis and b) TEM images of DNA-modified SPs. Sample for transmission electron microscopy (TEM) analysis was prepared according to the published procedure.<sup>[8]</sup> AFM of SPs modified with DNA strands were analysed on APTES-modified mica at 20 °C. Conditions: oligomer **A**, **B**, **E**, **F** (a); oligomer **A**, **B** (b).

### 3.1.3.4 Photophysical and FRET Properties of the Fluorophores

The fluorophores in the photonic wires consist of phenanthrene as the primary donor, Cy3 and Cy5 as intermediate donors and Cy5.5 as the acceptor. Their normalized absorption and emission spectra (Figure 16) display well-separated absorption and emission bands, and also significant overlap between the emission and absorption of the neighbouring fluorophores with minimal spectral overlap between phenanthrene and Cy5.5. The details for selected photophysical and FRET properties of each dye including extinction coefficients, absorption/emission maxima, quantum yields (QY), overlap integral  $J$  values and Förster distances  $R_0$  are listed in Tables 2-3. These spectral features play a crucial role in the FRET process and the four fluorophores capture light throughout a significant part of the visible spectrum, similar to natural light harvesting antennas.

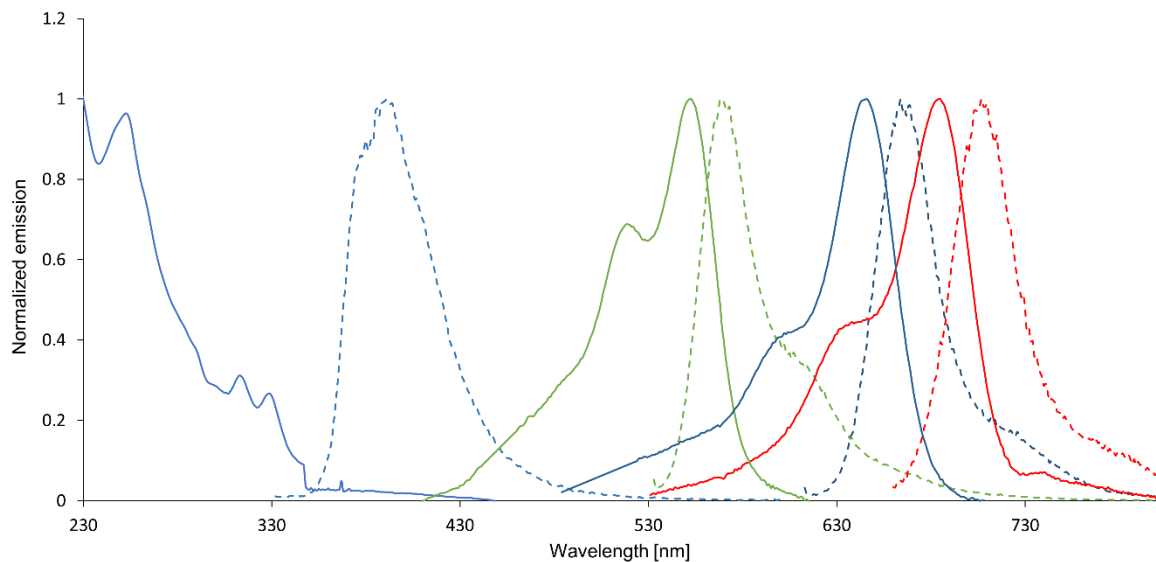


**Figure 16:** Normalized spectral overlap. Absorption (solid line) and emission (dotted line) spectra for LHCs: SPs (blue), Cy3 (green), Cy5 (blue) and Cy5,5 (red).

**Table 2.** Overlap Integral  $J$  [ $\text{nm}^4 \text{M}^{-1} \text{cm}^{-1}$ ] and  $R_0$  [nm]<sup>a)</sup>

	oligomerA [J / $R_0$ ]	Cy3 [J / $R_0$ ]	Cy5 [J / $R_0$ ]
Cy3	2.06E+14/2.2		
Cy5	3.64E+13/1.5	1.06E+16/5.9	
Cy5,5	0	4.74E+15/5.2	2.30E+16/6.7

a) Förster distances ( $R_0$ ) were calculated assuming values of 2/3 for  $x^2$  and 1.33 for  $n$ .

**Table 3** Selected photophysical and FRET properties of the fluorophores present in the light harvesting assemblies.

	QY <sup>a</sup>	$\varepsilon$ [ $\text{M}^{-1} \text{cm}^{-1}$ ]	$\lambda^{\text{abs}}_{\text{max}}$ [nm]	$\lambda^{\text{em}}_{\text{max}}$ [nm]
Oligomer A	0.038	106200	321	410
Oligomer B	0.072	177000	316	389
Cy3	0.254	111033	550	570
Cy5	0.261	203889	649	670
Cy5,5	0.206	158882	675	694

The quantum yields (QYs) were experimentally determined using the fluorescent standards Quinine Sulfate, Cresyl Violet, Rhodamine 6G, and Rhodamine 800 (LD 800) for Oligomer A and B, Cy3, Cy5 and Cy5,5, respectively.

### 3.1.3.5 Energy Transfer in Phenanthrene Based LHCs

A stepwise transfer of the excitation energy in **LHC3** is demonstrated in Figure 17. The excitation energy is transferred from the primary phenanthrene donor array to a Cy5.5 acceptor through intermediate Cy3 and/or Cy5 donors *via* a FRET.

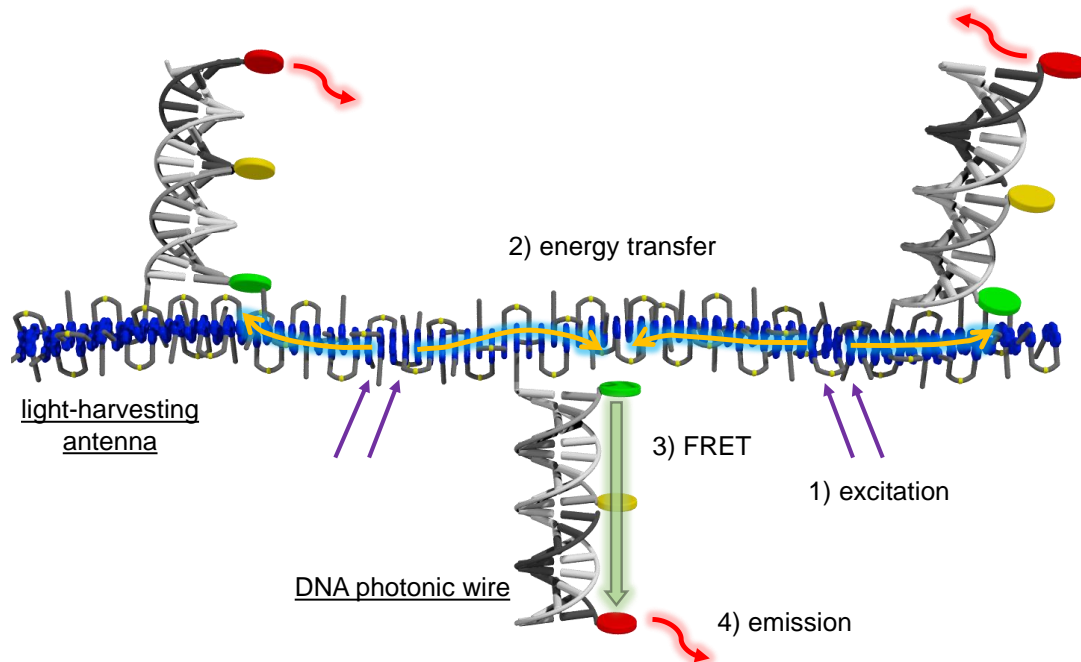


**Figure 17.** Illustration of light-harvesting complex **LHC3**: DNA photonic wires bearing suitable acceptor dyes (Cy3, Cy5 and Cy5.5 in green, yellow and red) are integrated into a supramolecular polymer ('antenna') composed of phenanthrenes (blue). Excitation energy absorbed by phenanthrene molecules is transferred along the antenna to the acceptor dye (Cy3) and further along the DNA photonic wire via FRET.

Hybridization of the phenanthrene-modified oligonucleotide **B** with various complementary single strands is expected to afford photonic wires with cascade energy transfer properties, as previously described in the DNA three-way junction (3WJ) system.<sup>[91]</sup> Initially, the light-harvesting suprapolymeric antenna was functionalized with a single Cy3-labeled DNA, such that the Cy3 acceptor was placed in close proximity to the antenna. The so formed **LHC1**, obtained from a mixture of oligomers **A** (0.5 µM), **B** (15

nM) and complementary single strand **H** (15 nM), shows significant fluorescence at 575 nm (Figure 18), which is characteristic for Cy3 emission and indicates energy transfer from phenanthrene to the Cy3 acceptor after excitation (322 nm). Control experiments, e.g. with **LHC4** bearing no cyanine acceptor in the self-assembled DNA, or a mixture of oligomers **A** or **B** with **H**, reveal weak or no emission at 575 nm, due to very limited or no energy transfer. Thus, DNA photonic wires can be successfully integrated into light-harvesting SPs in a simple self-assembly process which results in the formation of a LHC.

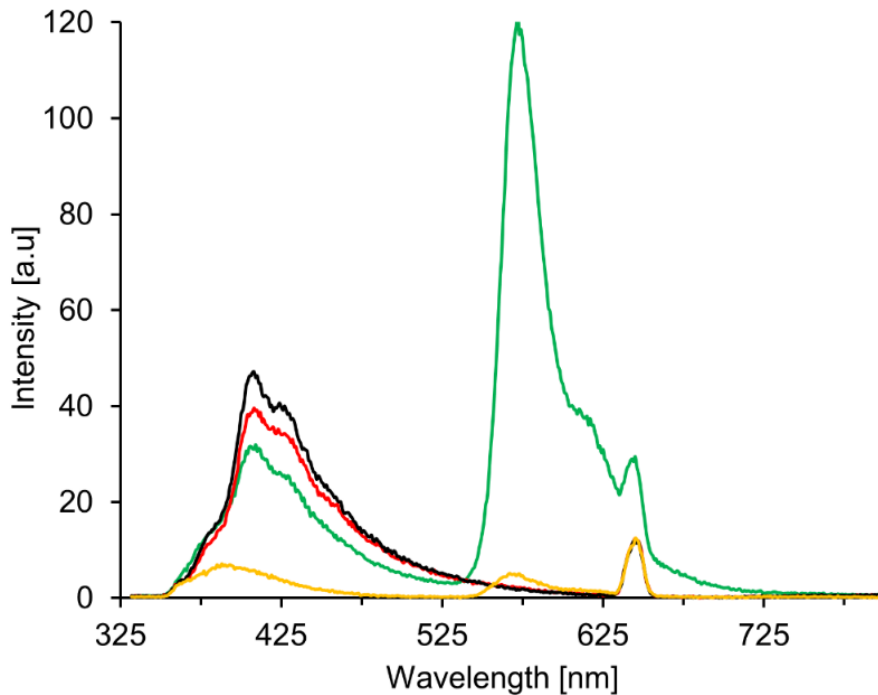


**Figure 18.** Fluorescence intensities of **LHC1** (green), **LHC4** (black) or a mixture of either oligomer **A** (red) or **B** (light brown) in combination with the Cy3-derived oligonucleotide **H**. Concentration of oligomers: **A** (0.5  $\mu$ M), **B** and **H** (15 nM); conditions: 10 mM sodium phosphate buffer, pH 7.2, 120 mM NaCl,  $\lambda_{\text{ex}} = 322$  nm.

To gain insight into the self-assembly process, the influence of increasing amounts of hybrid **B\*G** on Cy3 emission after excitation of the phenanthrene antenna was investigated (Figure 19). As expected, Cy3 fluorescence at 570 nm grows with increasing amounts of hybrid **B\*G**. Cy3 emission appears already in the presence of 0.47 nM **B\*G**, which translates into 0.1% of Cy3 relative to oligomer **A**. A continuous growth is observed upon further addition of **B\*G**. Parallel to the increase in Cy3 emission, the phenanthrene

fluorescence band centred at 415 nm gradually decreases up to a 15 nM concentration of **B<sup>\*</sup>G**. The latter concentration corresponds to approx. 3% of Cy3 acceptors relative to oligomer **A**. Beyond this concentration, an increase in both phenanthrene and Cy3 emission occurs, which is probably the result of direct energy transfer from the five phenanthrene units of oligomer **B** to Cy3 in hybrid **B<sup>\*</sup>G**, independently from the light-harvesting antenna. This assumption was verified by subtracting the corresponding concentration-dependent emission spectra of hybrid **B<sup>\*</sup>G** from the emission spectra (Figure 20). This results in a plateau (Figure 21) that serves as an indication that the SPs are saturated, i.e. additional **B<sup>\*</sup>G** is not anymore integrated into the SPs.

Hence, the efficiency of this LHC is, initially, strongly affected by the ratio of **B<sup>\*</sup>G** to oligomer **A**. Beyond a ratio of 3%, however, the harvesting efficiency levels off. It can be estimated that a maximum of 3% of duplex **B<sup>\*</sup>G** can be incorporated into the SPs. The observed maximum loading of the supramolecular light harvesting antenna with the DNA photonic wire is likely due to steric demand and electrostatic repulsion between the highly charged polyanionic components.

### 3.1.3.6 Titration Experiments

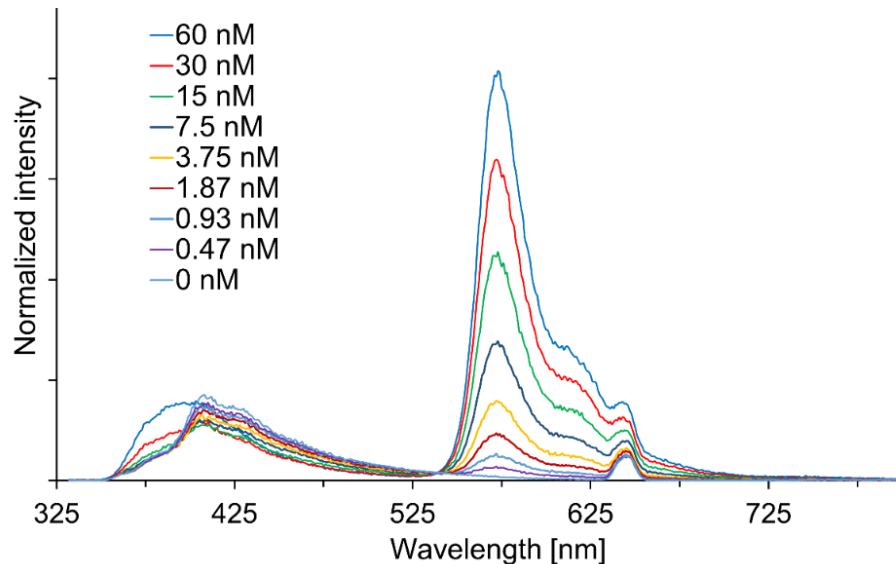


**Figure 19.** Emission spectra of oligomer **A** (0.5  $\mu$ M) in the presence of different concentrations of hybrid **B<sup>\*</sup>G** after phenanthrene excitation (322 nm). Normalization was done by dividing the emission spectra by the absorption value of each individual sample at 322 nm.

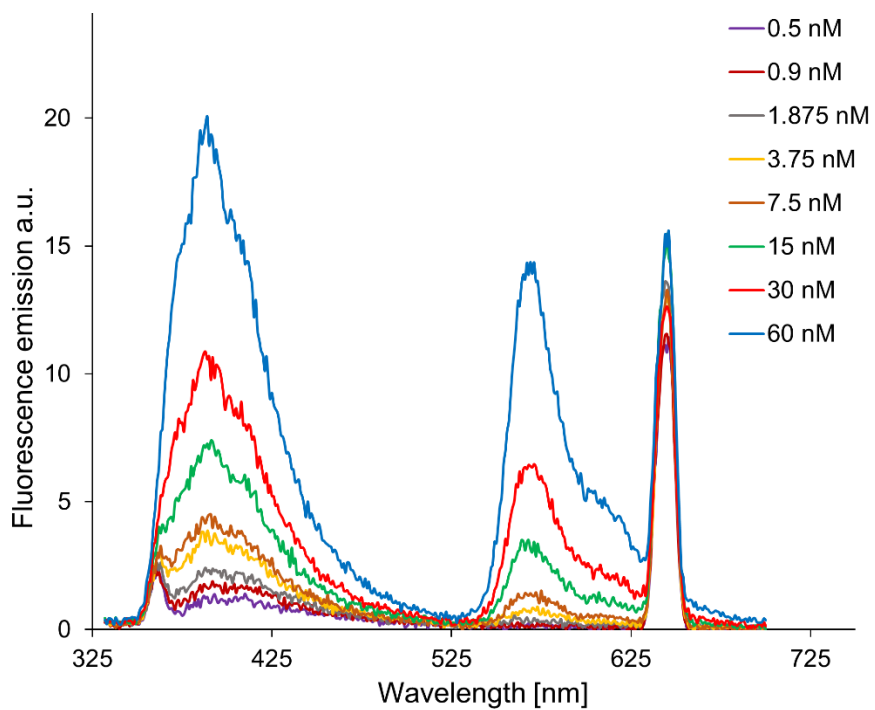


**Figure 20.** Emission spectra of different concentrations of hybrid **B\*G** after excitation at 322 nm.

### 3.1.3.7 Additional Titration Experiments

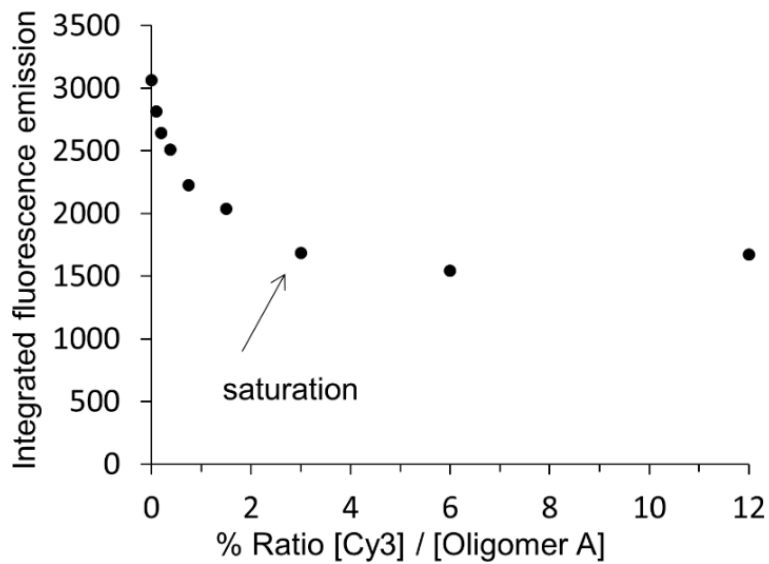


**Figure 21.** Indication that the SPs are saturated. Change of integrated fluorescence (340-525 nm) after correction for **B\*G** contribution.

Additionally, we tested the self-assembly of oligomer **K** containing only three phosphodiester-linked phenanthrene units instead of five units (as in oligomer **B**) in combination with SPs formed by oligomer **A**. As shown in the emission titration experiment (Figure 22), the resulting DNA fails to integrate into the SPs. This suggests that a minimal number of phenanthrene units attached to the DNA scaffold is required for the successful incorporation during the formation of LHCs *via*  $\pi$ - $\pi$  interactions with the phenanthrene units forming the SPs.

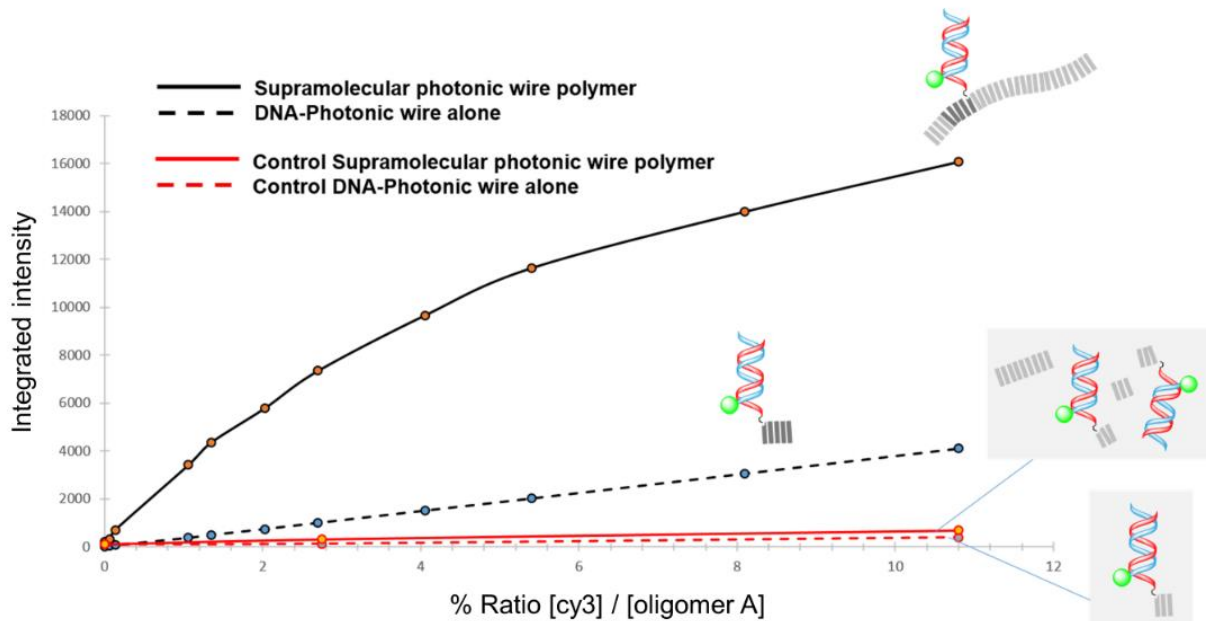


**Figure 22.** Fluorescence emission titration experiment of oligomers **B** (black curves) and **K** (red curves) in the presence of SP formed of oligomer **A** (note: oligomer **K** contains only three phenanthrenes and is not integrated into SPs). Fluorescence emission was integrated: 535 - 635 nm.

### 3.1.3.8 FRET Efficiency and Antenna Effects

To evaluate the FRET efficiency of each energy transfer step, a series of LHCs possessing different configurations of DNA photonic wires were prepared under identical conditions as described in Figure 23 and Table 4.

In **LHC2** and **LHC3**, two and three cyanine fluorophores with well-defined distances are positioned in the DNA photonic wires, respectively. Upon irradiation of **LHC2** at 322 nm

both, phenanthrene fluorescence at 415 nm and Cy3 emission at 575 nm, decrease substantially in intensity compared to that of the aforementioned **LHC1**, while a strong emission peak appears concomitantly at 675 nm characteristic of Cy5. In the case of **LHC3**, all three emission peaks are further quenched, accompanied by the appearance of Cy5.5 fluorescence at 725 nm (Figure 23). This demonstrates a directional, stepwise transfer of the excitation energy from the primary phenanthrene donor array to the Cy5.5 acceptor through the intermediate Cy3 and Cy5 donors *via* a FRET mechanism. FRET efficiencies were calculated based on the decrease in phenanthrene fluorescence compared to the control **LHC4**. The obtained average efficiencies of 43% (**LHC1**), 49% (**LHC2**) and 59% (**LHC3**, Table 4) are significantly higher than those of the corresponding DNA photonic wires lacking SPs (Figure 24 and Table 5).

**Table 4.** The average FRET efficiency ( $E$ ).

	Configuration	$E^{[a]}$
<b>LHC1</b>	SP – Cy3	43 ( $\pm 5$ )%
<b>LHC2</b>	SP – Cy3-Cy5	49 ( $\pm 11$ )%
<b>LHC3</b>	SP – Cy3-Cy5-Cy5.5	59 ( $\pm 10$ )%

[a] FRET efficiency is calculated according to the equation  $E = 1 - \frac{I_{DA}/A_{DA}}{I_D/A_D}$  where  $I_{DA}$  and  $I_D$  are the integrated areas of phenanthrene fluorescence emission between 335 nm and 520 nm with and without acceptors.  $A_{DA}$  and  $A_D$  are the absorbance of phenanthrene at 322 nm with and without acceptors.

The light-harvesting ability of the different LHCs was estimated by determining the antenna effect (AE, Table 5), which refers to the ratio of emission intensity of the acceptor upon excitation of the donor to that obtained by direct excitation of the acceptor.<sup>[95-97]</sup> Taking **LHC3** as an example, the overall AE is obtained following the equation:  $AE = I_{Cy5.5,322nm}/I_{Cy5.5,650nm}$ , where  $I_{Cy5.5,322nm}$  and  $I_{Cy5.5,650nm}$  are the emission intensities of Cy5.5 by excitation of phenanthrene donor at 322 nm and the direct excitation of Cy5.5 at 650 nm. All LHCs show an AE higher than 1, indicative of a highly efficient light-harvesting

process. For a given amount of light absorbed by the SPs, the overall AE value decreases when the number of intermediate donors is increased. This can be rationalized by a reduction in excitation energy transferred to the terminal acceptor along the wires, as would be expected from a FRET mechanism.

### 3.1.3.9 Spectroscopic Measurements

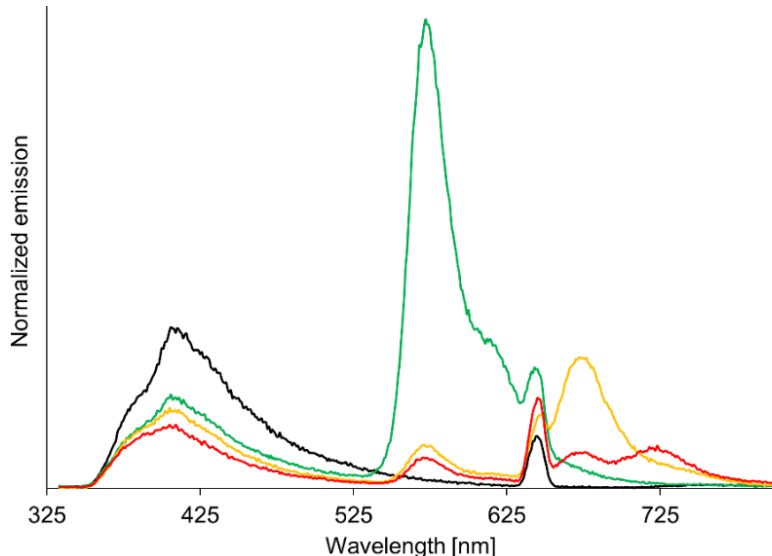


**Figure 23.** Fluorescence emission spectra of **LHC1** (green), **LHC2** (orange), **LHC3** (red) and **LHC4** (black). Concentration of oligomers: **A** (0.5  $\mu$ M), **B, C, D, E, F** and **H** (15 nM). Concentration of oligomers: **A** (0.5  $\mu$ M), **B C, D, E, F** and **H** (15 nM). Conditions: 10 mM sodium phosphate buffer, pH 7.2, 120 mM NaCl,  $\lambda_{\text{ex}} = 322$  nm.

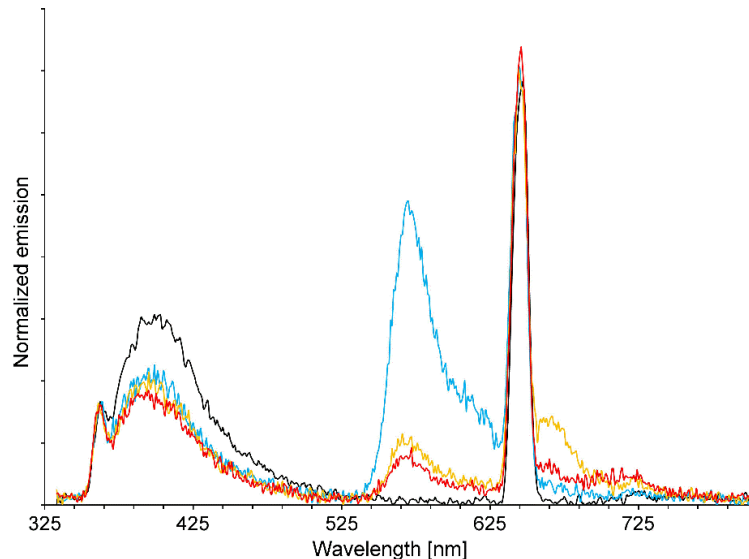


**Figure 24.** Fluorescence spectra of corresponding DNA photonic wires lacking SPs (corresponding to **LHC1** (blue), **LHC2** (orange), **LHC3** (red), **LHC4** (black)). Concentration of oligomers: 15 nM **B, C, D, E, F** and **G**; Conditions: 10 mM sodium phosphate buffer, pH 7.2, 120 mM NaCl,  $\lambda_{\text{ex}} = 322$  nm. Normalization was done by dividing the emission spectra by the absorption value of each individual sample at 322 nm.

To understand the effect of the intermediate donors on the FRET efficiency, fluorescence spectra of LHCs either lacking both, Cy3 and Cy5, or one of them were compared to those of **LHC3** (Figure 25). Direct energy transfer from the SP antenna to the most distant Cy5.5 acceptor is rather inefficient (3%) due to the poor spectral overlap and the relatively large distance between them. As expected, the insertion of intermediate donors Cy5 or Cy3 can circumvent these issues leading to a substantial increase in a FRET efficiency of up to 40% (Table 5), which corresponds to about 60% of the efficiency of **LHC3**. The same holds true for the corresponding DNA photonic wires lacking SPs (Figure 26 and Table 5). All these results demonstrate that the sequential arrangement of multiple chromophores facilitates a stepwise energy transfer cascade. [42-43, 98]

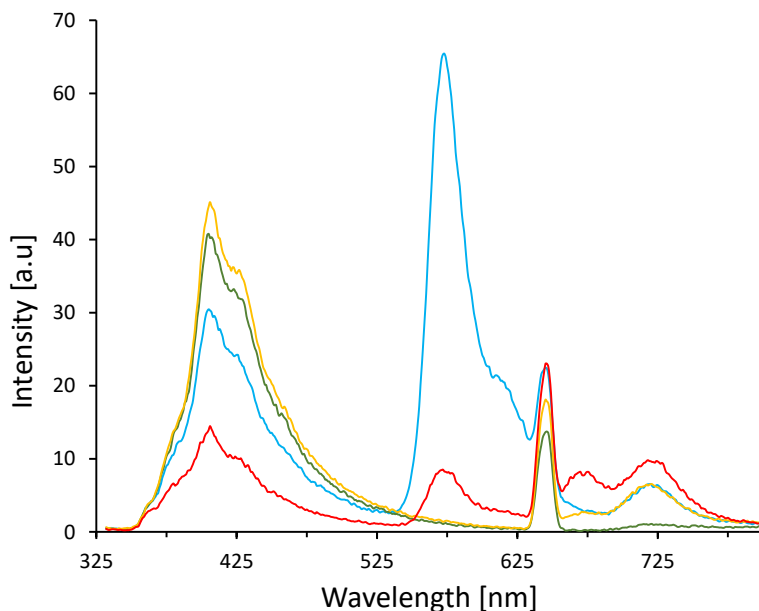


**Figure 25.** Fluorescence emission spectra of LHCs either lacking both Cy3 and Cy5 (green) or one of them (yellow and blue) compared to **LHC3** (red). Concentration of oligomers: **A** (0.5  $\mu$ M), 15 nM **B, C, D, E,** and **G**; Conditions: 10 mM sodium phosphate buffer, pH 7.2, 120 mM NaCl,  $\lambda_{\text{ex}} = 322$  nm.

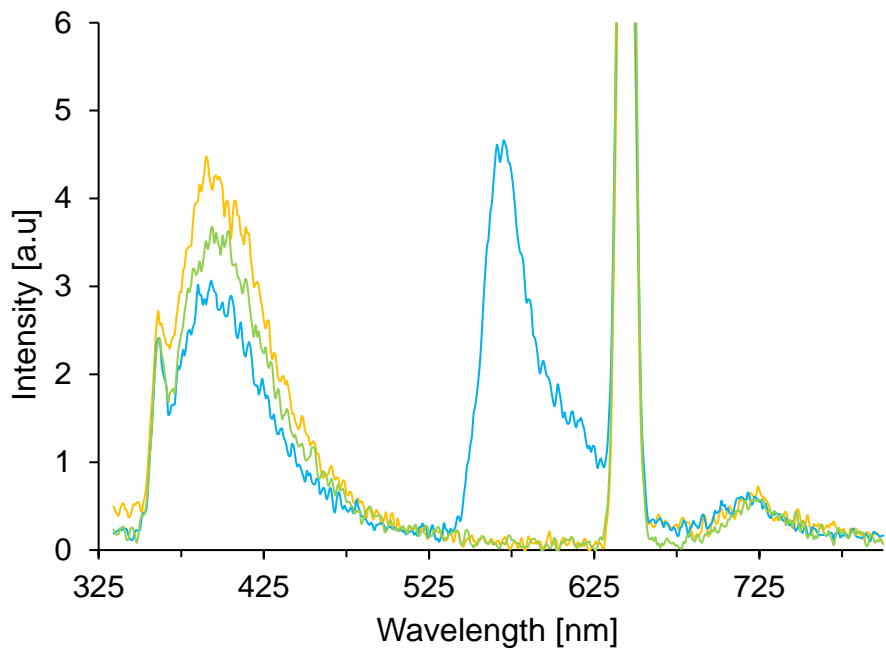


**Figure 26.** Fluorescence emission spectra of LHCs in the absence of oligomer **A** either lacking both Cy3 and Cy5 (green) or one of them (yellow and blue). Concentration of oligomers: 15 nM **B**, **C**, **D**, **E** and **G**; Conditions: 10 mM sodium phosphate buffer, pH 7.2, 120 mM NaCl,  $\lambda_{\text{ex}} = 322$  nm.

**Table 5.** Estimated donor energy losses for LHCs and corresponding DNA photonic wires. FRET efficiency calculation methods are described in Table 4. Antenna effect obtained by comparing the emission of the terminal acceptor by excitation of phenanthrene to the emission of the terminal acceptor by direct excitation

Configuration	FRET efficiency	AE
SP - Cy3	43.0%	22.8
SP - Cy3 - Cy5	49.0%	7.6
SP - Cy3 - Cy5 - Cy5,5	64.0%	1.6
SP - Cy3 - (----) - Cy5,5	39.6 %	3.2
SP - (----) - (----) - Cy5,5	3.1 %	0.9
SP - (----) - Cy5 - Cy5,5	13.7 %	0.5
Oligomer B - Cy3	21.8 %	2.0
Oligomer B - Cy3 - Cy5	28.7 %	- [a]
Oligomer B - Cy3 - Cy5 - Cy5,5	33.0 %	- [a]
Oligomer B - (----) - (----) - Cy5,5	7.5 %	- [a]
Oligomer B - Cy3 - (----) - Cy5,5	25.3 %	- [a]
Oligomer B - (----) - Cy5 - Cy5,5	24.1 %	- [a]

[a] not possible to define reliably due to low signal intensity

### 3.1.4 Conclusions

In conclusion, a novel approach combining light-harvesting, supramolecular phenanthrene polymers with DNA photonic wires has been described. DNA-derived scaffolds containing up to three fluorophores with defined inter-chromophore distances have been appended to SPs in a simple self-assembly process. A stepwise transfer of the excitation energy from the primary phenanthrene donor array to a Cy5.5 acceptor through intermediate Cy3 and/or Cy5 donors *via* a FRET mechanism proceeds with an efficiency of up to 59%. Antenna effects ranging from 1.4 up to 23 were observed for different LHCs. This work demonstrates that the combination of DNA-organized photonic wires with supramolecular polymers enables the assembly of artificial LHCs with excellent light-harvesting properties and high energy transfer efficiencies.

### 3.1.5 Supporting information

#### 3.1.5.1 Synthesis and purification of oligophosphates

The phenanthrene phosphoramidite building block required for the solid-phase synthesis was synthesized according to the published procedure.<sup>[61]</sup> All oligonucleotide sequences were prepared on a 1 µM scale using a standard cyanoethyl phosphoramidite protocol on an ABI 394 (Applied Biosystems Instruments) automated DNA synthesizer. Controlled pore glass support loaded with phenanthrene was used as solid support for the synthesis of oligomers **A**, **B** and **K**. Cleavage from the solid support was achieved with 1 ml of 30% NH<sub>4</sub>OH (aq) at 55 °C over 16 hours. After washing 2 times with EtOH/H<sub>2</sub>O (1:1 mixture) the supernatant was separated by centrifugation and lyophilized. After lyophilization the crude oligomers were purified by reversed phase HPLC; oligomer **A** was purified according to the procedure,<sup>[70]</sup> whereas oligomer **B** and **K** were eluted with Reprosil 100 RP8 column, 5 µm (*Dr. Maisch GmbH*, Ammerbuch, Germany) with 0.025 M TEAA as a buffer A and acetonitrile as eluent B. A gradient from 0-70% eluent B within 20 min for oligomer **B** and for oligomer **K** was performed. LC-MS was used to analyse the purity of the oligomer **B** and **K**.

### 3.1.5.2 Mass spectra of Oligomers

**Table 6.** Calculated and experimental masses of phenanthrene-modified oligomers **A**, **B** and **K**.

Oligomer	Molecular formula	Calc. mass	Exp. mass
<b>A</b>	C <sub>66</sub> H <sub>52</sub> O <sub>10</sub> P <sub>2</sub>	1067.1 Da	1066.3 Da
<b>B</b>	C <sub>306</sub> H <sub>328</sub> N <sub>86</sub> O <sub>133</sub> P <sub>24</sub>	8081.83 Da	8082.2 Da
<b>K</b>	C <sub>262</sub> H <sub>294</sub> N <sub>86</sub> O <sub>125</sub> P <sub>22</sub>	7329.13 Da	7328.4 Da

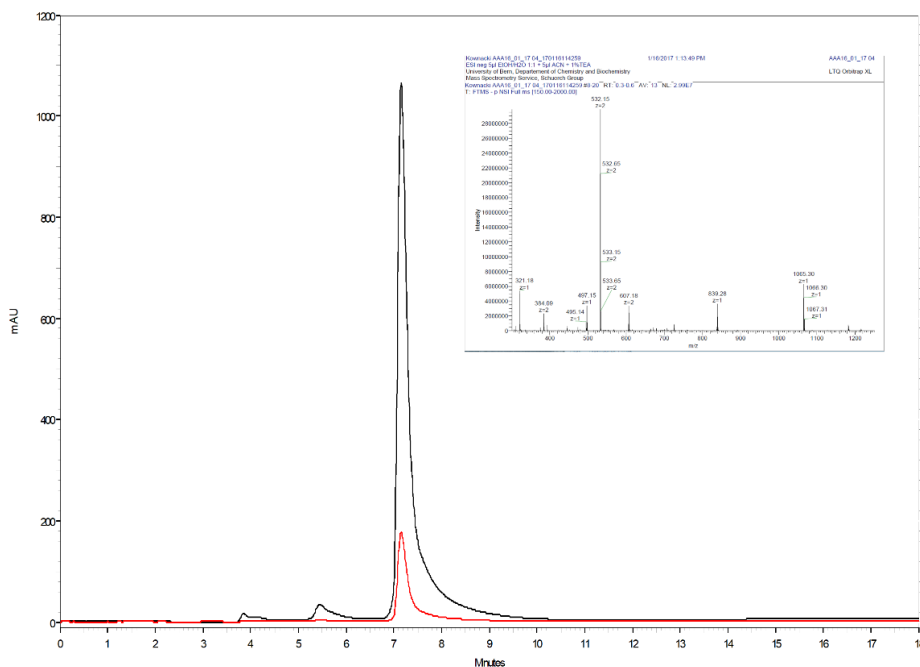


**Figure 27.** HPLC trace ESI -MS analysis of oligomer **A**.

### 3.1 Integrating DNA - Photonic Wires into Light-Harvesting Supramolecular Polymers

---

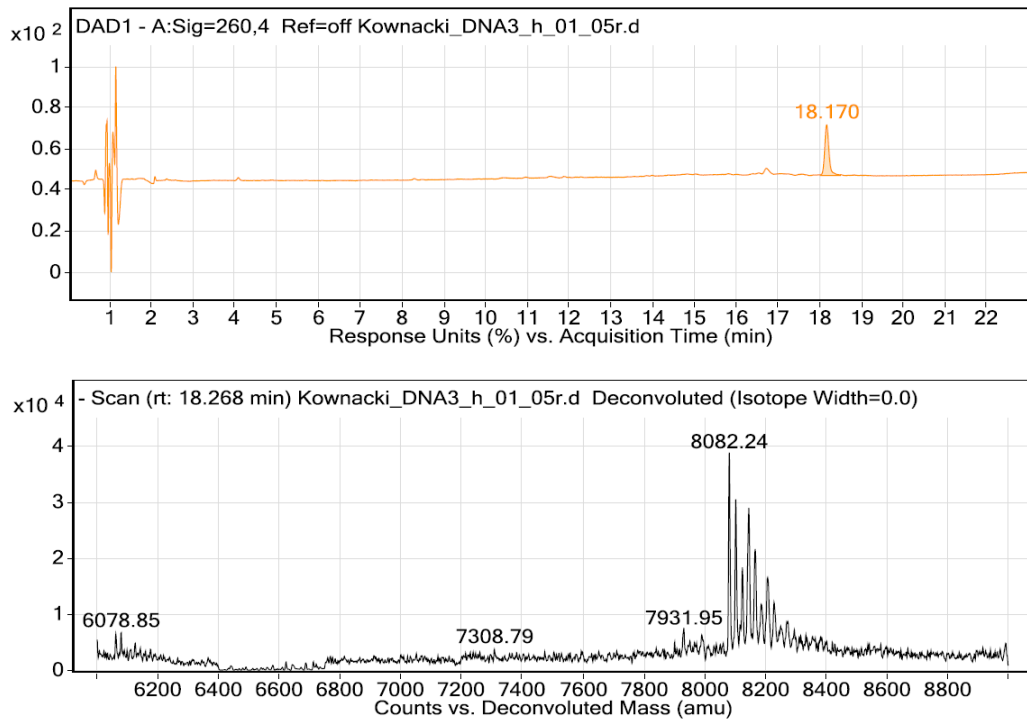


**Figure 28.** LC-MS analysis of oligomer **B**.

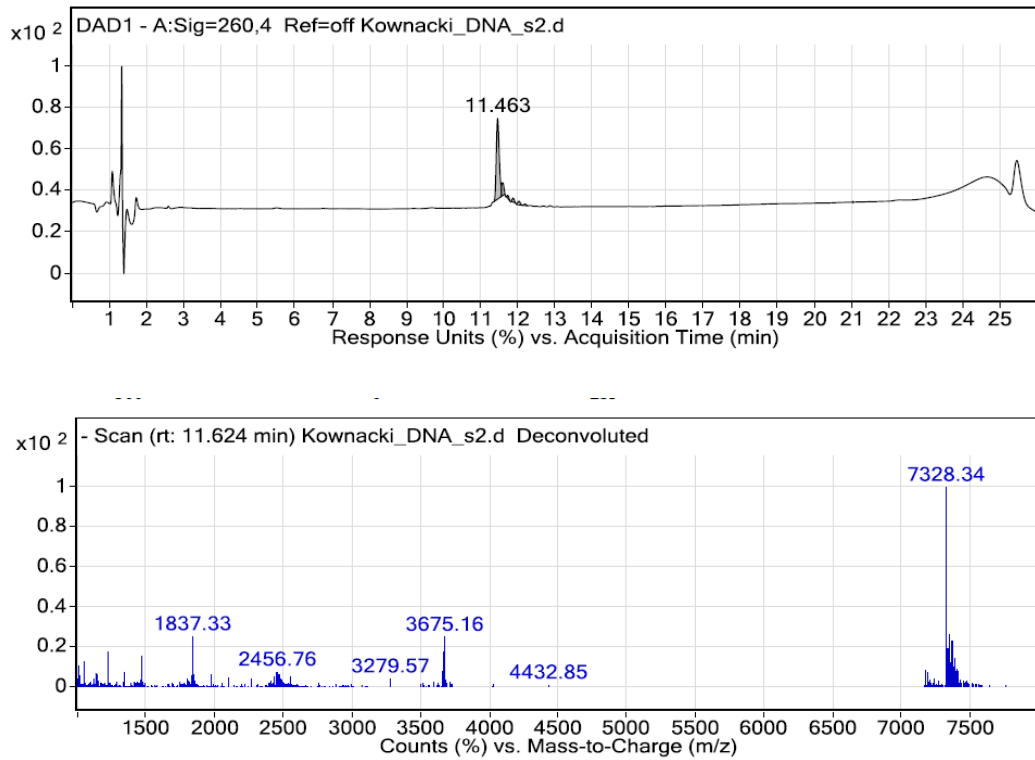


**Figure 29.** LC-MS analysis of oligomer **K**.

### 3.1.5.3 UV-Vis Spectra

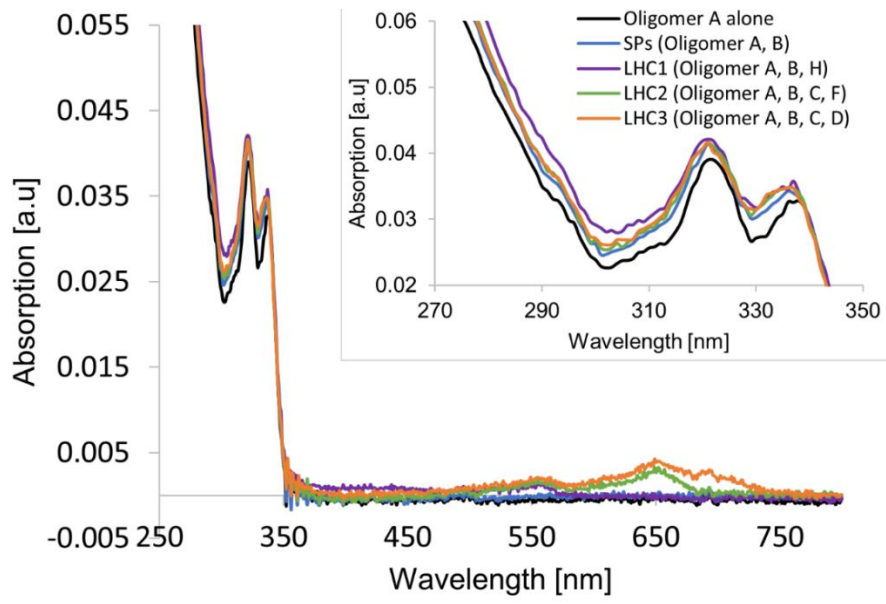


**Figure 30.** Absorption spectra of oligomer **A** alone, SPs (oligomer **A + B**), **LHC1**, **LHC2** and **LHC3** (0.5  $\mu$ M oligomer **A**, 0.015  $\mu$ M oligomer **B**, **C**, **D**, **F**, **H**). Insert: Enlargement of region 270-350 nm from spectra shown in a). Conditions: 10 mM sodium phosphate buffer, pH 7.2, 120 mM of NaCl.

### 3.1.5.4 Fluorescence Spectra of Cy7 (Cyanine)-Containing Light-Harvesting Complexes

**Table 7.** Oligomers used in fluorescence emission experiment in Figure 31.

Oligomer	Sequence
<b>A</b>	(Phe) <sub>3</sub>
<b>B</b>	(Phe) <sub>5</sub> –GAA GGA ACG TAG CCT GGA AC - 5'
<b>E</b>	5' - CTT CCT TGC A
<b>G</b>	Cy3 - CTT CCT TGC A - 3'
<b>P</b>	CTT CCT TGC ATC GGA CCT TG – Cy5 - 3'
<b>R</b>	TC GGA CCT TG – Cy5 - 3'
<b>S</b>	TC GGA CCT TG – Cy7 - 3'

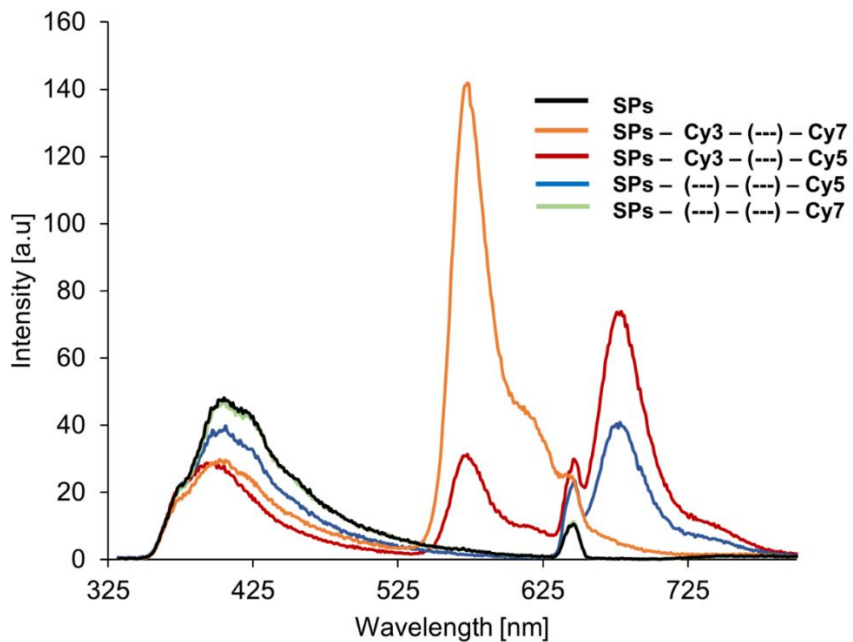


**Figure 31.** Additional fluorescence emission spectra for LHCs missing the first or the intermediate donor-acceptor. Concentration of oligomers: **A** (0.5  $\mu$ M) and **B, E, G, P, R, S** (15 nM). Conditions: 10 mM sodium phosphate buffer, pH 7.2, 120 mM NaCl,  $\lambda_{\text{ex}} = 322$  nm.

### 3.1.5.5 Structures of the Cyanine Fluorophores used for FRET Cascade Design

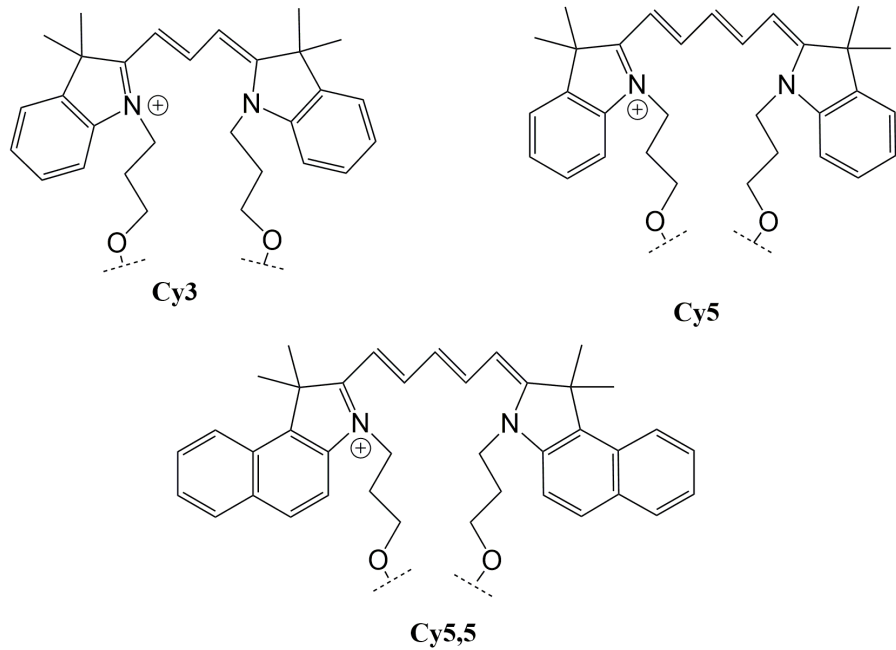


**Figure 32.** Structures of the non-nucleosidic building blocks (donors – acceptors) in DNA photonic wire.

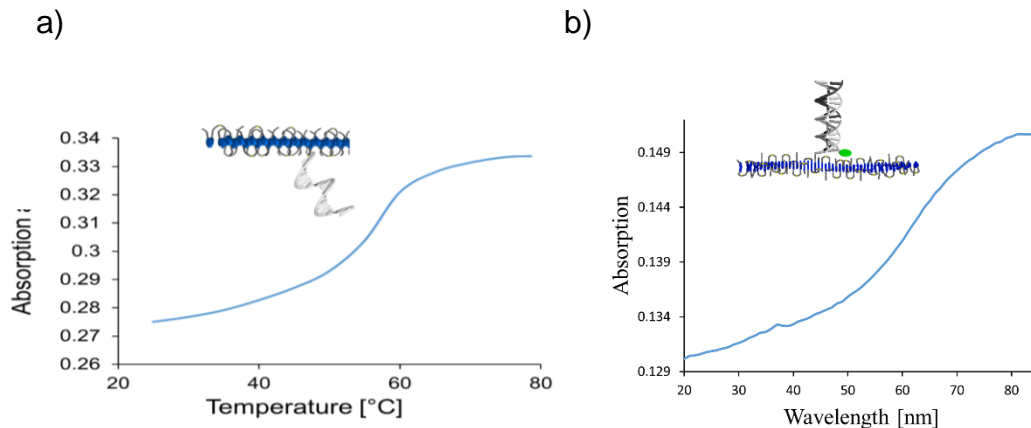
### 3.1.5.6 Spectra of $T_m$ Measurements

**Table 8.** Summary of melting temperatures.

Figure	Oligomers (conc.)	$T_m^a)$
a)	<b>A, B</b> (0.5 $\mu$ M, 150 nM*)	52 °C
b)	<b>A, B, H</b> (0.5 $\mu$ M, 15 nM*, 15 nM*)	58 °C
c)	<b>B, H</b> (0.5 $\mu$ M, 0.5 $\mu$ M)	70 °C
d)	<b>B, E, F</b> (0.5 $\mu$ M, 0.5 $\mu$ M, 0.5 $\mu$ M)	68 °C
e)	<b>I, H</b> (0.5 $\mu$ M, 0.5 $\mu$ M)	68 °C
f)	<b>E, F, I</b> (0.5 $\mu$ M, 0.5 $\mu$ M, 0.5 $\mu$ M)	38 °C
g)	<b>E, I</b> (0.5 $\mu$ M, 0.5 $\mu$ M)	38 °C
h)	<b>F, I</b> (0.5 $\mu$ M, 0.5 $\mu$ M)	37 °C
i)	<b>A, B, C, D</b> (0.5 $\mu$ M, 15 nM, 15 nM, 15 nM)	60 °C
j)	<b>A, B, C, F</b> (0.5 $\mu$ M, 15 nM, 15 nM, 15 nM)	59 °C
k)	<b>A, B, D, E</b> (0.5 $\mu$ M, 15 nM, 15 nM, 15 nM)	59 °C

<sup>a)</sup> Melting temperatures of different complexes and hybrids. The cooling ramp was measured with a rate of 0.3 °C/min. Absorbance was recorded at 250 nm. Conditions: 10 mM sodium phosphate buffer, pH 7.2, 120 mM of NaCl. Melting temperatures were determined by the maximum of the first derivative (average of the two cooling ramps; est. error  $\pm 1^\circ\text{C}$ ).

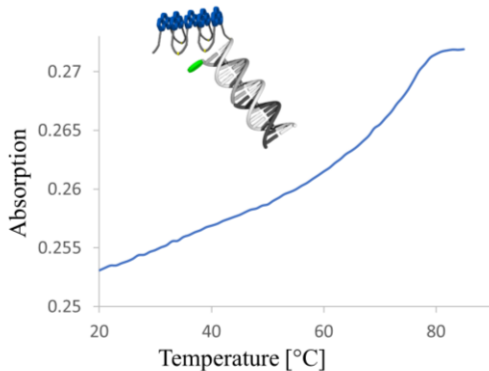
\* 150 nM concentration of DNA strands was used in order to observe hypochromicity



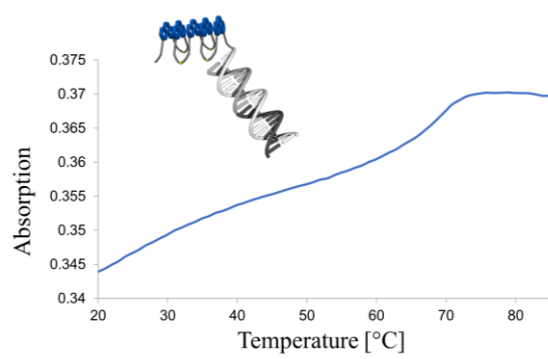
### 3.1 Integrating DNA - Photonic Wires into Light-Harvesting Supramolecular Polymers

---

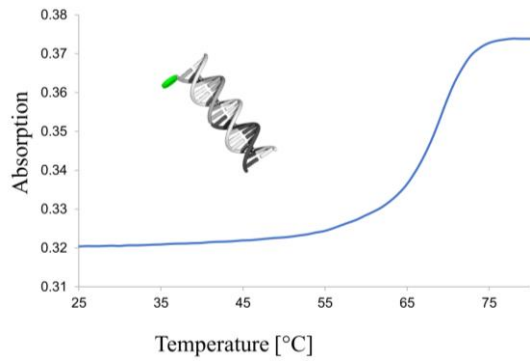
b)



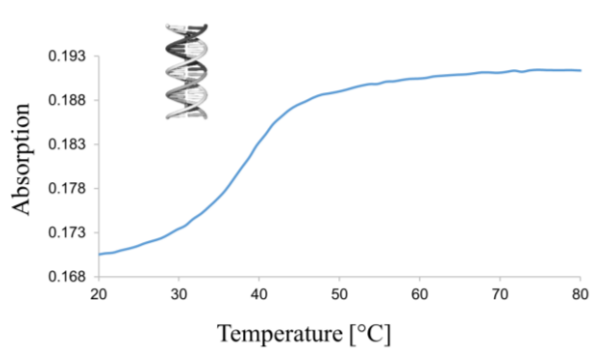
d)



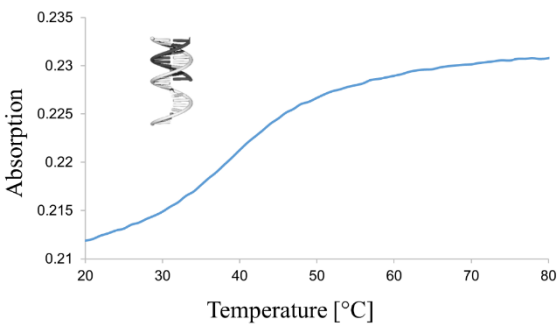
e)



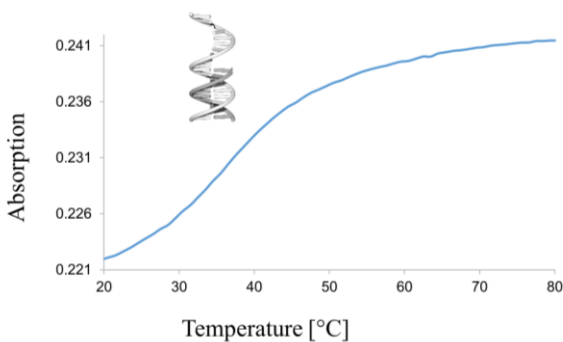
f)



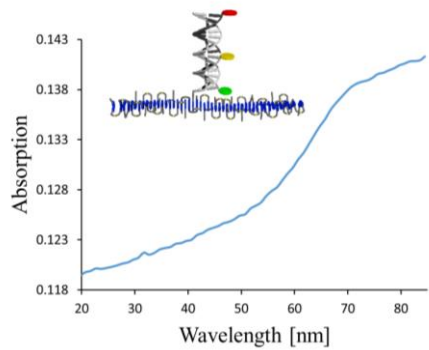
g)



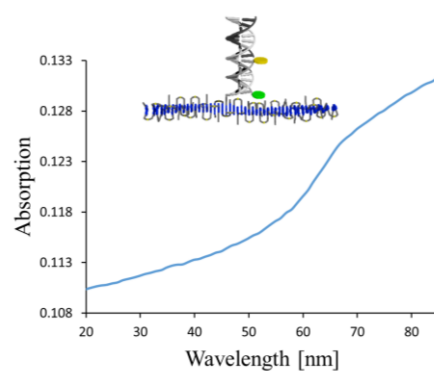
h)



i)



j)



k)

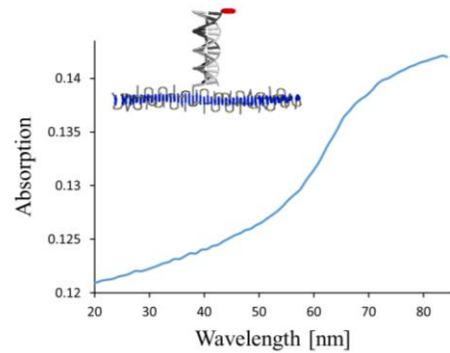


**Figure 33.** Melting curves of complexes: a) A and B; b) A, B and H (LHC1); c) B and H; d) B, E and F; e) I and H; f) I, E and F; g) I and E; h) I and F; i) A, B,C and D (LHC3); j) A, B, C and F (LHC2); k) A, B, D and E. Conditions: see Table 8.

## 3.2 Further Experiments

### 3.2.1 Introduction

Efficient propagation of the energy transfer is strongly influenced by the LHCs composition. In this study, a new phenanthrene-modified oligonucleotides with an additional pyrene acceptor and / or PEG linker building block were synthesized and incorporated into SPs. Hybridization with the Cy3- or Cy5-labelled complementary strand affords the LHCs presented in Figure 34. The PEG linker-containing LHCs were constructed in order to investigate a distance dependent ET between the phenanthrene antenna and the cyanine acceptor. Additionally, the precise arrangement of the acceptor on the 3`- or 5`-end of the complementary strand give an insight into distance dependent ET. Moreover, the influence of the pyrene donor-acceptor on the ET in LHCs was investigated.

### 3.2.2 Results and Discussion

#### 3.2.2.1 Composition of Light Harvesting Complexes and DNA Sequences

The synthesis of 1,8-dibutynyl-substituted pyrene phosphoramidite<sup>[99]</sup> was performed according to the published procedure.<sup>[70]</sup> The tetraethylene glycol phosphoramidite (**3**) was prepared in two steps (3.2.4.2 Supporting Information, Figure 50). Firstly the commercially available diol was transformed into DMT-protected alcohol **2** which was converted into phosphoramidite **3**. The pyrene and PEG linker phosphoramidites were used to prepare oligomer **L**, **M** and **N** in the same way as previously described oligomers **A** and **B** (3.1.3 Results). All five oligomers were assembled by automated oligonucleotide synthesis, purified by reverse phase HPLC and analysed by mass spectrometry (4.1.4 Supporting Information). The complementary Cy3- and Cy5-labelled DNA strands were purchased from *Microsynth*. The oligomers used in this study as well as dye-labelled oligonucleotides are presented in Table 9. The compositions of the LHCs are summarized in Figure 34.

### 3.2 Further Experiments

**Table 9.** Top: Sequences of oligomers used in this study, bottom: LHCs compositions.

Oligomer	Sequence		
<b>A</b>	(Phe) <sub>3</sub>		
<b>B</b>	(Phe) <sub>5</sub> - GAA GGA ACG TAG CCT GGA AC - 5'		
<b>L</b>	(Phe) <sub>5</sub> - PEG - GAA GGA ACG TAG CCT GGA AC - 5'		
<b>M</b>	Phe - Py - (Phe) <sub>3</sub> - GAA GGA ACG TAG CCT GGA AC - 5'		
<b>N</b>	Phe - Py - (Phe) <sub>3</sub> - PEG - GAA GGA ACG TAG CCT GGA AC - 5'		
<b>H</b>	Cy3 - CTT CCT TGC ATC GGA CCT TG - 3'		
<b>O</b>	5' - CTT CCT TGC ATC GGA CCT TG - Cy3		
<b>P</b>	5' - CTT CCT TGC ATC GGA CCT TG - Cy5		
<b>LHC1: (A,B,H)</b>	<b>LHC5: (A,L,H)</b>	<b>LHC6: (A,M,H)</b>	<b>LHC7: (A,N,H)</b>
<b>LHC10: (A,N,P)</b>	<b>LHC11: (A,M,P)</b>	<b>LHC12: (A,N,O)</b>	

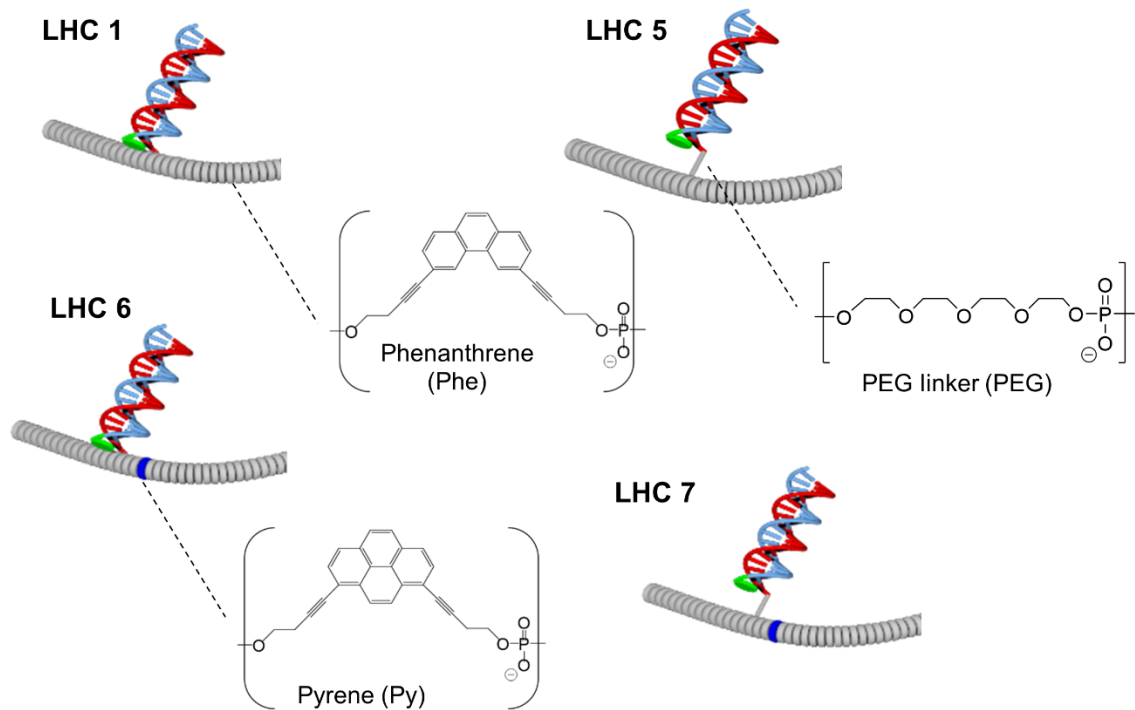


**Figure 34.** Illustrations of different LHCs: pyrene (dark blue), phenanthrene (grey), PEG linker (grey bar), Cy3 (green).

### 3.2.2.2 Spectroscopic Measurements

The photophysical properties of the SPs composed of the phosphate linked phenanthrene trimer **A** and tiny amounts of oligomer **N** (1% of pyrene in comparison to the phenanthrene) were investigated (Figure 35). Oligomer **A** (0.5  $\mu$ M) is mixed with oligomer **N** (15 nM) in sodium phosphate buffer in the presence of NaCl. Afterwards, the solution is heated to 80°C and cooled down to 20°C. The formation of SPs takes place between 60 and 50°C (melting curves, 3.2.4 Supporting Information).

Excitation of the phenanthrene polymer (0.5  $\mu$ M oligomer **A**) at 322 nm exhibit very weak fluorescence emission (Figure 36, black curve). However, addition of 15 nM pyrene-containing oligomer **N** results in strong fluorescence emission band at 406 nm (Figure 36, yellow curve). Based on this results, oligomer **N** can be incorporated into SP.

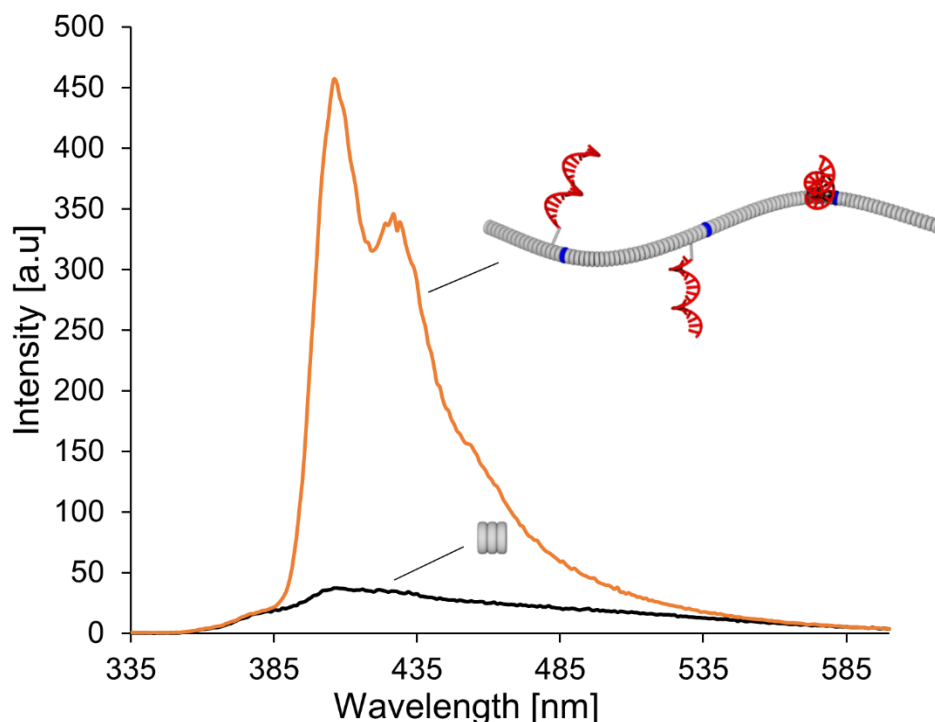


**Figure 35.** Fluorescence spectra of oligomer **A** (0.5  $\mu$ M, black) and self-assembled SPs composed of oligomer **A** (0.5  $\mu$ M) and oligomer **N** (15 nM) in 10 mM sodium phosphate buffer, pH 7.2, 120 mM NaCl,  $\lambda_{\text{ex.}}$ : 322 nm.

Similar strong fluorescence emission is observed for the SPs composed of oligomer **A** and **M** (Figure 36). The SPs in the absence of PEG linker exhibit lower fluorescence emission in comparison to the SPs with the incorporated spacer. The fluorescence emission results show the influence of the PEG linker on the SPs formation. Incorporated PEG linker into SPs ensure improved self-assembly due to the lower steric demand and electrostatic repulsion between highly charged polyanionic components.

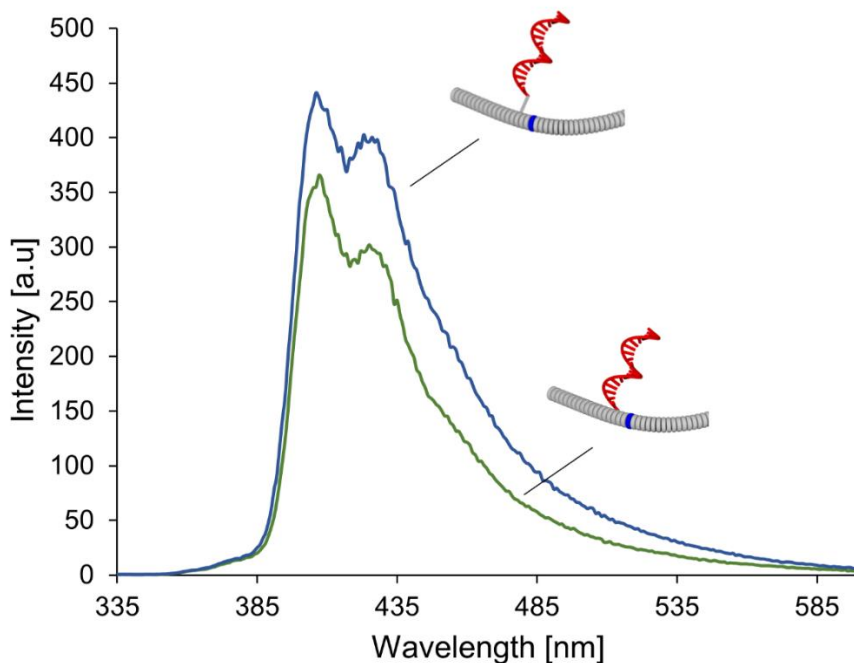


**Figure 36.** Fluorescence spectra of self-assembled SPs composed of oligomer **A** (0.5  $\mu$ M) and either oligomer **N** (15nM) or oligomer **M** (15nM) in sodium phosphate buffer, pH 7.2, 120 mM NaCl,  $\lambda_{\text{ex.}}$ : 322 nm.

Figure 37 and 38 shows UV-vis absorption spectra of the aforementioned SPs in the assembled (20 °C) and the disassembled (80 °C) state. A blue shift is observed in the phenanthrene region (at 330 nm) while comparing the spectra at 20 °C and at 80 °C. This indicates that at 20 °C the oligomer **A** and **N** are assembled (solid curve) and at 80 °C disassembled (dashed curve). A very distinct absorption shift is observed for the SPs (**A**, **N**) containing the PEG linker (Figure 37), as well as for the SPs (**A**, **M**) lacking the spacer (Figure 38). Besides, both SPs exhibit substantial change in the absorption intensity at 250 nm.

### 3.2 Further Experiments

---

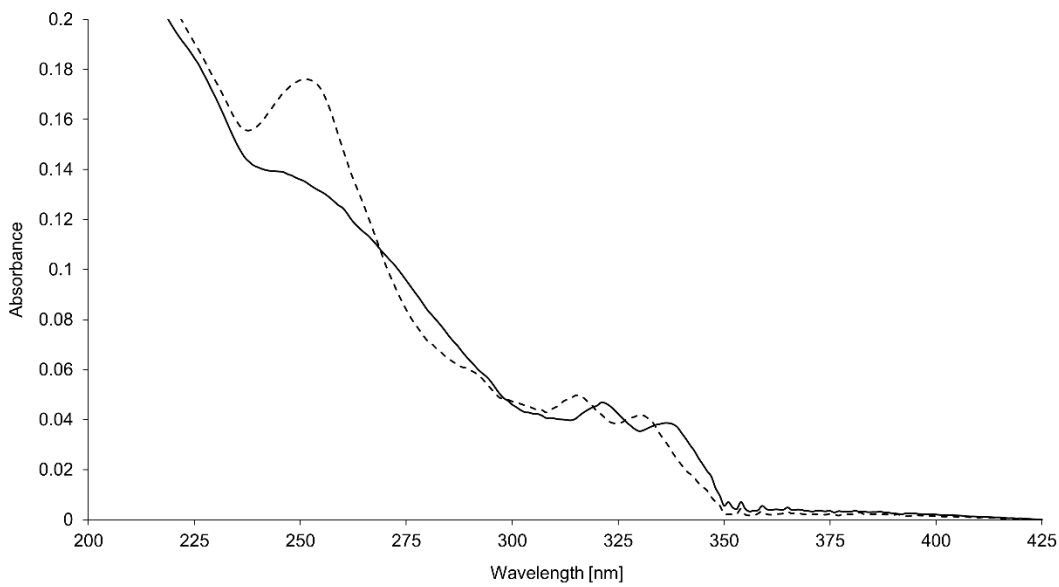


**Figure 37.** UV-vis spectrum of SPs (oligomer **A** (0.5  $\mu$ M) and oligomer **N** (15nM)) in assembled (20 °C, solid curve) and the disassembled state (80 °C, dashed curve) in 10 mM sodium phosphate buffer, pH 7.2, 120 mM NaCl,  $\lambda_{\text{ex.}}$ : 322 nm.

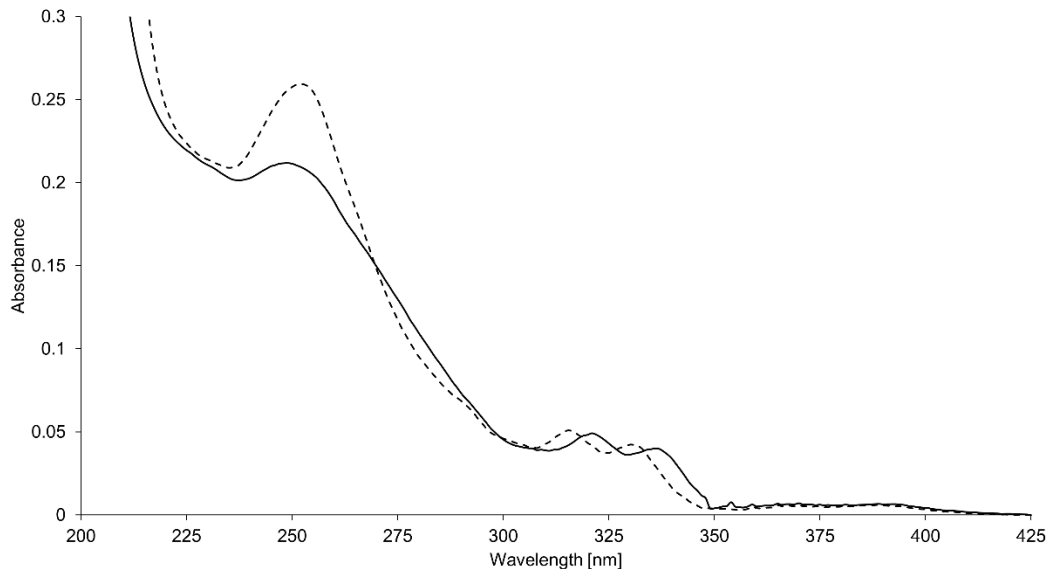


**Figure 38.** UV-vis spectrum of SPs (oligomer **A** (0.5 $\mu$ M) and oligomer **M** (15nM)) in the assembled (20 °C, solid curve) and the disassembled state (80 °C, dashed curve) in 10 mM sodium phosphate buffer, pH 7.2, 120 mM NaCl,  $\lambda_{\text{ex.}}$ : 322 nm.

#### 3.2.2.3 Energy Transfer in Modified Light-Harvesting Complexes

The new LHCs were designed to investigate the influence of the PEG linker as well as the 1,8-dibutynylpyrene building block on the energy transfer.

Aforementioned, SPs containing PEG linker show higher fluorescence emission in comparison to the SPs lacking the spacer (Figure 36). Higher fluorescence emission is a result of incorporated PEG linker into SPs which ensure improved SPs formation. Better formation of the SPs would be expected to drive more efficient ET from the phenanthrene antenna to the Cy3 acceptor after addition of the Cy3 labelled complementary strand to the SPs. In this experiment, the opposite fluorescence emission results are observed.

Self-assembly experiments were typically carried out by mixing oligomer **A** (0.5 µM) and an equimolar ratio of oligomer **N** / **M** and the cyanine-labeled oligonucleotide **H** (15 nM) in sodium phosphate buffer (10 mM, pH 7.2) in the presence of NaCl (120 mM). Upon heating to 80 °C and cooling to room temperature over a period of 5 min, the oligomeric building blocks self-organize into **LHC6** or **LHC7**.

The so-formed LHCs show a significant emission band at 575 nm after excitation of the phenanthrene antenna at 322 nm (Figure 39). The emission band is characteristic for the Cy3 emission which indicates that the energy absorbed by the phenanthrene antenna is transferred to the Cy3 acceptor. The Cy3 emission band is substantially higher in the **LHC6** than in the **LHC7**. Additionally, the excitation of the phenanthrene polymer in **LHC6** leads to a strong decrease of the fluorescence pyrene emission band at 406 nm. However, in case of **LHC7** there is a very limited decrease in the pyrene fluorescence emission in comparison to the SPs (**A**, **N**), as demonstrated in Figure 36. The **LHC6** lacking the PEG linker shows more efficient energy transfer from the phenanthrene antenna to the Cy3 acceptor. In **LHC7**, the longer distance between light harvesting polymer and Cy3 acceptor resulting in less efficient ET.

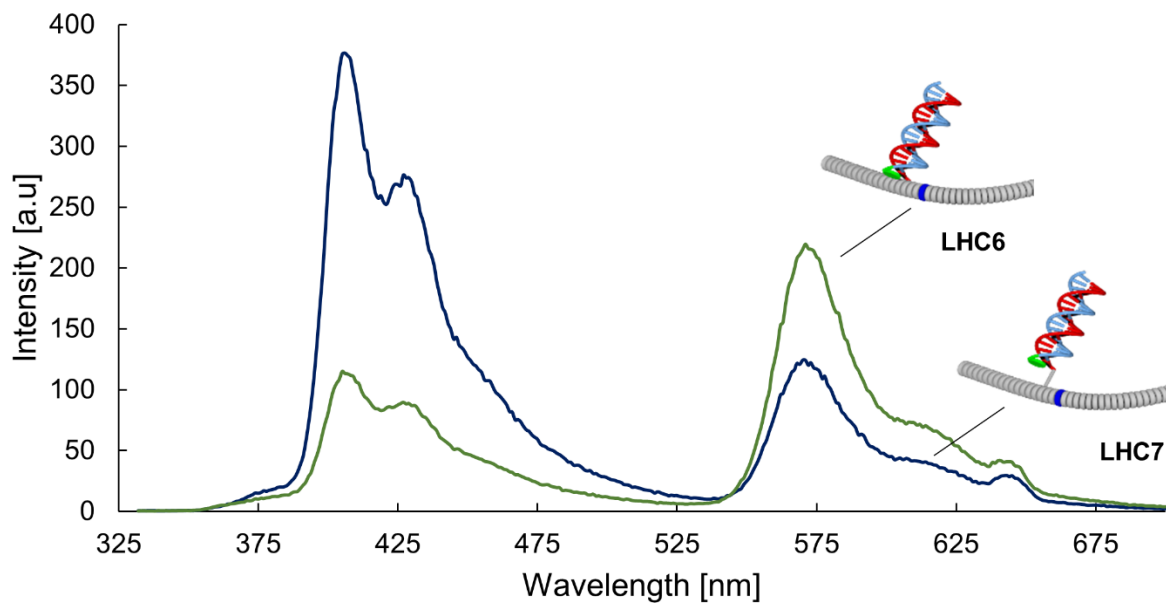


**Figure 39.** Fluorescence emission spectra of **LHC6** (blue) and **LHC7** (green). Conditions: concentration of oligomers: **A** (0.5  $\mu$ M), **N, M, H** (15 nM); 10 mM sodium phosphate buffer, pH 7.2, 120 mM NaCl,  $\lambda_{\text{ex.}}$ : 322 nm.

In this studies such SPs functionalized with the single Cy3-labeled oligonucleotide show efficient ET from the phenanthrene antenna to the Cy3 acceptor. However, incorporation of the PEG linker into **LHC7** affords less efficient ET than in **LHC6**. This results demonstrate the importance of the Cy3 acceptor proximity to the phenanthrene antenna for efficient ET. The ET efficiency in the **LHC6** with the Cy3 in the proximity to the phenanthrene antenna surpass the ET efficiency in **LHC7** containing the PEG linker, despite the improved formation of the SPs (**A, N**). Presence of the PEG linker in the **LHC6** extend the distance between the phenanthrene antenna and the Cy3 acceptor. The PEG monomer length is 0.35 nm.<sup>[100]</sup> The tetraethylene glycol length is around 1.4 nm. The distance between phenanthrene antenna and the Cy3 acceptor in **LHC7** is around 1.4 nm longer than in **LHC6**. Highly distance-dependent FRET explains the influence of the PEG linker on the ET efficiency in the designed complexes.

### 3.2.2.4 Influence of the PEG Linker on Phenanthrene Based Light-Harvesting Complexes

The **LHC5** (Figure 34) was designed to study the influence of the PEG linker on the supramolecular structure and on the ET efficiency. The **LHC5** was self-assembled from a mixture of oligomers **A** (0.5  $\mu$ M), **L** (15 nM) and complementary single strand **H** (15 nM). Upon heating-cooling process the Cy3-functionalized SP was formed. The Cy3-labelled single DNA strand (**H**) was hybridized with the phenanthrene-modified oligonucleotide and self-assembled into SPs in the way that Cy3 acceptor was placed in close proximity to the phenanthrene antenna. In **LHC5** the PEG linker was used to extend the distance between the antenna and the Cy3 acceptor. Figure 40 shows the fluorescence emission spectra of **LHC1** and **LHC5**. The excitation of the phenanthrene antenna results in formation of the new Cy3 emission band at 575 nm with two times higher emission intensity for **LHC1** than **LHC5**. The energy transfer from the phenanthrene antenna to the Cy3 (**LHC1**) is much more efficient than in **LHC5**. Similar like in **LHC6** and **LHC7**, the ET efficiency in the **LHC1** with the Cy3 in the proximity to the phenanthrene antenna surpass the ET efficiency in **LHC5** containing the PEG linker.

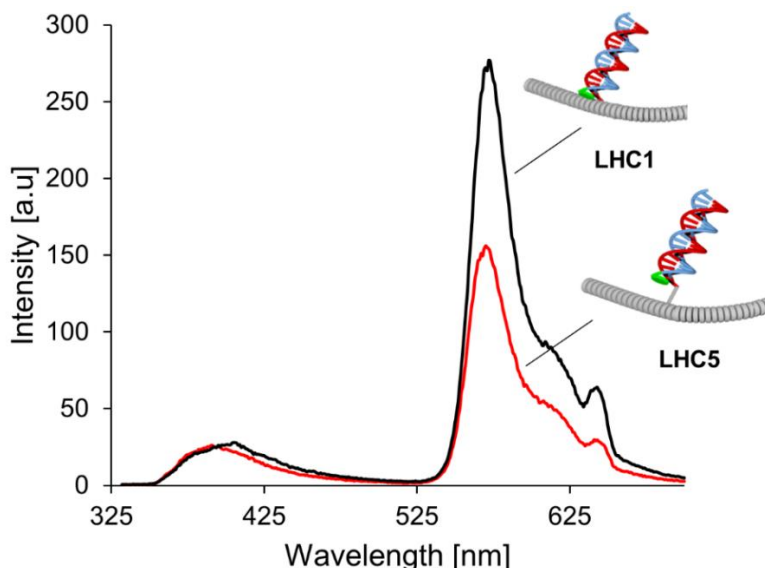


**Figure 40.** Fluorescence emission spectra of **LHC1** (black) and **LHC5** (red). Concentration of oligomers: **A** (0.5  $\mu$ M), **B**, **L**, **H** (15 nM); Conditions: 10 mM sodium phosphate buffer, pH 7.2, 120 mM NaCl,  $\lambda_{\text{ex.}}$ : 322 nm.

### 3.2.2.5 Pyrene Influence on the Phenanthrene Based Light-Harvesting Complexes

In this study, the energy transfer efficiency in **LHC1** and **LHC6** will be compared. The **LHC1** has already been used for the integration of photonic wires into light-harvesting SPs (3.1.3 Results). The **LHC6** containing an additional pyrene building block was used for ET studies (3.2.2.3). Figure 41 (left) shows the fluorescence emission spectra of the **LHC1** and **LHC6**. Excitation of phenanthrene polymer at 322 nm results in significant emission band at 575 nm characteristic for Cy3 emission. The **LHC1** exhibits slightly higher Cy3-emission intensity than **LHC6**. This indicates a similar energy transfer efficiency for both complexes. Besides, Figure 41 (right) shows the fluorescence emission spectra of the **LHC5** and **LHC7** modified with the additional pyrene chromophore. Excitation of phenanthrene polymer (at 322 nm) results in Cy3 emission. Similar like in the previously compared **LHC1** and **LHC6**, the Cy3 emission intensity is slightly lower in the pyrene containing **LHC7** than in **LHC5**.

The lower Cy3 emission in **LHC6** and **LHC7** (in comparison to **LHC1** and **LHC5**) can be explained by a multi-step FRET mechanism. The excitation energy absorbed by phenanthrene antenna is transferred to the Cy3 acceptor through the intermediate pyrene donor. The stepwise energy transfer leads to a partial energy loss resulting in lower fluorescence emission.

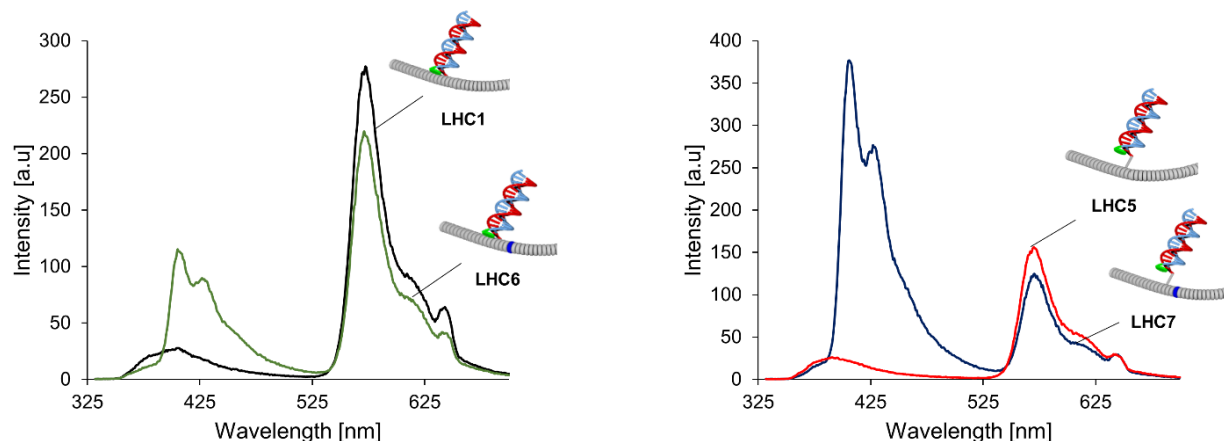


**Figure 41.** Fluorescence emission spectra. Left: **LHC1** (black) and **LHC6** (green). Right: **LHC5** (red) and **LHC7** (blue). Concentration of oligomers: **A** (0.5  $\mu$ M), **B**, **L**, **M**, **N**, **H** (15 nM); Conditions: 10 mM sodium phosphate buffer, pH 7.2, 120 mM NaCl,  $\lambda_{\text{ex.}}$ : 322 nm.

Figure 42 shows fluorescence emission spectra for all LHCs containing Cy3-acceptor in close proximity to the phenanthrene antenna. Direct ET from primary phenanthrene donor arrays to the Cy3 acceptor is much more efficient in **LHC1** than in **LHC5-7**. Presence of the PEG linker in **LHC5** and **LHC7** results in less efficient energy transfer due to the extended distance between the phenanthrene antenna and Cy3 acceptor. Further, in **LHC6**, the presence of additional intermediate pyrene donor has weaken the ET efficiency in comparison to the **LHC1** as a result of the stepwise transfer of energy from the phenanthrene antenna through the pyrene chromophore to the final Cy3 acceptor.

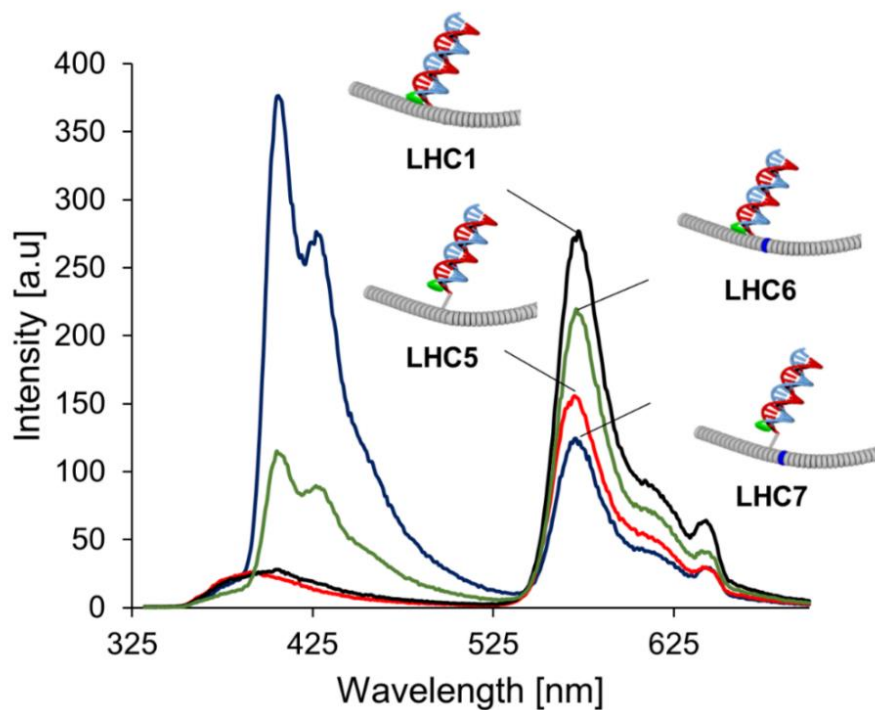


**Figure 42.** Fluorescence emission spectra of **LHC1** (black), **LHC5** (red), **LHC6** (blue) and **LHC7** (green). Concentration of oligomers: **A** (0.5  $\mu$ M) and 15 nM **B**, **L**, **M**, **N** and **H**; Conditions: 10 mM sodium phosphate buffer, pH 7.2, 120 mM NaCl,  $\lambda_{\text{ex.}}$ : 322 nm.

### 3.2.2.6 Distance Dependent Energy Transfer

DNA is used as a versatile platform for precise arrangement of chromophores.<sup>[47, 78]</sup> In this studies the SPs were functionalized with the complementary DNA single strands containing cyanine dye at the 3`-end (oligomer **O**) or at the 5`-end (oligomer **H**). The LHCs are demonstrated in Figure 43. In **LHC6** the Cy3 acceptor is in close proximity to the phenanthrene/pyrene antenna, whereas in **LHC12** the Cy3 is 20 base pairs away from the antenna (Figure 43). The oligomers used for the construction of **LHC6** and **LHC12** are shown in Figure 34. Oligomers **A** and **N** were prepared the way as described previously (3.1.3 Results). The cyanine labeled oligonucleotides were purchased from *Microsynth*.

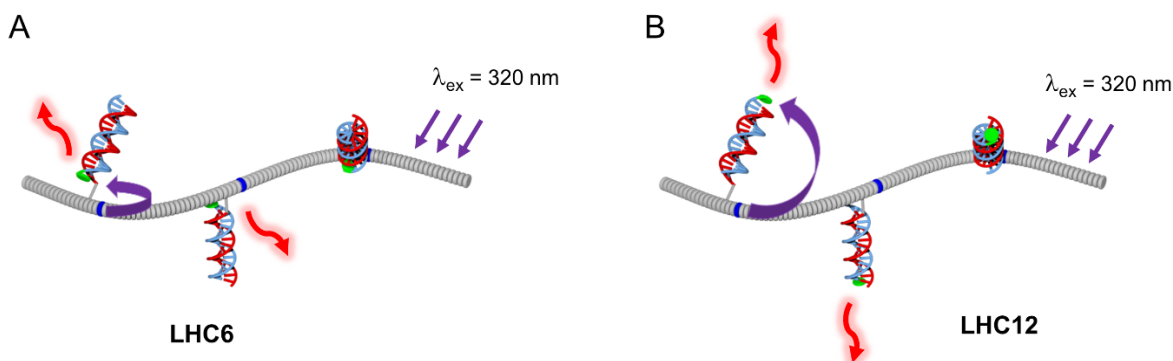


**Figure 43.** Illustration of the short-distance energy transfer in **LHC6** (A) and long-distance energy transfer in **LHC12** (B).

The LHCs fluorescence emission spectra are demonstrated in the Figure 44. Excitation of the phenanthrene antenna results in a decrease of phenanthrene fluorescence emission and an increase of a new Cy3 emission band at 575 nm.

The new Cy3 emission band is much more prominent in **LHC6** than in **LHC12**. The 20 nucleobases distance between phenanthrene antenna and the Cy3-acceptor in **LHC12** results in a significant decrease of Cy3 fluorescence emission.

### 3.2 Further Experiments

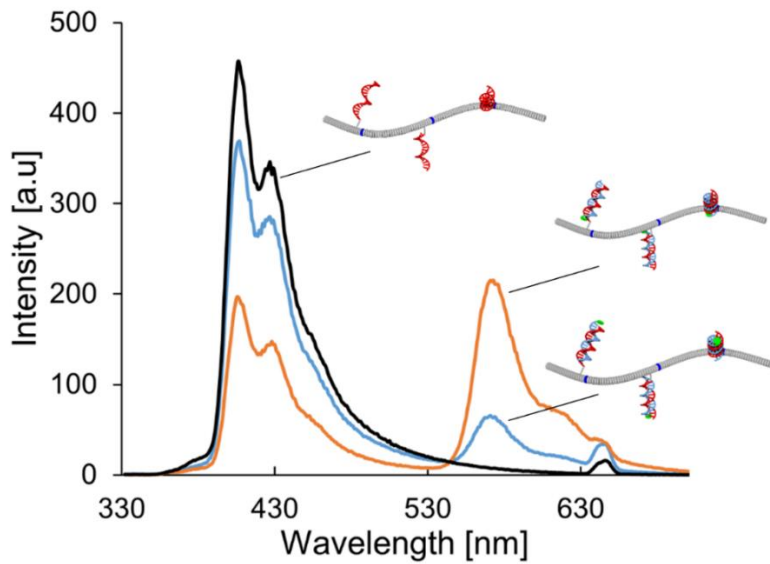


**Figure 44.** Fluorescence spectra of **LHC6** (orange), **LHC12** (blue) and self-assembled **SPs** (black) composed of oligomer **A** and **N**. Concentration of oligomers: **A** (0.5  $\mu$ M) and 15 nM, **N**, **H** and **O**; Conditions: 10 mM sodium phosphate buffer, pH 7.2, 120 mM NaCl,  $\lambda_{\text{ex.}}$ : 322 nm.

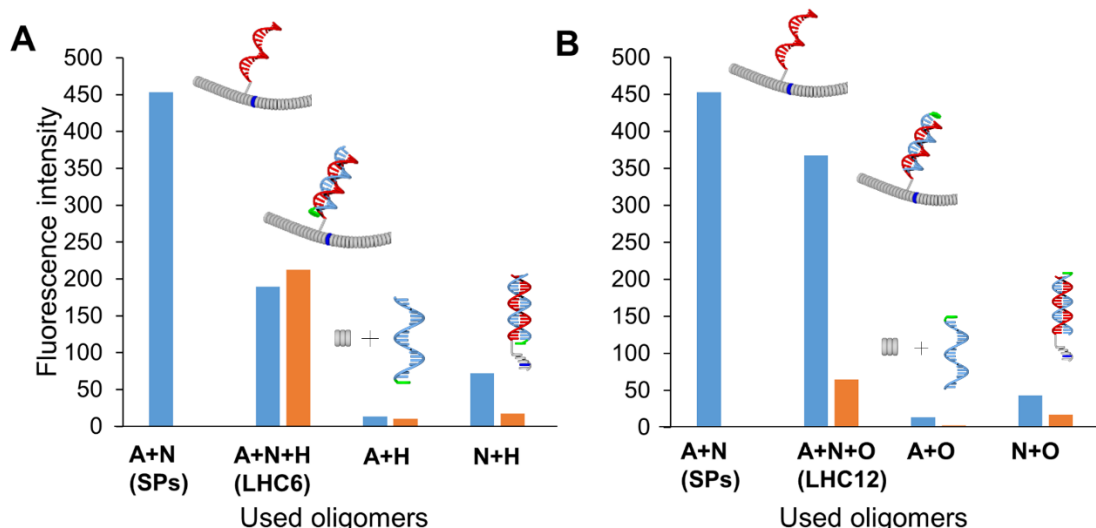


**Figure 45.** Diagram with the integrated fluorescence emission spectra of SPs alone (oligomer **A**, **N**) **LHC6** (A) or **LHC12** (B) as well as a mixture of either oligomer **A** or **N** in combination with the Cy3-derived oligonucleotide **H** (A) or **O** (B). Integrated fluorescence emission of phenanthrene/pyrene fluorescence / between 335 nm and 520 nm; blue bars) and Cy3 (between 525 nm and 630 nm; orange bars).

Figure 45 demonstrates the integrated fluorescence emission for the SPs (**A**, **N**), **LHC6** (**A**, **N**, **H**) and **LHC12** (**A**, **N**, **O**) as well as for the corresponding controls lacking either

### 3.2 Further Experiments

oligomer **A** or **N**. The energy transfer in **LHC12** is around 3 times less efficient than in **LHC6**. Very low energy transfer is observed for the mixture of either oligomer **A** or **N** functionalized with the single Cy3-labeled DNA (**H** or **O**). Mixture of oligomers **A** or **N** with **H** or **O**, reveal weak emission at 575 nm due to very limited energy transfer.

In **LHC12**, the distance between the donor and the acceptor is around 6.6 nm (20 nucleobases) longer than in **LHC6**. Additionally, the tetraethylene glycole has a length of 1.4 nm that results in total distance of 8 nm between phenanthrene antenna and Cy3 acceptor. The greater distance between the phenanthrene donor and Cy3 acceptor significantly influence the FRET efficiency. The ET efficiency depends on the inverse sixth-distance between phenanthrene-pyrene donor and Cy3 acceptor.

DNA addressability allows precise arrangement of the chromophores along the DNA scaffold. In this experiment, DNA functionalized SPs were hybridized with the complementary strand labeled at the 5'-end with Cy5. In such complexes the Cy5 dye and the phenanthrene antenna is separated by 20 nucleobases and the PEG linker. Excitation of the phenanthrene polymer results in Cy5 fluorescence emission at 675 nm (Figure 46) as a result of ET from the phenanthrene to Cy5-acceptor through the pyrene donor.

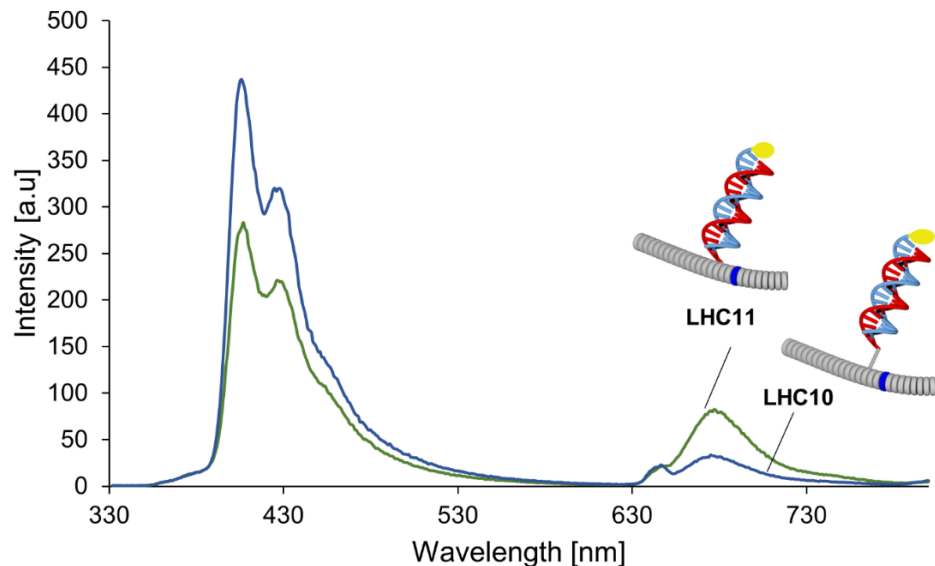


**Figure 46.** Fluorescence emission spectra of **LHC10** (blue) and **LHC11** (green). Conditions: concentration of oligomers: **A** (0.5  $\mu$ M), **N**, **M**, **P** (15 nM); 10 mM sodium phosphate buffer, pH 7.2, 120 mM NaCl.

### 3.2.2.7 Conclusions

In conclusion, a novel light-harvesting supramolecular polymers were constructed for further functionalization with DNA photonic wires in order to efficiently propagate the energy transfer. DNA-appended supramolecular phenanthrene polymers containing either additional pyrene acceptor and/or PEG linker building block has been developed in a simple self-assembled fashion. The self-assembly of the different cyanine dyes along the DNA of the growing antenna is described. Stepwise transfer of the excitation energy from the primary phenanthrene donor array to a Cy3- or Cy5-acceptor through intermediate pyrene donor via a FRET mechanism proceeds with high efficiency. The energy transfer from phenanthrene to pyrene can be explained by quantum coherent mechanism.<sup>[70]</sup>

Herein, we show that the combination of DNA-organized photonic wires with supramolecular polymers containing pyrene and / or PEG linker building block enables the assembly of artificial LHCs. Such DNA-functionalized supramolecular polymers have excellent light-harvesting properties. However, modified LHCs with the PEG linker and/or pyrene chromophore results in less efficient FRET in comparison to the phenanthrene based LHCs.

### 3.2.4 Supporting Information

#### 3.2.4.1 Mass Spectra of Oligomers

**Table 10.** Calculated and experimental masses of phenanthrene-modified oligomers **L, M, N.**

Oligomer	Molecular formula	Calc. mass	Exp. mass
<b>L</b>	C <sub>313</sub> H <sub>347</sub> N <sub>86</sub> O <sub>140</sub> P <sub>25</sub>	8335,6	8338,4
<b>M</b>	C <sub>308</sub> H <sub>333</sub> N <sub>86</sub> O <sub>133</sub> P <sub>24</sub>	8104,8	8108,9
<b>N</b>	C <sub>262</sub> H <sub>294</sub> N <sub>86</sub> O <sub>125</sub> P <sub>22</sub>	8357,0	8361,6

### 3.2 Further Experiments

---

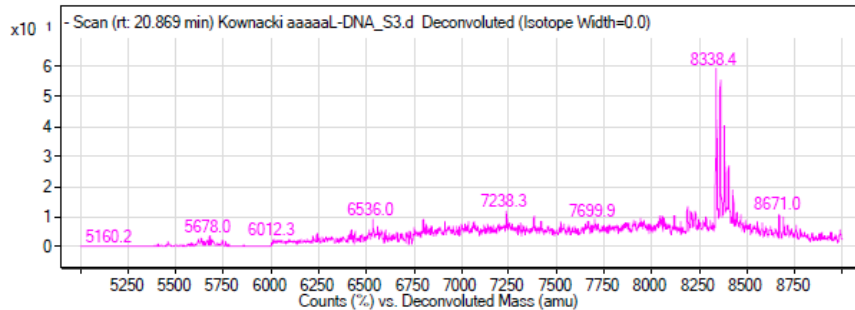


**Figure 47.** MS analysis of oligomer L.

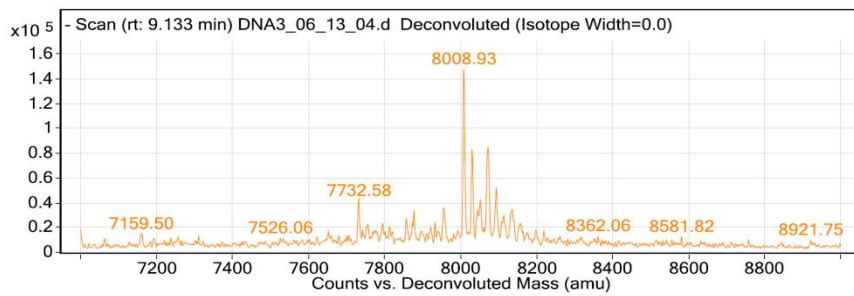


**Figure 48.** MS analysis of oligomer M.

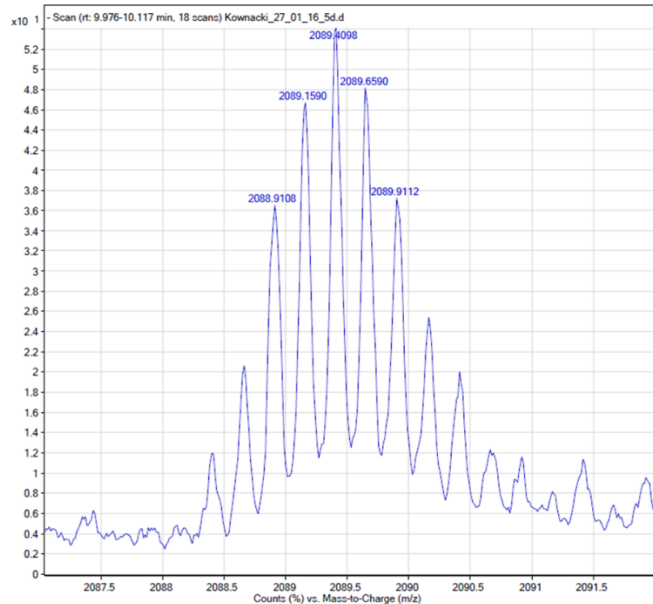


**Figure 49.** ESI -MS analysis of oligomer N.

### 3.2.4.2 Syntheses of PEG linker Derivatives and Phosphoramidites

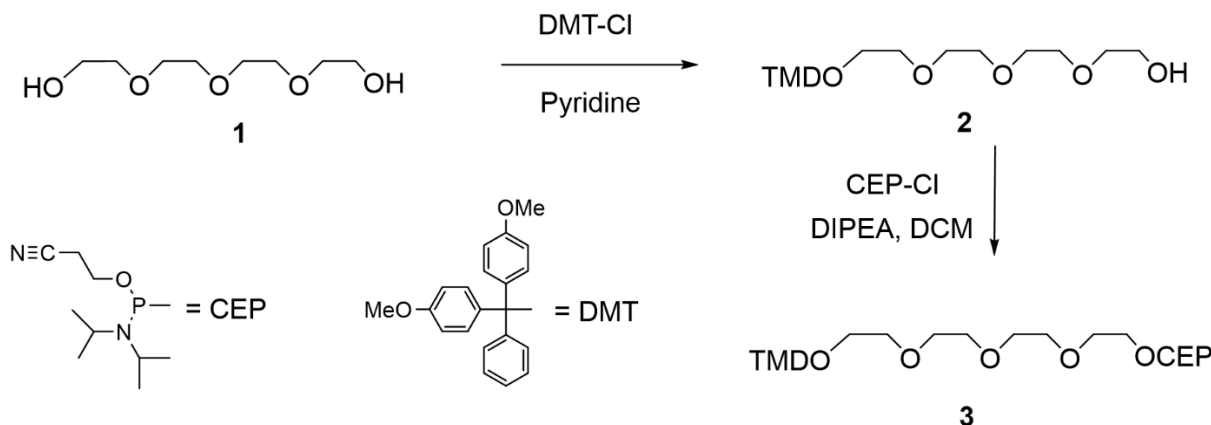


**Figure 50.** Synthesis of the PEG linker building block.

### 4-(6-(4-(bis(4-methoxyphenyl)(phenyl)methoxy)tetra(ethylene glycol)) (2)

The compound was synthesized according to the literature.<sup>[3]</sup>

Tetraethylene glycol **1** (0.308g, 1.59mmol) was dissolved in DCM (5ml) and pyridine (3 mL). Next, 4,4'-dimethoxyltrityl chloride (0.538g, 1.59 mmol) was added in small portions under argon atmosphere. The mixture was stirred at room temperature for 4h. 10 ml of DCM was added to the solution and washed with 5% NaHCO<sub>3</sub> (10 ml) and with H<sub>2</sub>O (10ml). The organic phase was dried with anhydrous sodium sulfate, filtered, and concentrated to an oily residue under reduced pressure. The crude product was purified by column chromatography (EtOH/TEA 98:2). The pure product **2** was obtained (316 mg, 42%) as a pale yellow oil: R<sub>f</sub> 0.35 (EtOAc).

<sup>1</sup>H NMR (CDCl<sub>3</sub>, ppm) 2.56 (s, 1H, OH), 3.24 (t, 2H, J=5 Hz, DMTOCH<sub>2</sub>), 3.59-3.62 (m, 2H, CH<sub>2</sub>CH<sub>2</sub>OH), 3.67-3.78 (m, 12H, OCH<sub>2</sub>CH<sub>2</sub>O), 3.80 (s, 6H, OCH<sub>3</sub>), 6.82-6.85 (m, 4H, arom H), 7.21-7.49 (m, 9H, aromH).

### 3.2 Further Experiments

#### 4-(6-(4-(bis(4-methoxyphenyl)(phenyl)methoxy)tetra(ethylene glycol) (2-cyanoethyl) diisopropylphosphoramidite (3)

To a solution of **2** (0.496 g 1.00 mmol) dissolved in  $\text{CH}_2\text{Cl}_2$  (7 mL) were added DIPEA (226  $\mu\text{L}$ , 1.75 mmol) and a solution of 2-cyanoethyl-*N,N*-diisopropylchlorophosphoramidite (0.71 g, 3.00 mmol) which were previously dissolved in 4ml of  $\text{CH}_2\text{Cl}_2$ . The mixture was stirred for 1 h. The reaction was concentrated and the residue was purified by column chromatography (hexane/ethyl acetate/ $\text{NEt}_3$  2:1:2%). The product was obtained in 55% yield (0.383 g).  $^1\text{H}$  NMR ( $\text{CDCl}_3$ , ppm) 1.15-1.19 (2d, 12H,  $\text{CH}(\text{CH}_3)_2$ ), 2.61 (t, 2H,  $J=6$  Hz,  $\text{CH}_2\text{CN}$ ) 3.22 (t, 2H,  $J=5$  Hz,  $\text{DMTOCH}_2$ ), 3.67-3.79 (m, 24H,  $\text{OCH}_3$ ,  $\text{OCH}_2\text{CH}_2\text{O}$ ,  $\text{CH}_2\text{OP}$ ,  $\text{POCH}_2\text{CH}_2\text{CN}$ ,  $\text{NCH}(\text{CH}_3)_2$ ), 6.81-6.83 (m, 4H, arom H), 7.21-7.49 (m, 9H, aromH);  $^{31}\text{P}$  NMR ( $\text{CDCl}_3$ , ppm) 148.6.

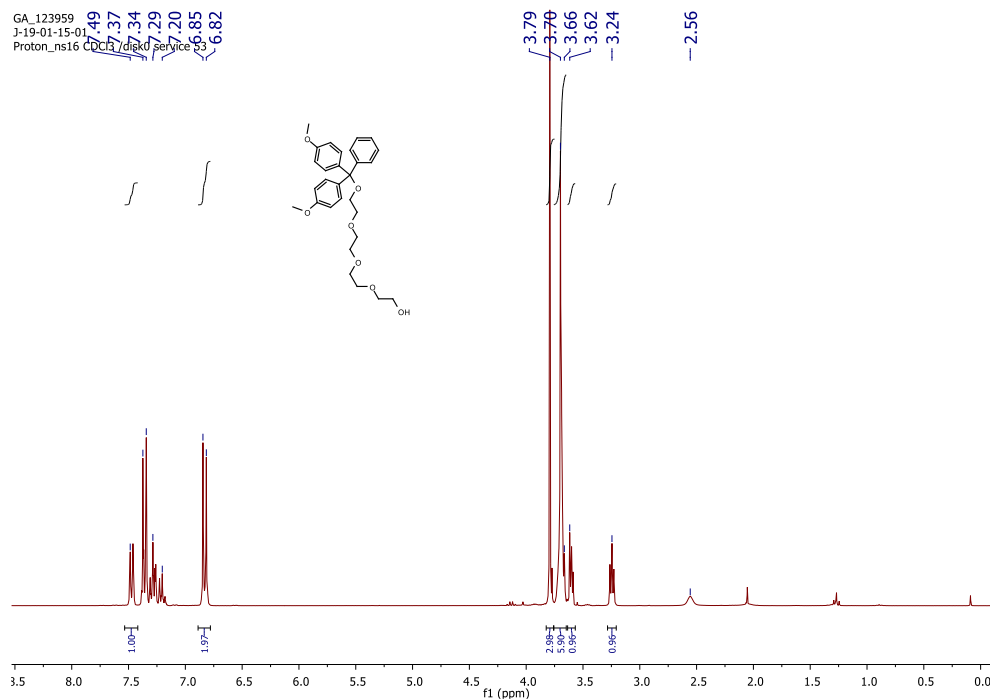


Figure 51.  $^1\text{H}$  NMR of compound **2** in  $\text{CDCl}_3$ .

### 3.2 Further Experiments

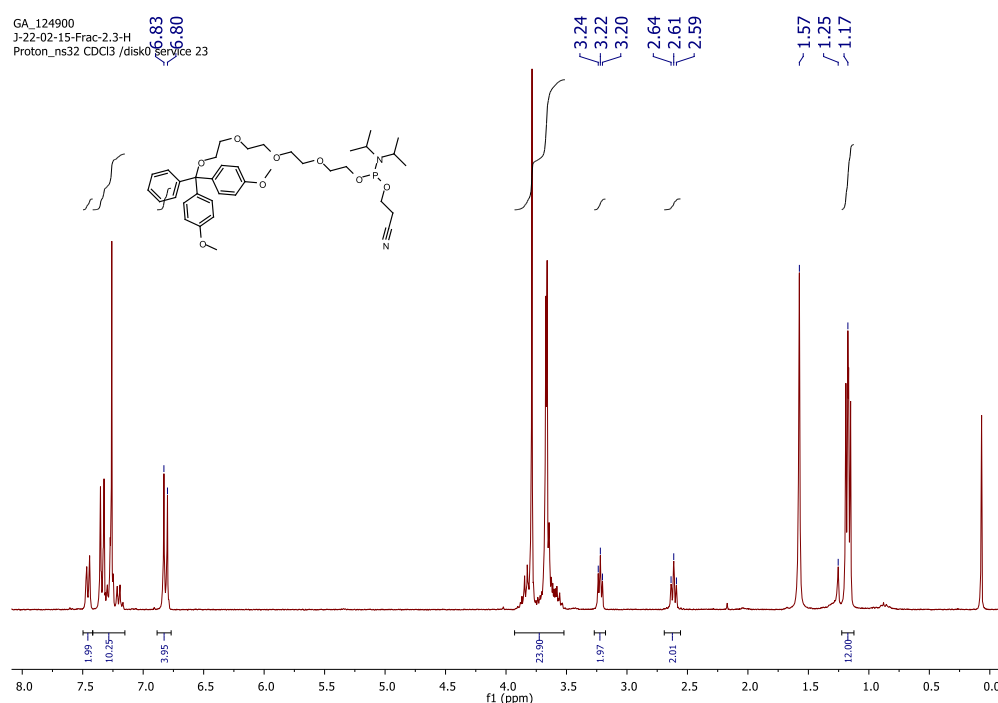


Figure 52. <sup>1</sup>H NMR of compound 3 in CDCl<sub>3</sub>.

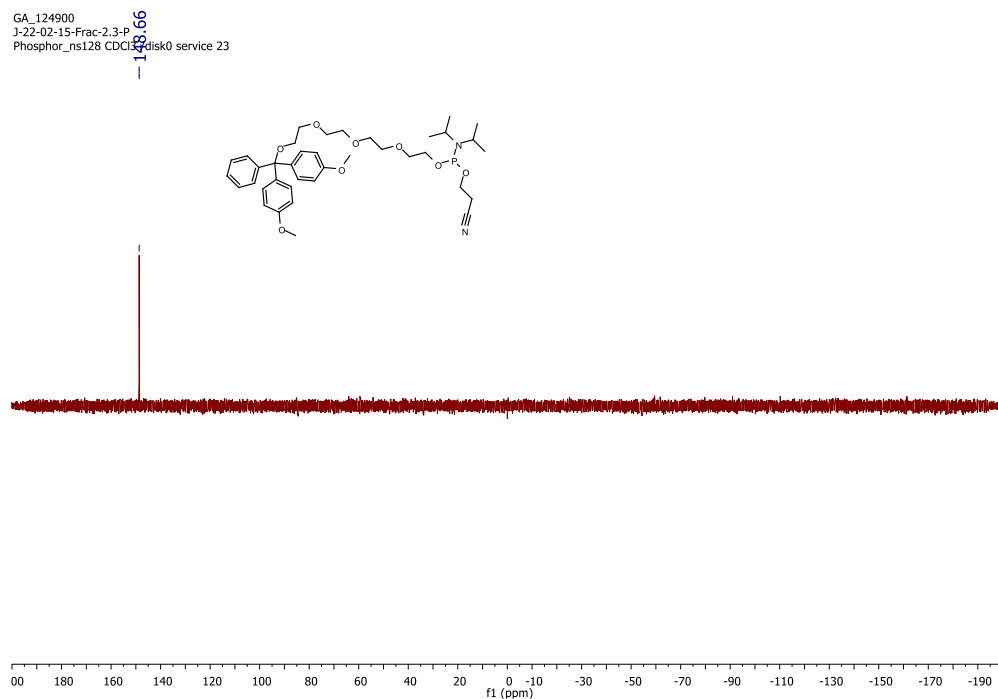


Figure 53. <sup>31</sup>P NMR of compound 3 in CDCl<sub>3</sub>.

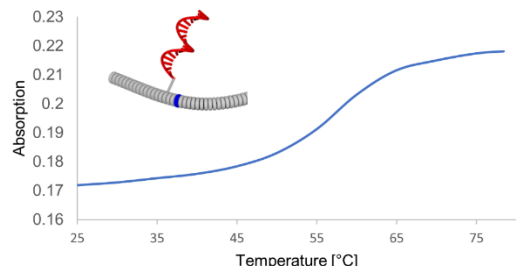
#### 3.2.4.3 Spectra of $T_m$ Measurements

**Table 11.** Summary of melting temperatures.

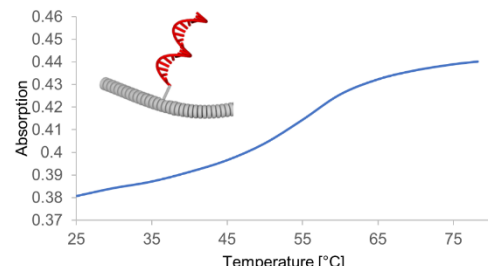
Figure	Oligomers (conc.)
l)	A, N (0.5 $\mu$ M, 15 nM)
m)	A, L (0.5 $\mu$ M, 15 nM)
n)	A, M (0.5 $\mu$ M, 15 nM)
o)	A, N, H (0.5 $\mu$ M, 15 nM, 15 nM)
p)	A, L, H (0.5 $\mu$ M, 15 nM, 15 nM)
q)	A, M, H (0.5 $\mu$ M, 15 nM, 15 nM)

a) Melting temperatures of different complexes and hybrids. The cooling ramp was measured with a rate of 0.3 °C/min. Absorbance was recorded at 250 nm. Conditions: 10 mM sodium phosphate buffer, pH 7.2, 120 mM of NaCl.

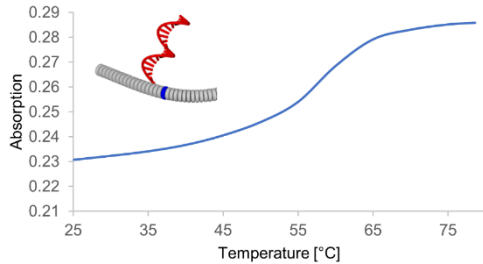
l)



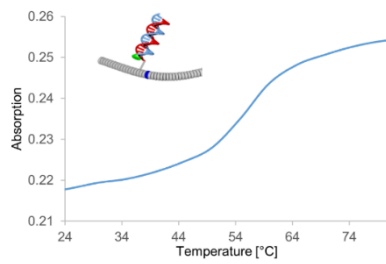
m)



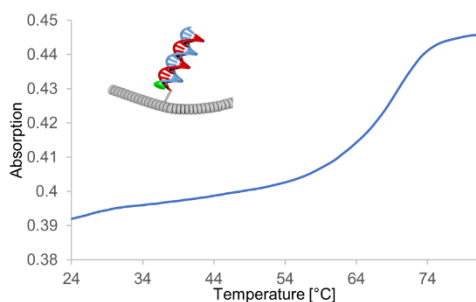
n)



o)



p)



q)

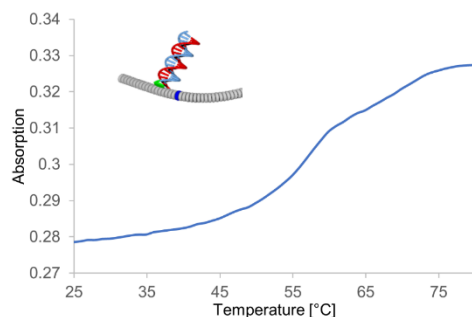


**Figure 54.** Melting curves of complexes: l) A and N; m) A and L; n) A and M; o) A, N and H; p) A, L and H; q) A, M and H; Condition: see Table 11.3.3 Integration of DNA-Modified Gold Nanoparticles into Supramolecular Polymers

### 3.3 Integration of DNA-Modified Gold Nanoparticles into Supramolecular Polymers

#### 3.3.1 Introduction

Gold nanoparticles (Au-NP) are commonly used for decoration of DNA nanostructures<sup>[21-22, 59]</sup>, in drug delivery<sup>[101]</sup> or in detecting DNA arrays<sup>[102]</sup>. Recently, in our group as well as in the Kieltyka group DNA-functionalized AuNPs were introduced along the supramolecular polymers.<sup>[21-22]</sup> The AuNPs were reversibly loaded on the supramolecular platform containing complementary sequence to the AuNP-functionalized one by DNA hybridization. Figure 55 illustrates functionalization of DNA-grafted SPs with AuNPs.<sup>[22]</sup> The DNA-grafted SPs were assembled from seven 2,7-pentynyl pyrene units attached to 10 nucleotide long oligonucleotide. Subsequent AuNPs immobilization along the both edges of the helical polymer is visualized by TEM microscopy.

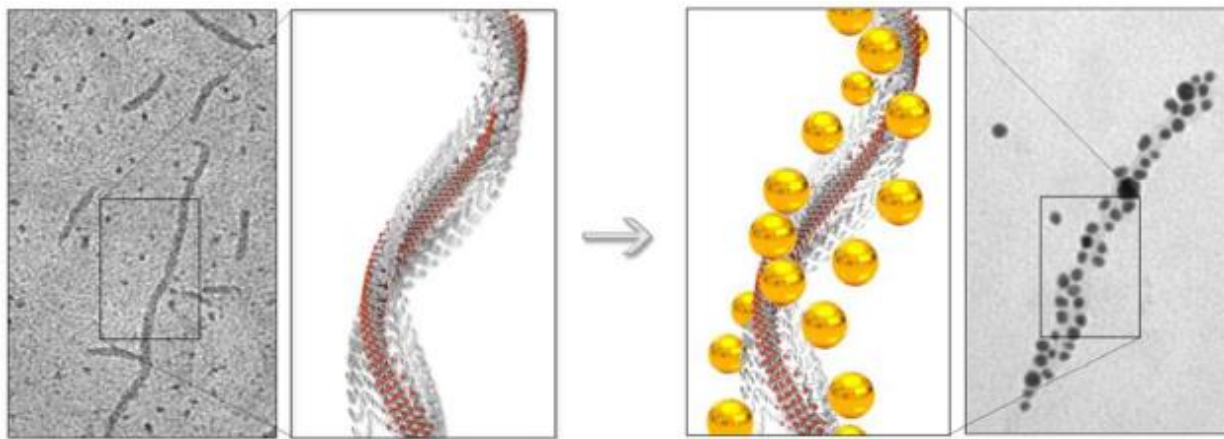


**Figure 55.** Functionalization of the DNA-grafted SPs with AuNPs. Taken from [22].

In this study, the incorporation of the AuNP-functionalized DNA into SPs is demonstrated. For this purpose AuNPs with an average height of 20 nm were prepared by the citrate reduction method (Supporting Information), followed by incubation with thiol-modified oligonucleotides in order to afford DNA-conjugated AuNPs. Such conjugates were mixed with oligomeric building blocks and self-organize into AuNP-functionalized SPs that reach a length of several micrometers. The self-assembly of the different components into AuNP-functionalized SPs is illustrated in Figure 56.

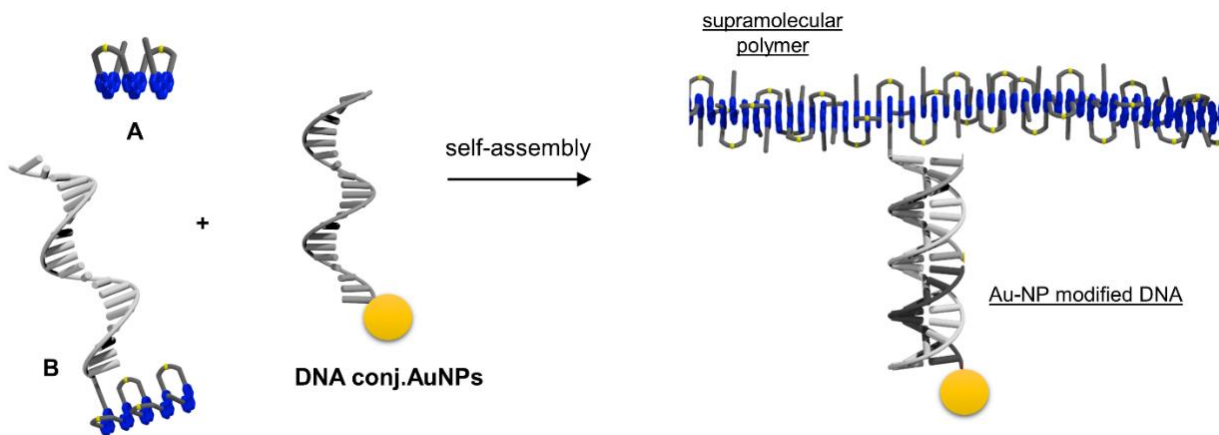


**Figure 56.** Illustration of the gold nanoparticles immobilization on the fibrillar supramolecular polymer.

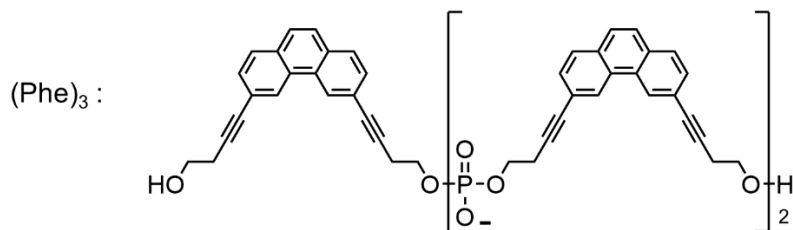
### 3.3.2 Results

#### 3.3.2.1 DNA Sequences

Table 12 shows the oligomers used in this work. Oligomer **A** and **B** self-assemble into DNA-appended supramolecular polymers. The supramolecular polymerization process is previously described in 3.1.3 Results. AuNPs were prepared by citrate reduction method, followed by conjugation with excess of thiolated DNA to ensure densely grafted AuNPs (3.3.4 Supporting Information). In this work synthesized Au-NPs were conjugated with DNA and amenable to sequence-specific hybridization with DNA-appended SPs.

**Table 12.** Top: DNA sequences of oligomers used in this studies, bottom: chemical structure of the phenanthrene building block.

Oligomer	Sequence
<b>A</b>	(Phe) <sub>3</sub>
<b>B</b>	(Phe) <sub>5</sub> - GAA GGA ACG TAG CCT GGA AC - 5'
<b>T</b>	5' - CTT CCT TGC ATC GGA CCT TG – (CH <sub>2</sub> ) <sub>6</sub> - S - Au



#### 3.3.2.2 Arrangements of Gold Nanoparticles

In a previous studies it was demonstrated that SPs composed of oligomer **A** (0,5 μM) and 15 nM **B**, which translaes into 3% of oligomer **B** relative to oligomer **A**, results in several micrometers long supramolecular platform accessible for further functionalization (Figure

16, 3.1.3 Results).<sup>[103]</sup> Herein, such DNA-appended supramolecular polymers are used for the alignment of AuNPs along the polymer.

Self-assembly experiments were typically carried out by mixing oligomer **A** (3  $\mu$ M) and 3% of oligomer **B** (0.09  $\mu$ M) with the excess (0.45  $\mu$ M) of DNA-labeled AuNP (**T**) in sodium phosphate buffer (10 mM, pH 7.2) in the presence of NaCl (120 mM). The oligomeric building blocks self-organize upon heating to 80 °C and cooling to room temperature over 3 hours resulting in AuNPs aligned along the supramolecular polymer (Figure 57).

A three-fold excess in AuNPs (0.45  $\mu$ M) ensured improved loading (Figure 57, right). AuNPs revealed uniform shape with an average height of 15-20 nm (Figure 58).

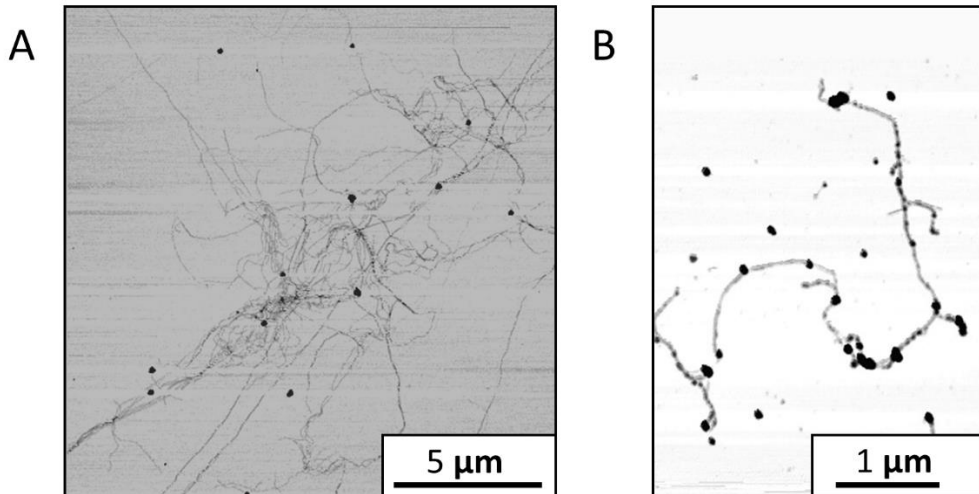


**Figure 57.** AFM images of the supramolecular polymers loaded with Au-NPs. Used concentrations for assembly of SPs; left: oligomer **A** (3  $\mu$ M), **B** (90 nM), **T** (150 nM); right: oligomer **A** (3  $\mu$ M), **B** (90 nM), and **T** (450 nM) in 10 mM sodium phosphate buffer, pH 7.2, 120 mM NaCl.

To ensure densely decorated SPs, initially used conditions were modified. SPs were self-assembled from oligomer **A** (3  $\mu$ M) and 0.45  $\mu$ M **B**, which translates into 15% of **B** relative to **A**. As a result higher AuNPs density was observed (Figure 58).

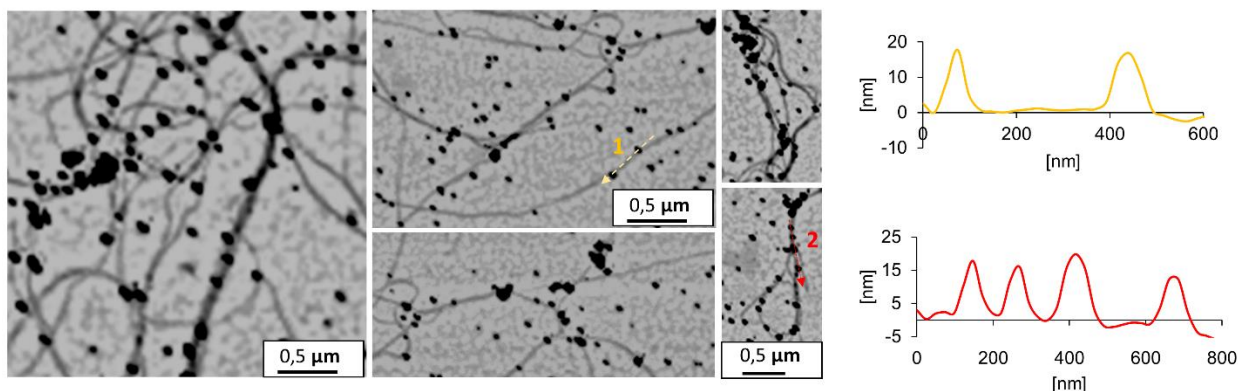


**Figure 58.** AFM images of the Au-NP modified DNA integrated into supramolecular polymer and the cross-sections profiles. Conditions: oligomer **A** (3  $\mu$ M), **B** (0.45  $\mu$ M), **T** (0.9  $\mu$ M) in 10 mM sodium phosphate buffer, pH 7.2, 120 mM NaCl.

### 3.3.3 Conclusions and outlook

In conclusion, we have demonstrated self-assembly of multicomponent SPs. In such hybrids we are merging DNA-functionalized supramolecular polymers with gold nanoparticles. The reversibility of DNA hybridization and pronounced stimulus-responsiveness of the SPs allows to design uniquely adaptive/tunable systems that can be used as a cargo for the delivery of nanoparticles but also small molecules and proteins.

### 3.3.4 Supporting Information

#### 3.3.4.1 Synthesis of Gold Nanoparticles

Citrate reduction method was used for the synthesis of 20 nm (in height) AuNPs. As a co-reductant tannic acid was used.<sup>[104]</sup> 100 ml of 0.3 mM chloroauric acid was refluxed. 2 ml of 1% citric acid and 7 ml of 1% tannic acid was added. The color of the solution changed to burgundy, it was left refluxed for another 3 min and cooled then to room temperature. Afterwards the AuNPs solution was filtered through a syringe filter with a pore size of 0.2  $\mu$ m. More stable phosphine ligands were used to exchange the citrate shell in the citrate coated nanoparticles. Thus, 11 mg of BSPP (bis(p-sulfonatophenyl) - phenylphosphine dipotassium salt) was added to 10 ml of the AuNPs solution and was shaken overnight at

low speed. AuNPs were precipitated by slowly adding solid NaCl until the color changed from red to gray-blue. The solution was centrifuged for 15 min at 4400 rpm and the supernatant was removed. The AuNPs were resuspended in 500  $\mu$ l of an aqueous 0.5 mM BSPP solution. The centrifugation and resuspension were repeated twice. For the concentration determination, photometric analysis at 520 nm was performed (assuming a molar extinction coefficient for the AuNP of  $1 \cdot 10^7 \text{ M}^{-1} \cdot \text{cm}^{-1}$ ).

### 3.3.4.2 AuNPs-DNA conjugation

One part of commercially available thiol-modified oligonucleotide was mixed with 17 parts of freshly synthesized AuNPs in a  $0.5 \times$  TBE buffer (Tris base, boric acid, EDTA, pH 8.0). The mixture was incubated for 36 hours at 20 °C. The centrifugation and resuspension was used in order to remove excess of oligonucleotides. The concentration was determined at 520 nm (assuming a molar extinction coefficient for the AuNP of  $1 \cdot 10^7 \text{ M}^{-1} \cdot \text{cm}^{-1}$ ).

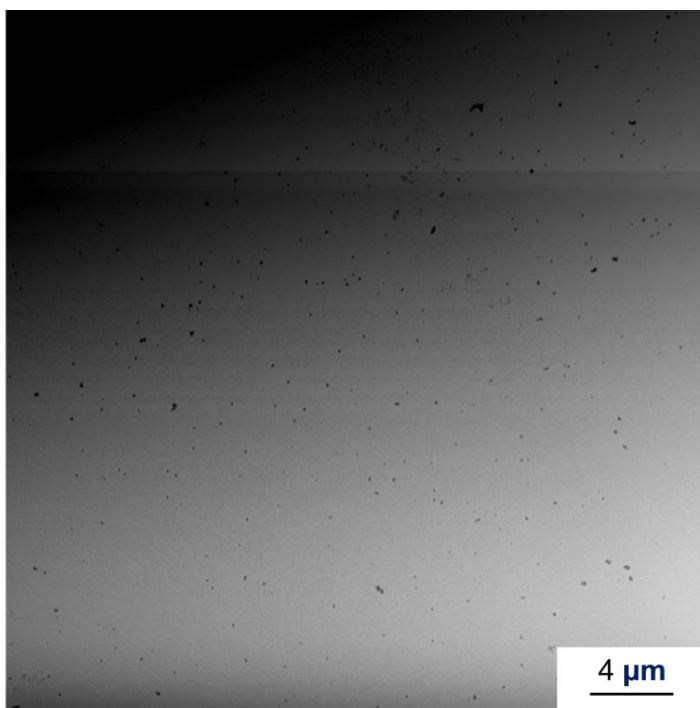


**Figure 59.** AFM image of the Au-NP modified DNA. Conditions: T (150 nM) in 10 mM sodium phosphate buffer, pH 7.2, 120 mM NaCl.

## 4 Self-Assembly and Aggregation-Induced Emission Properties of a Dialkynyl-Tetraphenylethylene Oligophosphate

### 4.1 Introduction

The construction of luminescent organic nanostructures received recently lots of attention.<sup>[105]</sup> Tang's group has presented a series of fluorophores which are almost non-emissive in the disassembled state but highly emissive in the aggregated state. [106-107] Such aggregation-induced emission (AIE) properties are exhibited by a certain class of fluorophores with a unique structure. Aggregated state is a result of restriction of the intramolecular rotational motions, and radiative decay is the main decay channel leading to the highly emissive state.<sup>[108]</sup> Propeller-shaped AIE molecules exhibit limited aggregation through π-π stacking.<sup>[109]</sup> Opposite to AIE in aggregation-caused quenching (ACQ) typical fluorophores have planar aromatic structure (e.g. perylene). For typical AIE luminogens (AI Egens) belongs molecules like tetraphenylethylene (TPE), hexaphenylsilole (HPS) or distyrylanthracene (DSA), which are demonstrated in Figure 60.<sup>[110]</sup> HPS is one of the first discovered AIE-active compound that is non-emissive in solution but highly emissive in aggregates (Figure 61). The incorporation of such fluorogens into polymer architectures result in the formation of functional luminescent materials. [111-113]

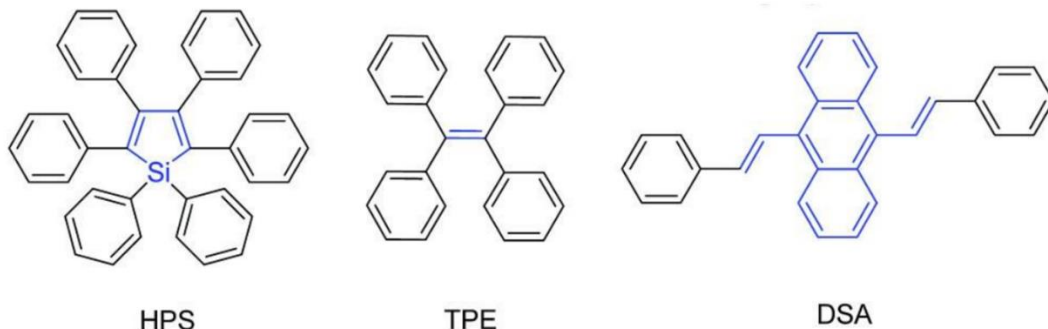


**Figure 60.** Examples of typical AI Egens. Taken from <sup>[110]</sup>.

#### 4 Self-Assembly and Aggregation-Induced Emission Properties of a Dialkynyl-Tetraphenylethylene Oligophosphate

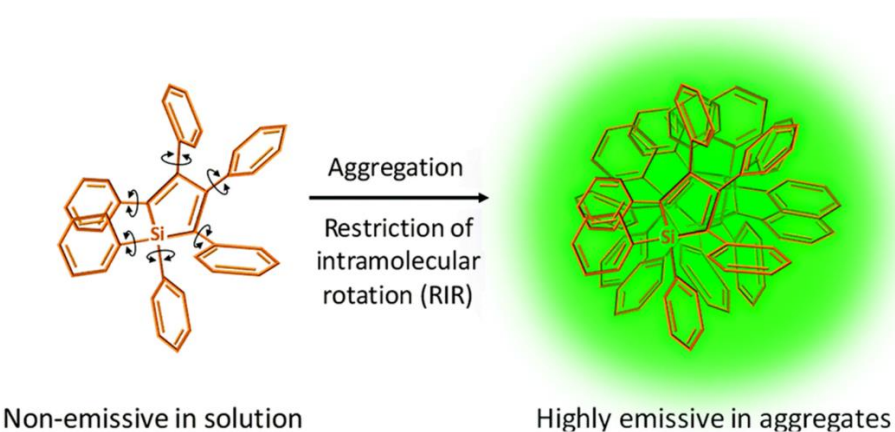


**Figure 61.** Illustration of AIE-active hexaphenylsilole. Taken from [108]

AIE-active compounds [114] and polymers [115-116] with stimuli-responsiveness for temperature, pH, light, forces, or solvents were intensively investigated. In our group, we have reported the control of AIE by hybridization of dialkynyl-tetraphenylethylene (DATPE) modified DNA strands (Figure 62). AIE features are of interest in diverse areas including fluorescence sensors and OLEDs.<sup>[118-119]</sup> Such luminophores are often used in physiological environments or aqueous media and are promising candidates for diagnostic probes.<sup>[120]</sup>

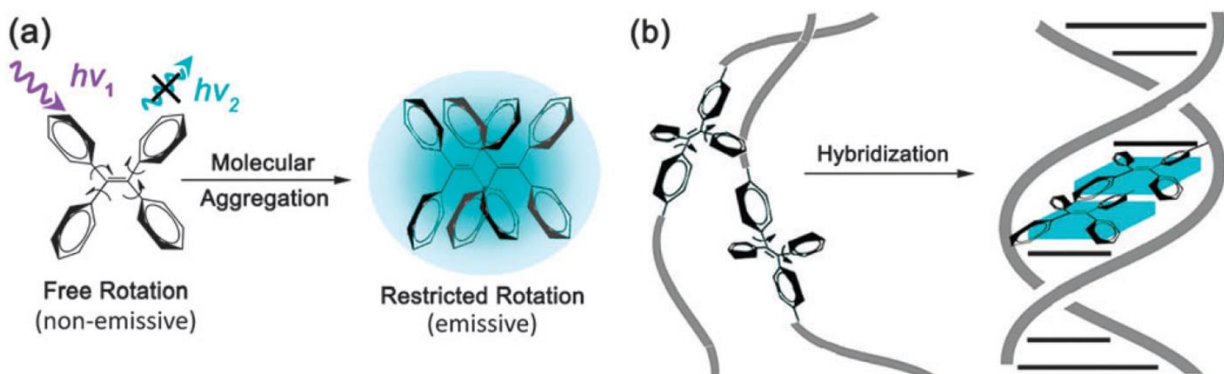


**Figure 62.** DATPE-modified DNA conjugates which exhibit AIE. Taken from [117].

Design, synthesis and control of self-assembly process of AIE-active supramolecular polymers is the main challenge in this studies.

## 4.2 Results

### 4.2.1 Oligomer Synthesis

Oligomer **1** is composed of three *Z*-dialkynyl-tetraphenylethylene (DATPE) units (Figure 63) linked via phosphodiesters and was partially synthesized according to previously described procedure.<sup>[117]</sup> Firstly, dibromotetraphenylethylene was prepared by reductive coupling of carbonyls to olefins and afforded a mixture of *E*- and *Z*-TPE isomers.<sup>[121]</sup> Next, alkynyl-linkers were introduced by a Sonogashira reaction. The two stereoisomers were separated by column chromatography. *Z*-DAPTE diol was used for the DMT-protection followed by conversion into the phosphoramidite. The trimer was synthesized by solid phase synthesis using a CPGs-TPE-modified solid support, purified by RP-HPLC and characterized by MS-ESI (4.4 Supporting Information).

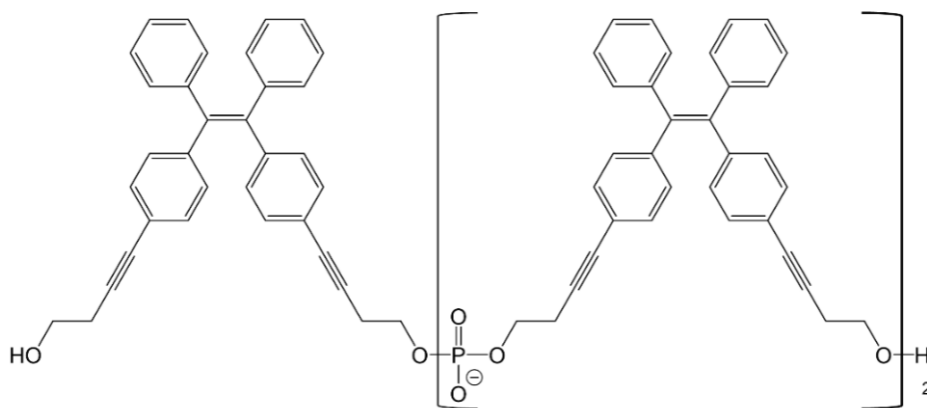


**Figure 63.** The phosphodiester-linked *Z*-DATPE trimer (**1**).

### 4.2.2 Photophysical Properties

The polarity of the solvent has a significant influence on the AIE-active fluorophores. In ‘poor’ solvent like ethanol, oligomer **1** is nearly non-emissive (Figure 64) due to the free rotation of C(sp<sup>2</sup>)–C(sp<sup>2</sup>) bonds of TPE. Addition of ‘good’ solvent promotes the AIE-effect (restricted rotational motion) resulting in the formation of a new fluorescence emission

band between 400-650 nm. The maximum of the emission is centered around 490 nm ( $\lambda_{\text{ex.}}$ : 335 nm).

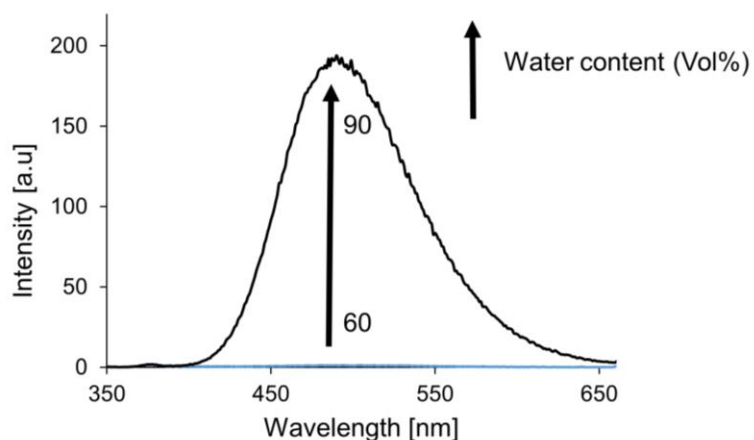


**Figure 64.** Fluorescence spectra of oligomer **1** in EtOH / water mixtures with different contents of water (black: 10 vol% EtOH, blue: 60 vol% EtOH). Concentration of oligomer **1**: 1  $\mu$ M, 10mM sodium phosphate buffer pH 7.2, 20 vol% EtOH, RT,  $\lambda_{\text{ex.}}$ : 335 nm.

Changes in AIE with the variation of the water / ethanol ratio are demonstrated in Figure 65. The minimal water content in which oligomer **1** aggregates is around 70vol%. With the additional increase of water content, the fluorescence emission is greatly enhanced. Based on this results, a mixed solvent system composed of a buffered system with ethanol (20 vol%) and aqueous sodium phosphate buffer pH 7.2 (80 vol%) was further used to analyze the AIE properties of **1**.

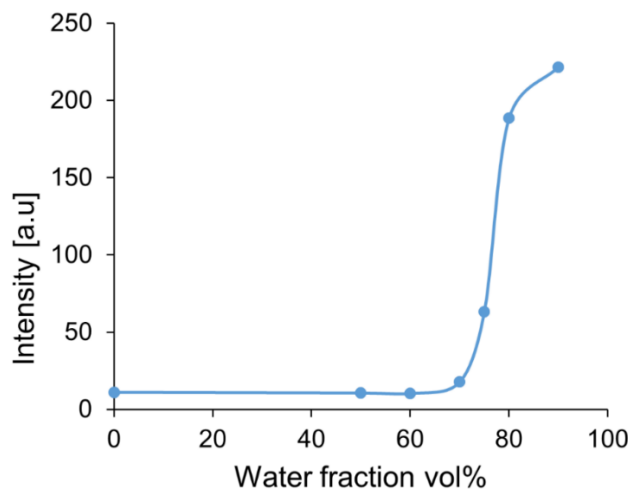


**Figure 65.** Changes in the fluorescence intensity of oligomer **1** with variation of the water / EtOH ratio. Concentration of oligomer **1**: 1  $\mu$ M, 10mM sodium phosphate buffer pH 7.2,  $\lambda_{\text{ex}}$ : 335 nm.

#### 4.2.3 Temperature Dependent AIE

Figure 66 shows the temperature dependent absorption spectrum of oligomer **1** in aqueous medium and ethanol. A distinct blue shift of the tetraphenylethylene absorption maximum band from  $\lambda_{\text{abs}}= 334 \text{ nm}$  at  $20 \text{ }^{\circ}\text{C}$  to  $\lambda_{\text{abs}}= 326 \text{ nm}$  at  $70 \text{ }^{\circ}\text{C}$  is observed. Additionally, the band around  $\lambda_{\text{abs}}= 260 \text{ nm}$  shows changes in intensity.

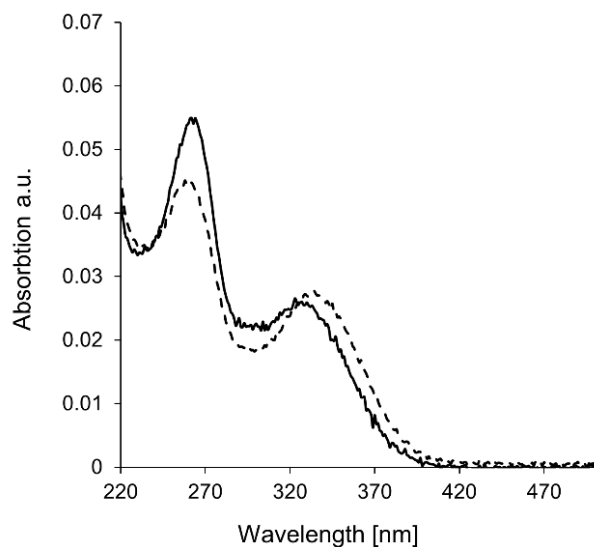


**Figure 66.** UV-Vis spectra of the aggregated ( $20 \text{ }^{\circ}\text{C}$ , dashed) and disassembled ( $70 \text{ }^{\circ}\text{C}$ , solid curve) state. Concentration of oligomer **1**: 1  $\mu$ M, 10mM sodium phosphate buffer pH 7.2, 20 vol% EtOH.

#### 4 Self-Assembly and Aggregation-Induced Emission Properties of a Dialkynyl-Tetraphenylethylene Oligophosphate

Temperature dependent fluorescence spectra of **1** ( $[1] = 1 \mu\text{M}$ ) are shown in Figure 67. Oligomer **1** shows high fluorescence emission at  $20^\circ\text{C}$  (solid curve). Heating of the solution to  $70^\circ\text{C}$  decreases the fluorescence emission completely (dashed curve). The following controlled cooling of the solution ( $1^\circ\text{C}/\text{min}$ ) results in nearly non-emissive self-assembled state.

Initial high fluorescence emission is a result of the AIE activated state with the restriction in the rotation of the intramolecular  $\text{C}(\text{sp}^2)-\text{C}(\text{sp}^2)$  bonds of DATPE molecules. Disassembled state at  $70^\circ\text{C}$  shows no fluorescence. Surprisingly, the fluorescence of the solution does not return to its original state upon controlled cooling. Highly probably, formed supramolecular polymers lack enhanced fluorescence emission due to free intermolecular motion of the TPE groups. Heating – cooling curves of oligomer **1** (4.4 Supporting Information) indicate that the assembly takes place in the temperature range between  $60$  and  $50^\circ\text{C}$ .

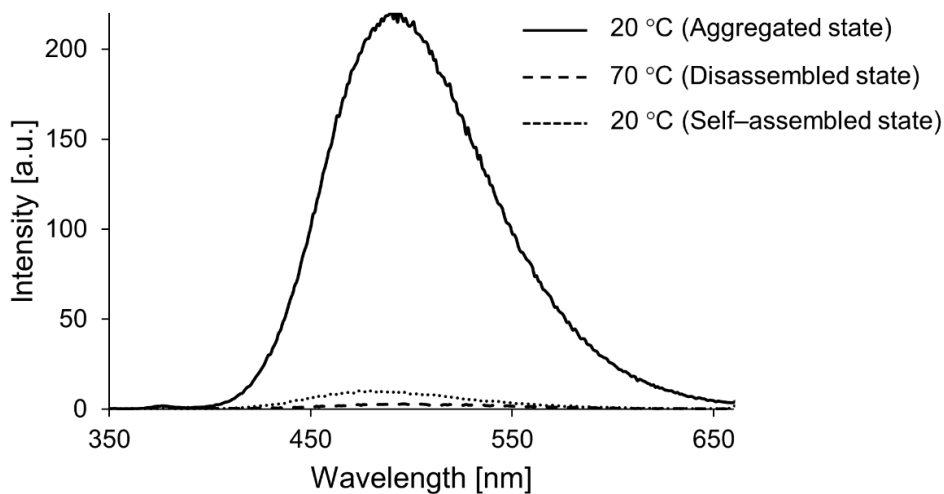


**Figure 67.** Fluorescence spectra of aggregated state:  $20^\circ\text{C}$  (solid curve), disassembled state:  $70^\circ\text{C}$  (dashed curve) and self-assembled:  $20^\circ\text{C}$  (dotted curve); self-assembly was performed with slow cooling ( $1^\circ\text{C}/\text{min}$ ) from  $70^\circ\text{C}$  to  $20^\circ\text{C}$ . Conditions: oligomer **1** ( $1 \mu\text{M}$ ),  $10 \text{ mM}$  sodium phosphate buffer, pH 7.2, 20 vol% EtOH,  $\lambda_{\text{ex.}}$ :  $335 \text{ nm}$ .

In case of higher concentrated solution ( $[1] = 10 \mu\text{M}$ ) only partial quenching of the fluorescence emission is observed upon heating to  $70^\circ\text{C}$  (Figure 68). Nevertheless, controlled cooling ( $1^\circ\text{C}/\text{min}$ ) results in a significant decrease in fluorescence emission with a blue shift in the fluorescence maximum from  $490 \text{ nm}$  at  $70^\circ\text{C}$  to  $475 \text{ nm}$  at  $20^\circ\text{C}$ .

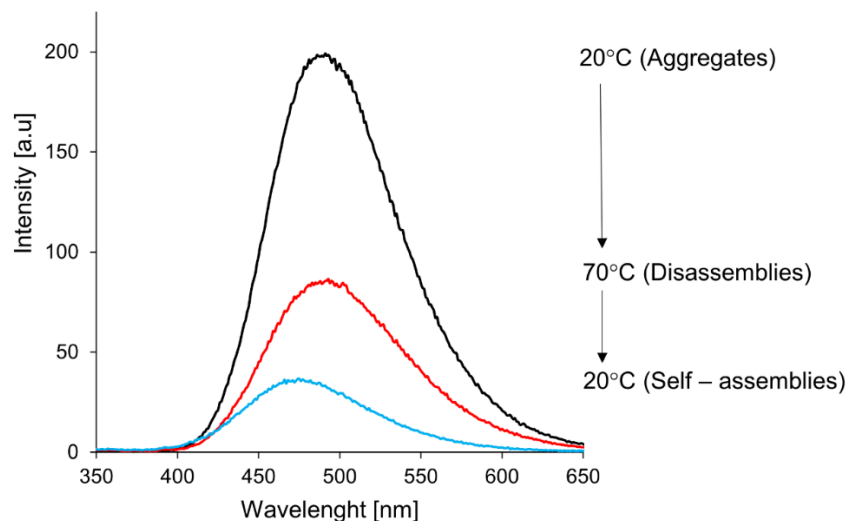


**Figure 68.** Fluorescence spectra of aggregated state:  $20^\circ\text{C}$  (black curve), disassembled state:  $70^\circ\text{C}$  (red) and self-assembled:  $20^\circ\text{C}$  (blue); self-assembly was performed with cooling ( $1^\circ\text{C}/\text{min}$ ) from  $70^\circ\text{C}$  to  $20^\circ\text{C}$ . Conditions: oligomer **1** ( $10 \mu\text{M}$ ),  $10 \text{ mM}$  sodium phosphate buffer, pH 7.2, 20 vol% EtOH,  $\lambda_{\text{ex.}}$ :  $335 \text{ nm}$ .

#### 4.2.4 AFM Images

The aggregated and the self-assembled state of **1** is visualized by the AFM (Figure 69). In order to obtain aggregated state, the solution ( $[1] = 1 \mu\text{M}$ ) was adsorbed on the APTES-modified mica sheet for two minutes, washed with water and dried. AFM images revealed big aggregates with a height ranging from  $10 - 40 \text{ nm}$  and non-uniform shape (Figure 69, top).

The same solution was used for the formation of the self-assemblies. After heating to  $70^\circ\text{C}$  and controlled cooling ( $1^\circ\text{C}/\text{min}$ ) to  $20^\circ\text{C}$  the sample for AFM analysis was prepared in the same way as described above for the aggregated state. Self-assembly process leads to the formation of spherical objects ( $5 - 6 \text{ nm}$  in height) with uniform shape and the size ranging from:  $120 - 160 \text{ nm}$  (Figure 69, bottom).

#### 4 Self-Assembly and Aggregation-Induced Emission Properties of a Dialkynyl-Tetraphenylethylene Oligophosphate

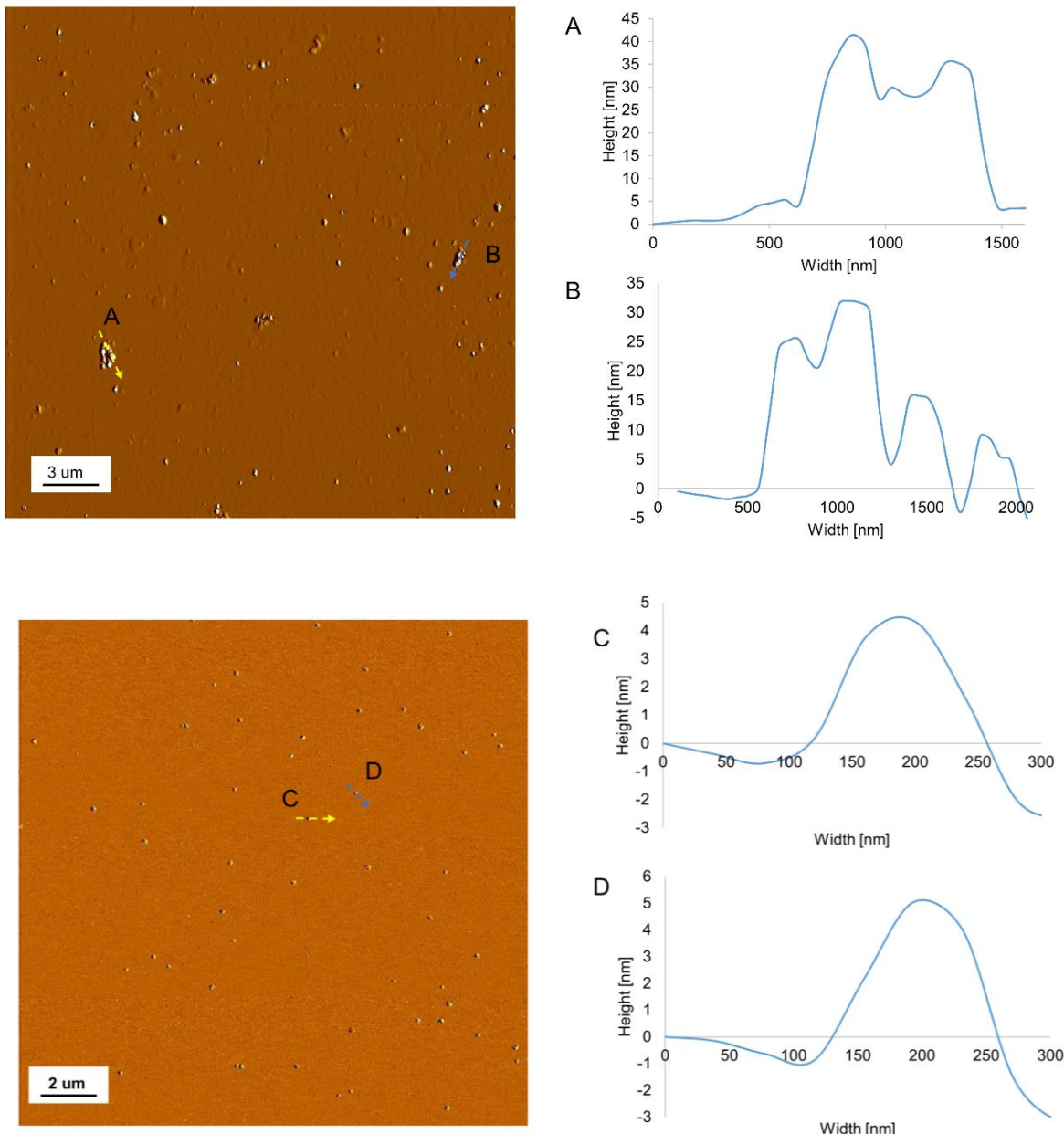


**Figure 69.** AFM images of the oligomer **1** in the aggregated state (top left) and in the self-assembled state (bottom left). Self-assembly results in spherical nanoparticles. Self-assembly was performed with slow cooling ( $1^{\circ}\text{C}/\text{min}$ ) from  $70^{\circ}\text{C}$  to  $20^{\circ}\text{C}$ . Conditions: oligomer **1** ( $1 \mu\text{M}$ ),  $10 \text{ mM}$  sodium phosphate buffer, pH 7.2, 20 vol% EtOH.

Self-assembly of oligomer **1** with increased concentration ( $[1] = 10 \mu\text{M}$ ) in above mentioned conditions leads to similar results (Figure 70) (size and shape of the vesicles) like in case of 10-times lower concentration of **1** (Figure 69, bottom).

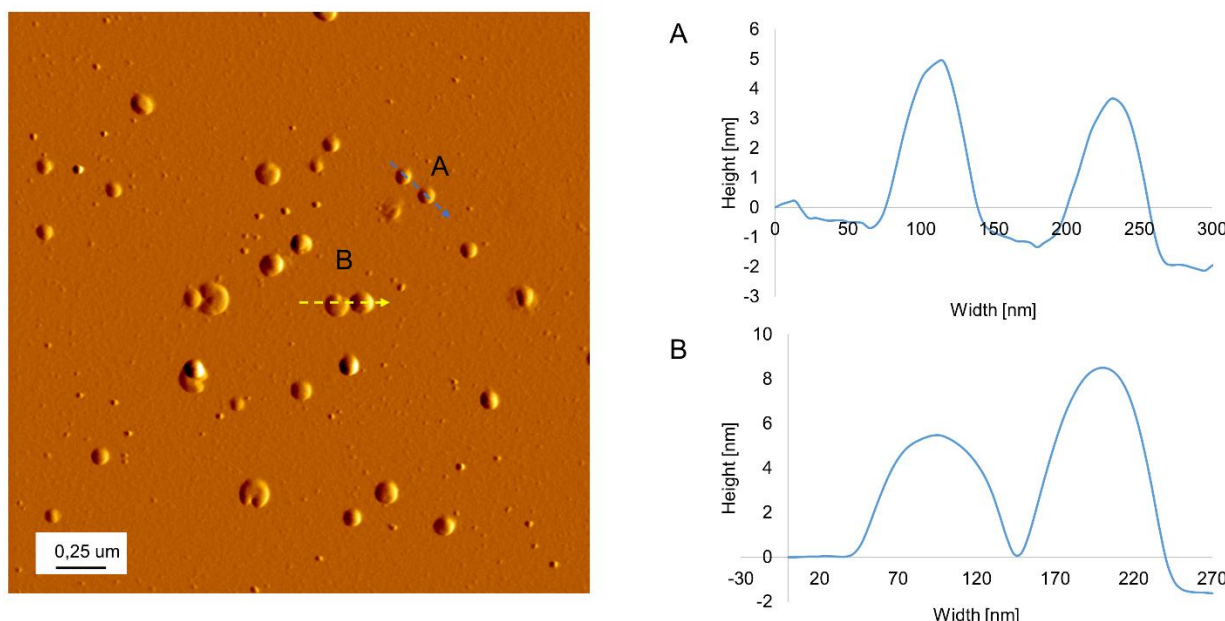


**Figure 70.** AFM images and cross-section profiles of the self-assembled oligomer **1**. Self-assembly was performed with slow cooling ( $1^\circ\text{C}/\text{min}$ ) from  $70^\circ\text{C}$  to  $20^\circ\text{C}$ . Conditions: oligomer **1** ( $10 \mu\text{M}$ ),  $10 \text{ mM}$  sodium phosphate buffer, pH 7.2, 20 vol% EtOH,

### 4.3 Conclusions

As a conclusion, it was possible to successfully synthesize, purify and characterize the phosphodiester-linked dialkynyl-tetraphenylethylene (DATPE) trimer (**1**). Oligomer **1** is a weak emitter when it is molecularly dissolved in ethanol. However, addition of the ‘good’ solvent (water) leads to aggregation-induced emission. The self-assembly of **1** results in spherical supramolecular polymers with a uniform shape. In contrast to the AIE-active random aggregates, formation of the TPE-SPs resulted in almost non-emissive polymers. The self-assembly of **1** with increased concentration leads to the same spherical morphology with slightly improved AIE-properties. Disassembled aggregates exhibit no AIE activity due to the free intramolecular  $\text{C}(\text{sp}^2)-\text{C}(\text{sp}^2)$  bond rotation. High fluorescence

emission of the molecularly aggregated state is a consequence of the restriction in the intramolecular C(sp<sup>2</sup>)–C(sp<sup>2</sup>) bond rotation.

## 4.4 Supporting Information

### 4.4.1 Oligomers Synthesis

CPGs-TPE-modified solid support was used for the synthesis of oligomer **1**. The Z-TPE-phosphoramidite building block for solid phase synthesis was prepared according to the previously published procedure.<sup>[117]</sup> Cleavage from the solid support was achieved with 1 ml of 30% NH<sub>4</sub>OH (aq) at 55 °C over 16 hours. After washing 2 times with EtOH/H<sub>2</sub>O (1:1 mixture) the supernatant was separated by centrifugation and lyophilized. The final trimer **1** was eluted with Reprosil 100 RP18 column, 5 µm (Dr. Maisch GmbH, Ammerbuch, Germany) with 0.1 M ammonium acetate buffer (eluent A) and acetonitrile (eluent B). A gradient from 60-100% eluent B within 15 min was performed.

### 4.4.2 Mass Spectra of Oligomer 1

**Table 13:** Calculated and experimental mass of oligomer **1**.

Oligomer	Molecular formula	Calc. mass	Exp. mass
<b>1</b>	C <sub>102</sub> H <sub>82</sub> O <sub>10</sub> P <sub>2</sub>	1528.53 Da	763.76 (z = 2)

#### 4 Self-Assembly and Aggregation-Induced Emission Properties of a Dialkynyl-Tetraphenylethylene Oligophosphate

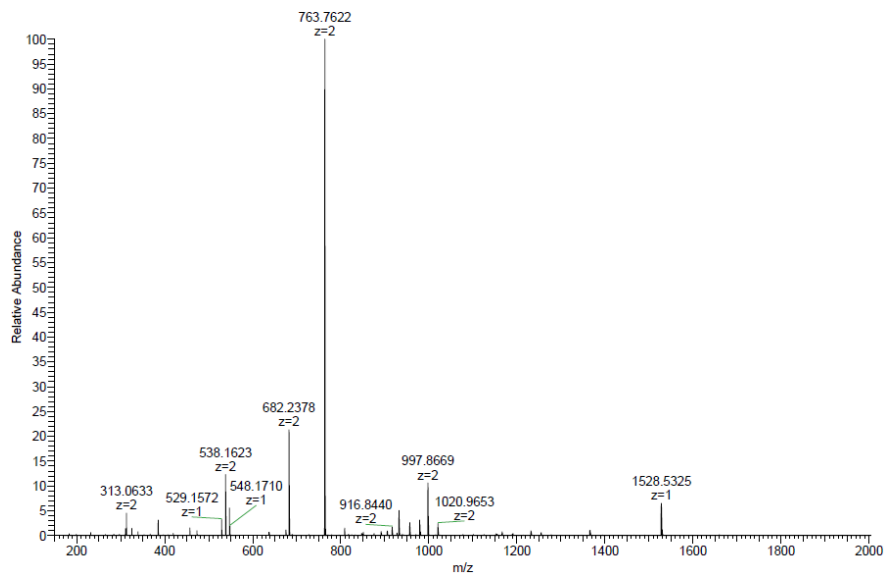


**Figure 71.** ESI-MS analysis of oligomer 1.

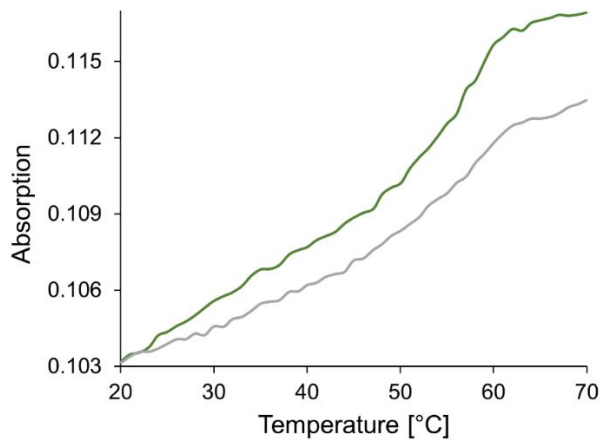


**Figure 72.** Heating–cooling curve of oligomer 1. Ramp 1: cooling (green), ramp 2: heating (gray). Concentration of oligomer 1: 1  $\mu$ M, 10mM sodium phosphate buffer pH 7.2,  $\lambda_{\text{ex.}}$ : 335 nm. Temperature gradient: 0,3 °C/min. Absorbance was recorded at 250 nm

## 5 References

- [1] T. F. A. de Greef, E. W. Meijer, *Nature* **2008**, *453*, 171-173.
- [2] X. Ma, H. Tian, *Accounts of Chemical Research* **2014**, *47*, 1971-1981.
- [3] T. Aida, E. W. Meijer, S. I. Stupp, *Science* **2012**, *335*, 813-817.
- [4] K. Matyjaszewski, M. Möller, A. H. E. Müller, *Polymer science : a comprehensive reference*. 6, 6, Elsevier, Amsterdam, **2012**.
- [5] T. F. A. De Greef, M. M. J. Smulders, M. Wolffs, A. P. H. J. Schenning, R. P. Sijbesma, E. W. Meijer, *Chemical Reviews* **2009**, *109*, 5687-5754.
- [6] M.M.J. Smulders, M.M.L. Nieuwenhuizen, T.F.A. de Greef, P. van der Schoot, A.P.H.J. Schenning, E.W. Meijer, *Chemistry - A European Journal* **2010**, *16*, 362-367.
- [7] S. P. W. Wijnands, E. W. Meijer, M. Merkx, *Bioconjug Chem* **2019**.
- [8] Y. Vyborna, M. Vybornyi, R. Häner, *J Am Chem Soc* **2015**, *137*, 14051-14054.
- [9] S. P. W. Wijnands, W. Engelen, R. P. M. Lafleur, E. W. Meijer, M. Merkx, *Nature Communications* **2018**, *9*.
- [10] R. R. Sinden, **2012**.
- [11] J. SantaLucia, Jr., D. Hicks, *Annu Rev Biophys Biomol Struct* **2004**, *33*, 415-440.
- [12] D. L. Nelson, M. M. Cox, A. L. Lehninger, *Lehninger principles of biochemistry*, W.H. Freeman, New York, **2013**.
- [13] C. R. Cantor, P. R. Schimmel, *The conformation of biological macromolecules*, W.H. Freeman, New-York, **1980**.
- [14] W. Saenger, *Principles of nucleic acid structure*, Springer, New York, **1984**.
- [15] N. C. Seeman, *Nature* **2003**, *421*, 427-431.
- [16] J. J. Storhoff, C. A. Mirkin, *Chemical reviews* **1999**, *99*, 1849-1862.
- [17] R. R. Sinden, **2012**.
- [18] A. R. Clapp, I. L. Medintz, J. M. Mauro, B. R. Fisher, M. G. Bawendi, H. Mattoussi, *J Am Chem Soc* **2004**, *126*, 301-310.
- [19] G. Tikhomirov, S. Hoogland, P. E. Lee, A. Fischer, E. H. Sargent, S. O. Kelley, *Nature Nanotechnology* **2011**, *6*, 485-490.
- [20] J. R. McMillan, C. A. Mirkin, *J Am Chem Soc* **2018**, *140*, 6776-6779.
- [21] W. E. M. Noteborn, V. Saez Talens, R. E. Kieltyka, *ChemBioChem* **2017**, *18*, 1995-1999.
- [22] Y. Vyborna, M. Vybornyi, R. Häner, *Chemical Communications* **2017**, *53*, 5179-5181.
- [23] C. B. Winiger, S. M. Langenegger, O. Khorev, R. Häner, *Beilstein Journal of Organic Chemistry* **2014**, *10*, 1589-1595.

- [24] S. M. Langenegger, R. Haner, *Chem Commun* **2004**, 2792-2793.
- [25] S. M. Langenegger, R. Haner, *Chembiochem* **2005**, 6, 848-851.
- [26] C. Wagner, H. A. Wagenknecht, *Org Lett* **2006**, 8, 4191-4194.
- [27] W. Wang, W. Wan, H. H. Zhou, S. Niu, A. D. Li, *J Am Chem Soc* **2003**, 125, 5248-5249.
- [28] D. Ackermann, R. Häner, *Helvetica Chimica Acta* **2004**, 87, 2790-2804.
- [29] S. M. Langenegger, R. Häner, *ChemBioChem* **2005**, 6, 2149-2152.
- [30] V. L. Malinovskii, D. Wenger, R. Haner, *Chem Soc Rev* **2010**, 39, 410-422.
- [31] R. Varghese, H.-A. Wagenknecht, *Chem Commun* **2009**.
- [32] H. Kashida, M. Komiya, H. Asanuma, *Chem Lett* **2006**, 35, 934-935.
- [33] S. L. Beaucage, M. H. Caruthers, *Tetrahedron Letters* **1981**, 22, 1859-1862.
- [34] R. W. Sinkeldam, N. J. Greco, Y. Tor, *Chem Rev* **2010**, 110, 2579-2619.
- [35] G. D. Scholes, G. R. Fleming, A. Olaya-Castro, R. van Grondelle, *Nat Chem* **2011**, 3, 763-774.
- [36] X. Hu, A. Damjanovic, T. Ritz, K. Schulten, *Proc Natl Acad Sci U S A* **1998**, 95, 5935-5941.
- [37] Z. G. Fetisova, A. M. Freiberg, K. E. Timpmann, *Nature* **1988**, 334, 633-634.
- [38] R. R. Alfano, R. M. Clegg, M. Sener, Govindjee, in *Optical Biopsy VII*, **2010**.
- [39] G. D. Scholes, T. Mirkovic, D. B. Turner, F. Fassioli, A. Buchleitner, *Energy & Environmental Science* **2012**, 5, 9374-9393.
- [40] D. L. Andrews, Wiley Online Library, Hoboken, **2015**.
- [41] L. Ji, Y. Sang, G. Ouyang, D. Yang, P. Duan, Y. Jiang, M. Liu, *Angew Chem Int Ed Engl* **2019**, 58, 844-848.
- [42] B. Albinsson, J. K. Hannestad, K. Borjesson, *Coordin Chem Rev* **2012**, 256, 2399-2413.
- [43] K. Boeneman, D. E. Prasuhn, J. B. Blanco-Canosa, P. E. Dawson, J. S. Melinger, M. Ancona, M. H. Stewart, K. Susumu, A. Huston, I. L. Medintz, *J Am Chem Soc* **2010**, 132, 18177-18190.
- [44] E. Boulais, N. P. D. Sawaya, R. Veneziano, A. Andreoni, J. L. Banal, T. Kondo, S. Mandal, S. Lin, G. S. Schlau-Cohen, N. W. Woodbury, H. Yan, A. Aspuru-Guzik, M. Bathe, *Nature materials* **2018**, 17, 159–166
- [45] P. K. Dutta, R. Varghese, J. Nangreave, S. Lin, H. Yan, Y. Liu, *J Am Chem Soc* **2011**, 133, 11985-11993.
- [46] M. Heilemann, P. Tinnefeld, G. S. Mosteiro, M. Garcia-Parajo, N. F. Van Hulst, M. Sauer, *J Am Chem Soc* **2004**, 126, 6514-6515.
- [47] W. P. Klein, S. A. Diaz, S. Buckhout-White, J. S. Melinger, P. D. Cunningham, E. R. Goldman, M. G. Ancona, W. Kuang, I. L. Medintz, *Advanced Optical Materials* **2018**, 6, 1700679.

- [48] C. M. Spillmann, S. Buckhout-White, E. Oh, E. R. Goldman, M. G. Ancona, I. L. Medintz, *Chem Commun* **2014**, *50*, 7246-7249.
- [49] K. Trofymchuk, A. Reisch, P. Didier, F. Fras, P. Gilliot, Y. Mely, A. S. Klymchenko, *Nature Photonics* **2017**, *11*, 657-663.
- [50] R. W. Wagner, J. S. Lindsey, *J Am Chem Soc* **1994**, *116*, 9759-9760.
- [51] J. K. Hannestad, P. Sandin, B. Albinsson, *J Am Chem Soc* **2008**, *130*, 15889-15895.
- [52] F. Nicoli, A. Barth, W. Bae, F. Neukirchinger, A. H. Crevenna, D. C. Lamb, T. Liedl, *ACS Nano* **2017**, *11*, 11264-11272.
- [53] W. P. Klein, S. A. Diaz, S. Buckhout-White, J. S. Melinger, P. D. Cunningham, E. R. Goldman, M. G. Ancona, W. Kuang, I. L. Medintz, *Adv Opt Mater* **2018**, *6*.
- [54] C. M. Spillmann, S. Buckhout-White, E. Oh, E. R. Goldman, M. G. Ancona, I. L. Medintz, *Chem Commun* **2014**, *50*.
- [55] N. Appukutti, C. J. Serpell, *Polymer Chemistry* **2018**, *9*, 2210-2226.
- [56] A. T. Haedler, K. Kreger, A. Issac, B. Wittmann, M. Kivala, N. Hammer, J. Köhler, H.-W. Schmidt, R. Hildner, *Nature* **2015**, *523*, 196.
- [57] A. J. Markvoort, H. M. M. t. Eikelder, P. A. J. Hilbers, T. F. A. de Greef, *ACS Central Science* **2016**, *2*, 232-241.
- [58] B. N. S. Thota, X. Lou, D. Bochicchio, T. F. E. Paffen, R. P. M. Lafleur, J. L. J. van Dongen, S. Ehrmann, R. Haag, G. M. Pavan, A. R. A. Palmans, E. W. Meijer, *Angew Chem Int Edit* **2018**, *57*, 6843-6847.
- [59] S. K. Albert, I. Sivakumar, M. Golla, H. V. P. Thelu, N. Krishnan, L. J. K. Ashish, R. Varghese, *J Am Chem Soc* **2017**, *139*, 17799-17802.
- [60] M. Á. Alemán García, E. Magdalena Estrado, L. G. Milroy, L. Brunsved, *Angew Chem Int Edit* **2018**, *57*, 4976-4980.
- [61] C. D. Bösch, S. M. Langenegger, R. Häner, *Angew Chem Int Edit* **2016**, *55*, 9961-9964.
- [62] O. A. Krasheninnina, D. S. Novopashina, E. K. Apartsin, A. G. Venyaminova, *Molecules* **2017**, *22*, 2108.
- [63] V. L. Malinovskii, A. L. Nussbaumer, R. Häner, *Angew Chem Int Edit* **2012**, *51*, 4905-4908.
- [64] L.-B. Meng, D. Li, S. Xiong, X.-Y. Hu, L. Wang, G. Li, *Chem. Commun. (Cambridge, U. K.)* **2015**, *51*, 4643-4646.
- [65] A. L. Nussbaumer, D. Studer, V. L. Malinovskii, R. Häner, *Angew Chem Int Edit* **2011**, *50*, 5490-5494.
- [66] G. Pan, X. Jin, Q. Mou, C. Zhang, *Chinese Chemical Letters* **2017**, *28*, 1822-1828.

- [67] M. Vybornyi, Y. B. C. Hechevarria, M. Glauser, A. V. Rudnev, R. Häner, *Chem Commun* **2015**, 51, 16191-16193.
- [68] M. Vybornyi, A. Rudnev, R. Häner, *Chem Mater* **2015**, 27, 1426-1431.
- [69] M. Vybornyi, A. V. Rudnev, S. M. Langenegger, T. Wandlowski, G. Calzaferri, R. Häner, *Angew Chem Int Edit* **2013**, 52, 11488-11493.
- [70] C. B. Winiger, S. Li, G. R. Kumar, S. M. Langenegger, R. Häner, *Angew. Chem., Int. Ed.* **2014**, 53, 13609-13613.
- [71] N. Zhang, W.-Y. Lo, A. Jose, Z. Cai, L. Li, L. Yu, *Adv Mater* **2017**, 29, 1701248.
- [72] O. O. Adeyemi, V. L. Malinovskii, S. M. Biner, G. Calzaferri, R. Häner, *Chem Commun* **2012**, 48, 9589-9591.
- [73] M. Balaz, S. Tannir, K. Varga, *Coordin Chem Rev* **2017**, 349, 66-83.
- [74] É. Boulais, N. P. D. Sawaya, R. Veneziano, A. Andreoni, J. L. Banal, T. Kondo, S. Mandal, S. Lin, G. S. Schlau-Cohen, N. W. Woodbury, H. Yan, A. Aspuru-Guzik, M. Bathe, *Nature materials* **2017**, 17, 159.
- [75] B. L. Cannon, D. L. Kellis, L. K. Patten, P. H. Davis, J. Lee, E. Graugnard, B. Yurke, W. B. Knowlton, *The Journal of Physical Chemistry A* **2017**, 121, 6905-6916.
- [76] P. K. Dutta, S. Levenberg, A. Loskutov, D. Jun, R. Saer, J. T. Beatty, S. Lin, Y. Liu, N. W. Woodbury, H. Yan, *J Am Chem Soc* **2014**, 136, 16618-16625.
- [77] F. Garo, R. Häner, *Angew Chem Int Edit* **2012**, 51, 916-919.
- [78] V. L. Malinovskii, D. Wenger, R. Häner, *Chem Soc Rev* **2010**, 39, 410-422.
- [79] W. Su, V. Bonnard, G. A. Burley, *Chem-Eur J* **2011**, 17, 7982-7991.
- [80] R. Varghese, H.-A. Wagenknecht, *Chem. Commun. (Cambridge, U. K.)* **2009**, 2615-2624.
- [81] J. G. Woller, J. K. Hannestad, B. Albinsson, *J Am Chem Soc* **2013**, 135, 2759-2768.
- [82] F. A. Aldaye, A. L. Palmer, H. F. Sleiman, *Science* **2008**, 321, 1795-1799.
- [83] C. Lin, Y. Liu, H. Yan, *Biochemistry-US* **2009**, 48, 1663-1674.
- [84] N. C. Seeman, *J Theor Biol* **1982**, 99, 237-247.
- [85] N. C. Seeman, *Nano Lett* **2010**, 10, 1971-1978.
- [86] V. Balzani, A. Credi, M. Venturi, *Chemsuschem* **2008**, 1, 26-58.
- [87] G. Calzaferri, M. Pauchard, H. Maas, S. Huber, A. Khatyr, T. Schaafsma, *J Mater Chem* **2002**, 12, 1-13.
- [88] B. L. Cannon, L. K. Patten, D. L. Kellis, P. H. Davis, J. Lee, E. Graugnard, B. Yurke, W. B. Knowlton, *The Journal of Physical Chemistry A* **2018**, 122, 2086-2095.
- [89] M. Endo, H. Sugiyama, *Chembiochem* **2009**, 10, 2420-2443.
- [90] J. M. Kinsella, A. Ivanisevic, *Langmuir* **2007**, 23, 3886-3890.

- [91] M. Probst, S. M. Langenegger, R. Häner, *Chem Commun* **2014**, *50*, 159-161.
- [92] N. L. Rosi, C. A. Mirkin, *Chemical reviews* **2005**, *105*, 1547-1562.
- [93] E. Stulz, *Acc. Chem. Res.* **2017**, *50*, 823-831.
- [94] C. W. Brown, A. Samanta, S. Buckhout-White, S. A. Díaz, S. A. Walper, E. R. Goldman, I. L. Medintz, in *SPIE Nanoscience + Engineering*, Vol. 10355, SPIE, **2017**, p. 9.
- [95] S. Buckhout-White, C. M. Spillmann, W. R. Algar, A. Khachatrian, J. S. Melinger, E. R. Goldman, M. G. Ancona, I. L. Medintz, *Nature Communications* **2014**, *5*, 5615.
- [96] L. Jing-Jing, C. Yong, Y. Jie, C. Ni, L. Yu, *Advanced Materials* **2017**, *29*, 1701905.
- [97] R. A. Miller, A. D. Presley, M. B. Francis, *J Am Chem Soc* **2007**, *129*, 3104-3109.
- [98] V. Garg, G. Kodis, P. A. Liddell, Y. Terazono, T. A. Moore, A. L. Moore, D. Gust, *The Journal of Physical Chemistry B* **2013**, *117*, 11299-11308.
- [99] H. Bittermann, D. Siegemund, V. L. Malinovskii, R. Haner, *J Am Chem Soc* **2008**, *130*, 15285-15287.
- [100] D. B. Chithrani, *Journal of Nanomedicine Research* **2014**, *1*.
- [101] G. Han, P. Ghosh, V. M. Rotello, *Nanomedicine* **2007**, *2*, 113-123.
- [102] T. A. Taton, C. A. Mirkin, R. L. Letsinger, *Science* **2000**, *289*, 1757-1760.
- [103] M. Kownacki, S. M. Langenegger, S.-X. Liu, R. Häner, *Angew Chem Int Edit* **2019**, *58*, 751-755.
- [104] D. A. Handley, *Colloidal gold : principles, methods and applications. Volume 1*, Academic Press, San Diego, **1989**.
- [105] L. Maggini, D. Bonifazi, *Chem. Soc. Rev.* **2012**, *41*, 211-241.
- [106] B. Chen, H. Nie, P. Lu, J. Zhou, A. Qin, H. Qiu, Z. Zhao, B. Z. Tang, *Chem Commun* **2014**, *50*.
- [107] J. Zhou, Z. Chang, Y. Jiang, B. He, M. Du, P. Lu, Y. Hong, H. S. Kwok, A. Qin, H. Qiu, Z. Zhao, B. Z. Tang, *Chem Commun* **2013**, *49*.
- [108] J. Liang, B. Z. Tang, B. Liu, *Chem Soc Rev* **2015**, *44*, 2798-2811.
- [109] H. Wang, E. Zhao, J. W. Y. Lam, B. Z. Tang, *Materials Today* **2015**, *18*, 365-377.
- [110] M. Chen, L. Li, H. Nie, J. Tong, L. Yan, B. Xu, J. Z. Sun, W. Tian, Z. Zhao, A. Qin, B. Z. Tang, *Chemical Science* **2015**, *6*, 1932-1937.
- [111] X. Zhang, K. Wang, M. Liu, X. Zhang, L. Tao, Y. Chen, Y. Wei, *Nanoscale* **2015**, *7*, 11486-11508.
- [112] A. Ranjanaware, D. Duc La, S. V. Bhosale, *RSC Advances* **2015**, *5*, 56270-56273.
- [113] Z. Qiu, X. Liu, J. W. Y. Lam, B. Z. Tang, *Macromolecular Rapid Communications* **2019**, *40*.

- [114] G. Huang, B. Ma, J. Chen, Q. Peng, G. Zhang, Q. Fan, D. Zhang, *Chemistry - A European Journal* **2012**, *18*, 3886-3892.
- [115] C.-T. Lai, R.-H. Chien, S.-W. Kuo, J.-L. Hong, *Macromolecules* **2011**, *44*, 6546-6556.
- [116] R. Hu, Y. Kang, B. Z. Tang, *Polymer Journal* **2016**, *48*, 359.
- [117] S. Li, S. M. Langenegger, R. Haner, *Chem Commun (Camb)* **2013**, *49*, 5835-5837.
- [118] J. Huang, Y. Jiang, J. Yang, R. Tang, N. Xie, Q. Li, H. S. Kwok, B. Z. Tang, Z. Li, *Journal of Materials Chemistry C* **2014**, *2*.
- [119] H. Shi, Z. Gong, D. Xin, J. Roose, H. Peng, S. Chen, J. W. Y. Lam, B. Z. Tang, *Journal of Materials Chemistry C* **2015**, *3*, 9095-9102.
- [120] Y. Hong, J. W. Y. Lam, B. Z. Tang, *Chem Soc Rev* **2011**, *40*.
- [121] J. E. McMurry, M. P. Fleming, *J Am Chem Soc* **1974**, *96*, 4708-4709.

## 6 Appendix

### 6.1 General Methods

The synthesis of the modified oligonucleotides was performed using a 394-DNA/RNA synthesizer *via* automated oligonucleotide synthesis by a standard solid-phase synthetic procedure by using CPGs-Phe-modified or CPGs-TPE-modified solid support. The commercially available oligonucleotides were purchased from *Microsynth* (Balgach, Switzerland) and used without further purification. Chemicals used for the building block preparation were purchased from commercial suppliers (Sigma-Aldrich, TCI, Alfa Aesar, Glen Research). Milli-Q purified water was used for the phosphate buffer preparation. A varian Cary-100 Bio-UV/VIS was used for collecting absorption spectra and determining melting temperatures ( $T_m$ ). A varian Cary Eclipse fluorescence spectrofluorimeter was used to record fluorescence emission and excitation spectra. TEM (Transmission Electron Microscopy) analysis was obtained on FEI Morgagni 268 (Institute of Anatomy, University of Bern) using operating voltage of 80 kV. AFM measurements were performed on a Nanoflex AFM (Nanosurf AG, Switzerland) at ambient conditions. Experimental masses were determined by a Thermo Fisher LTQ Orbitrap XL using Nano Electrospray Ionization as well as LC-MS for Oligonucleotides (Q-TOF).

### 6.2 Declaration

#### **Declaration of consent**

on the basis of Article 30 of the RSL Phil.-nat. 18

Name/First Name: Mariusz Kownacki

Matriculation Number: 15-126-238

Study program:

Bachelor  Master  Dissertation

Title of the thesis: Integration of Functional DNA-Nanoscaffolds into Supramolecular Polymers

Supervisor: Prof. Dr. Robert Häner

I declare herewith that this thesis is my own work and that I have not used any sources other than those stated. I have indicated the adoption of quotations as well as thoughts taken from other authors as such in the thesis. I am aware that the Senate pursuant to Article 28. RSL Phil.-nat. 05 is authorized to revoke the title awarded on the basis of this thesis.

For the purposes of evaluation and verification of compliance with the declaration of originality and the regulations governing plagiarism, I hereby grant the University of Bern the right to process my personal data and to perform the acts of use this requires, in particular, to reproduce the written thesis and to store it permanently in a database, and to use said database, or to make said database available, to enable comparison with future theses submitted by others.

Place/Date

Signature

### 6.3 Curriculum Vitae

Name	Mariusz Kownacki
Date of Birth	08.05.1990
Place of Birth	Mława, Poland
Address	3013 Bern, Hildanusstrasse 4
E-Mail	mkownacki90@gmail.com
Telefon	+417762296164

### Education

- 2015-2019 PhD with Prof. R. Häner at the University of Bern
- 2014-2015 Internship at Abnoba GmbH in Germany
- 2012-2014 Master in Chemistry at Adam Mickiewicz University in Poznan (Poland)
- 2009-2012 Bachelor in Chemistry at the University of Gdansk (Poland)

### Publications

M. Kownacki, S. M. Langenegger, S.-X. Liu, R. Häner, *Integrating DNA-Photonic Wires into Light-Harvesting Supramolecular Polymers*, *Angew. Chem. Int. Ed.*, **2019**, 58, 751-755.

### Other activities

Contribution to Swiss Science Concentrates, Chimia 2016-2017.